A PHASE SHIFTER USING RF MEMS TECHNOLOGY

A THESIS SUBMITTED TO
THE GRADUATE SCHOOL OF APPLIED AND NATURAL SCIENCES
OF
THE MIDDLE EAST TECHNICAL UNIVERSITY

BY

HÜSEYİN SAĞKOL

IN PARTIAL FULFILLMENT OF THE REQUIREMENTS FOR THE DEGREE OF
MASTER OF SCIENCE
IN
THE DEPARTMENT OF ELECTRICAL AND ELECTRONICS ENGINEERING

SEPTEMBER 2002

Approval of Graduate School of Natural and Applied Sciences.

Prof. Dr. Tayfur Öztürk
Director

I certify that this thesis satisfies all the requirements as a thesis for the degree of Master of Science.

Prof. Dr. Mübeccel Demirekler
Head of Department

This is to certify that we have read this thesis and that in our opinion it is fully adequate, in scope and quality, as a thesis for the degree of Master of Science.

Assoc. Prof. Dr. Tayfun AKIN
Co-Supervisor

Assoc. Prof. Dr. Sencer Koç
Supervisor

Examining Committee Members

Prof. Dr. Canan TOKER

Prof. Dr. Altunkan HIZAL

Assoc. Prof. Dr. Sencer KOÇ

Assoc. Prof. Dr. Tayfun AKIN

Sinan KORKAN

ABSTRACT

A PHASE SHIFTER USING RF MEMS TECHNOLOGY

Sağkol, Hüseyin
M. Sc., Department of Electrical and Electronics Engineering
Supervisor: Assoc. Prof. Dr. Sencer Koç
Co-Supervisor: Assoc. Prof. Dr. Tayfun Akın

September 2002, 148 pages

This thesis reports design, fabrication, and testing of RF MEMS switches and phase shifters. Shunt and series switches were designed, and they were employed in discrete and continuous phase shifters. Switches operate by pulling down metal beams or bridges on the signal line by electrostatic force, hence making short circuit. This short circuit is used, to either reflect signal as in shunt switches, or transmit it as in series switches. Switches are also used as tunable capacitive loads on a transmission line, changing its phase velocity, hence creating phase shift. This type of phase shifter is named as loaded line phase shifter. Also switches are used to

change the length of the line between input and output, by switching different length lines, to create phase shift. This type of phase shifter is named as switched line phase shifter.

In the scope of this study, three different types of switches and two different types of phase shifters are designed. Designed switches are series capacitive, shunt capacitive, and single-pole double-throw switch. Designed phase shifters are loaded line and switched line phase shifters. The design of switches and phase shifters are completed in the Middle East Technical University (METU), Department of Electrical and Electronics Engineering (EEE). The components are fabricated using a custom process developed in microelectronics fabrication laboratories of METU EEE. They were tested using the measurement setup in the millimeter wave laboratory of METU EEE.

Measurement results give better than 20 dB isolation at 1 GHz and a minimum insertion loss of 0.2 dB for the series capacitive switch. Results for the loaded line phase shifter indicate that the phase shifter can give a phase shift that is linearly increasing with frequency, which is 4^{o}/cm at 10 GHz. Insertion loss difference between minimum phase shift and maximum phase shift is <0.02 dB meaning a negligible amplitude variation in different insertion phases.

This research is the first national study on design and implementation of switches and phase shifters using RF MEMS technology.

Keywords: RF MEMS, Series capacitive switch, Shunt capacitive switch, Loaded line phase shifter, Switched line phase shifter, Micromachining.

ÖZ

RF MEMS TEKNOLOJİSİ İLE FAZ KAYDIRICI

Sağkol, Hüseyin
Yüksek Lisans, Elektrik ve Elektronik Mühendisliği Bölümü
Tez Yöneticisi: Yrd. Doç. Dr. Sencer Koç
Ortak Tez Yöneticisi: Yrd. Doç. Dr. Tayfun Akın

Eylül 2002, 148 sayfa

Bu tez RF MEMS anahtar ve faz kaydırıcıların tasarım, üretim ve testini bildirmektedir. Paralel ve seri anahtarlar tasarlanmış ve bu anahtarlar faz kaydırıcılarda kullanılmıştır. Anahtarlar metal kiriş veya köprülerin elektrostatik kuvvet kullanılarak sinyal hattının üzerine indirilmesi ve böylece kısa devre oluşturulması ile çalışır. Bu kısa devre ya parallel anahtarlarda olduğu gibi sinyali yansıtmak için veya seri anahtarlarda olduğu gibi sinyali iletmek için kullanılır. Anahtarlar aynı zamanda iletim hattı üzerine yerleştirilmiş olan ve iletim hattının faz hızını değiştirerek faz kayması yaratan ayarlanabilir sığaçlar olarak kullanılır. Bu tür

faz kaydırıcıya yüklenmiş hat faz kaydırıcısı denir. Aynı zamanda anahtarlar faz kayması yaratmak için giriş ile çıkış arasındaki hattın uzunluğunu farklı uzunluktaki hatları anahtarlayarak değiştirirler. Bu tür faz kaydırıcılara anahtarlanmış hat faz kaydırıcısı denir.

Bu çalışma kapsamında üç değişik anahtar türü ve iki değişik faz kaydırıcı türü tasarlanmıştır. Tasarlanmış olan anahtarlar seri sığasal (kapasitif), paralel sığasal (kapasitif), ve tek girişli iki çıkışlı anahtarlardır. Tasarlanmış olan faz kaydırcılar yüklenmiş hat ve anahtarlanmış hat faz kaydırıcılardır. Anahtarların ve faz kaydırıcıların tasarımı Ortadoğu Teknik Üniversitesi (ODTÜ) Elektrik Elektronik Mühendisliği (EE Müh.) bölümünde yapılmıştır. Yapılar ODTÜ EE Müh. bölümünde geliştirilmiş olan özel bir süreç kullanılarak ODTÜ EE Müh. bölümünün mikroelektronik laboratuvarlarında üretilmiştir. Yapılar ODTÜ EE Müh. bölümünün milimetrik dalga laboratuvarında bulunan ölçüm düzeneği kullanılarak ölçülmüştür.

Ölçüm sonuçlarına göre seri sığasal (kapasitif) anahtarın en az araya sokma yitimi 0.2 dB dir ve 1 GHz deki yalıtımı 20 dB den daha iyidir. Yüklenmiş hat faz kaydırıcılar içinde sonuçlar faz kaydırıcının frekansla doğru orantılı olarak arttığını ve 10 GHz de 4^{o}/cm faz farkı verebildiğini göstermektedir. Minimum faz kayması ve maksimum faz kayması arasındaki araya sokma yitimi farkı 0.02 dB den azdır. Bu da göstermektedir ki değişik araya sokma yitimlerindeki büyüklük değişimi ihmal edilebilecek kadar küçüktür.

Bu araştırma RF MEMS teknolojisi kullanan anahtar ve faz kaydırıcıların tasarım ve üretimi üzerine yapılmış olan ilk milli çalışmadır.

Anahtar kelimeler: RF MEMS, Seri sığasal (kapasitif) anahtar, Paralel sığasal (kapasitif) anahtar, Yüklenmiş hat faz kaydırıcı, Anahtarlanmış hat faz kaydırıcı, Mikroişleme

To My Parents...

ACKNOWLEDGEMENTS

I would like to thank my thesis advisors Prof. Sencer Koç and Prof. Tayfun Akın not only for their guidance and support, but also for their friendly and extremely kind attitude towards me.

I would like to thank Prof. Altunkan Hızal for providing the design and test environment in the millimeter wave laboratory, and for sharing his experience and ideas. I would like to thank Prof. Şimşek Demir and Prof. Özlem Aydın Çivi for their great contribution to the development of this research, and for their innovative ideas.

I would like to thank Mehmet Ünlü and Kağan Topallı for their great help in all phases of the research, and for their great friendship in the sleepless nights during design and fabrication of the devices. I would like to thank Orhan Akar for his guidance in the development of the fabrication process, for sharing his process experience with me, for his innovative ideas, and for his valuable friendship. I would like to thank Selim Eminoğlu for his software and hardware support, and for his friendship. I would like to thank Deniz Sabuncuoğlu Tezcan for her friendship and support. I would like to thank Özge Zorlu and Mahmud Yusuf Tanrıkulu for their support and friendship that made life easier. I would like to thank all of my office mates for the nice atmosphere they created for me during my thesis studies.

I am grateful to my family for their support and patience through all my life.

This research is supported by TÜBİTAK BİLTEN.

TABLE OF CONTENTS

LIST OF FIGURES

FIGURES

LIST OF TABLES

TABLES

CHAPTER 1

INTRODUCTION

Switches and phase shifters are two important components of today's microwave systems. Phase shifters are key components in phased arrays enabling electronic beam scanning, which improves the performance of radars significantly. Switches are basic building blocks of many elements such as multiplexers, frequency selective surfaces, phase shifters, and many other microwave circuits that are extensively used in telephone switching networks, radars, wireless communication devices, radio astronomy, material detection, and many other applications.

The applications mentioned above requires systems that are compact, high performance, low power, and low cost. Due to these requirements, switches and phase shifters used in the systems are mostly implemented using solid-state components such as PIN diodes and FETs. PIN diode and FET switches are very small components due to the nature of solid-state device fabrication, which employs photolithography technique to implement devices that are a few microns in size. They are also very cheap since they can be batch produced in large amounts easily. However, they are nonlinear devices, which leads to spurious responses and cross talk in the systems. Also their RF performance, especially insertion loss, does not

meet the requirements of some of today's low power communication systems. In addition their power consumption is high, which makes them unsuitable for handheld, mobile, and wireless systems.

RF MEMS switches, which are newly being developed, can be taken as an alternative that can solve the problems mentioned above. Their introduction to the science society dates back to 1995 [1, 2]. First step was to demonstrate a switch that is functional. Then characterization and modeling of the switch was made [3]. Next step was to improve the performance of the switch. In this phase many different switches were introduced. These switches proposed different structures to improve different aspects of performance. Mainly improvement of insertion loss [4, 5], isolation [6-9], response time, power handling capacity, and actuation voltage [10, 11], was made by the intensive research. Also new processes were developed to implement the switches on GaAs substrates to reduce substrate losses and to integrate RF MEMS with MMIC technology [12].

Besides improving switches, researchers worked on applying the switch to different structures. First idea was to use them as tunable capacitances [13, 14] and capacitor banks in filters [15]. Then, they were used in phase shifters both as switches and as capacitive loads. These phase shifters were simply the same as the semiconductor switch based phase shifters. The difference was that FET or PIN diode switches were replaced with MEMS switches and capacitors. The developed phase shifters are grouped in three groups: loaded line phase shifters [16, 17], switched line phase shifters [18, 19], and reflection type phase shifters [20]. Switched line and reflection type phase shifters change the total length of line between input and output to give phase shift. They are compact, but they cannot give continuously tunable phase shift opposite to the loaded line phase shifters, which change the phase velocity of transmission line to give phase shift.

After the introduction of RF MEMS phase shifters, switches were considered for use in industrial applications [21]. At this point reliability issues of RF MEMS switches were investigated, and effort was spent on improving reliability of the RF

MEMS switches [22]. Also new applications were introduced like impedance tuners [23, 24], MEMS antennas [25], and tunable arrays [26].

Current state of RF MEMS switches outperforms FET and PIN diode switches in linearity, RF performance, and power consumption. For this reason development of these switches are very important for the forthcoming industrial applications. Nowadays there is an extensive research in developing new switches for different applications, improving current applications, and introducing new structures.

This thesis reports the first study on the development and fabrication of RF MEMS switches and phase shifters constructed using these switches in Turkey. Two types of phase shifters, discrete and continuous, were developed. They employ both series and shunt RF MEMS switches. The switches are used both for switching and capacitive loading purposes.

This chapter briefly explains the previously developed switches and phase shifters, and the objectives of this research. Section 1.1 gives an overview of the switches. Section 1.2 briefly explains the phase shifters and their development. Section 1.3 gives information on the devices developed in this research. Section 1.4 gives the objectives and the organization of the thesis.

1.1 Overview of Switches

Switches are one of the widely used components in RF applications. Early switches were triodes implemented using vacuum tubes. They were large and bulky devices. They consumed very high power and were also very fragile. They were replaced with semiconductor switches like diodes and transistors, with the invention of solid-state technology. Semiconductor switches are significantly smaller than triode tubes. They are also cheaper and suitable for mass production. Besides, they have better RF performance compared to triode tubes, and they have significantly lower power consumption.

However, new type of switches that use MEMS technology outperform their performance. These RF MEMS switches were first introduced in 1995 [1, 2] by Goldsmith and Chang. They use mechanical movement to achieve short circuit or an open circuit in the RF transmission line [22]. Mechanical movement can be achieved with electrostatic, magnetostatic, piezoelectric, or thermal forces. Electrostatic force driven switch is the most common used type [22].

The advantages of RF MEMS switches over FET and PIN diode switches can be listed as:

- *Very high isolation*: RF MEMS switches have very low off state capacitances. Hence, they have good isolation behavior for a wide frequency range.

- *Very low insertion loss*: They have insertion loss less than 0.1 dB, which is significantly lower than the insertion loss of FET and PIN diode switches.

- *Linearity*: RF MEMS switches are very linear compared to semiconductor switches. They have intermodulation products, which are 30 dB better than semiconductor switches.

- *Low power consumption*: RF MEMS switches do not consume power in steady state. They only consume power during transition between on and off states.

They also have some disadvantages, which are:

- *Long response time*: Due to their mechanical nature RF MEMS switches have response times around 2-40 μs, which is very long compared to switching times of 1ns of FET and PIN diode switches.

- *Power handling*: Most switches cannot handle more than 20-50 mW limiting their use in high power systems.

- *High voltage drive*: Electrostatic switches require 20-80V for operation, which is a very high value compared to 5V operation voltage for FET or PIN diode switches.

- *Packaging*: Since development of these switches is new, absolute solutions for packaging are still under development, which makes their packaging nonstandard and difficult.

1.2 Overview of Phase Shifters

Phase shifters are used in RF field for a number of applications, including phased array systems. Ferrite based phase shifters, which are the first generation of phase shifters used in different applications, use ferrite materials to change the properties of the propagation medium. This change in medium, leads to rotation in the polarization of the field, leading to a phase shift. Since these devices use ferrites, they are very large in size and heavy, and they consume large power.

In order to make small and light systems, switch based phase shifters were developed as replacement for ferrite based phase shifters. Switch based phase shifters use switches in different circuit topologies to obtain phase shift. Two of these approaches are switched line phase shifters and loaded line phase shifters. Switched line phase shifters direct the signal through lines of different length, altering the insertion phase between input and output. Since discrete line lengths are used to complete the path, these phase shifters are discrete phase shifters. Typically PIN diode and FET switches are used to choose the desired lines. These switches generally result in high insertion losses of 6-7 dB [27], however when RF MEMS switches are used, this insertion loss decreases significantly to a value as low as 0.9 dB [27].

Second type of switch based phase shifters considered in this work is loaded line phase shifters. These structures use transmission lines that are loaded with shunt reactive loads, to create phase shift. When a transmission line is loaded with a

reactive load, its insertion phase changes from the unloaded case. Therefore, it is possible to obtain desired amount of phase shift by changing the amount of loading. This loading is typically done by shunt connecting the reactive load to the transmission line through a switch or using the switch impedance as the reactive load. Typically PIN diode and FET switches are used for connecting reactive loads to the line or their variable capacitance is used for loading action. In RF MEMS phase shifters, FET or PIN diode switches are replaced with RF MEMS switches. Since these switches can attain a large range of capacitances their capacitance is used as reactive loads simplifying the structure of the phase shifter. Also, this approach enables continuous tuning of phase shift since capacitance of MEMS switches can be changed in a continuous manner.

As observed in the switch based phase shifters, RF MEMS version of the phase shifter is simply generated by replacing the FET or PIN diode switch with the MEMS switch. This approach simplifies the design process, since there is a well-known design process for the PIN diode or FET switch based phase shifters. The designer only has to replace the FET or PIN diode switch with the MEMS switch. This replacement results in significant decrease in insertion loss, decrease in power consumption, and better linearity.

1.3 Devices Developed in This Research

In the framework of this research, various RF MEMS switches and two different kind of phase shifters have been developed. Figure 1.1 shows the circuit model of the switched line phase shifters developed in this study. Signal path is completed through path 1, path 2, or path 3. The length difference between each path determines the amount of phase shift given at each step. Each path is selected by the single-pole double-throw RF MEMS switches that are developed for this phase shifter in this research.

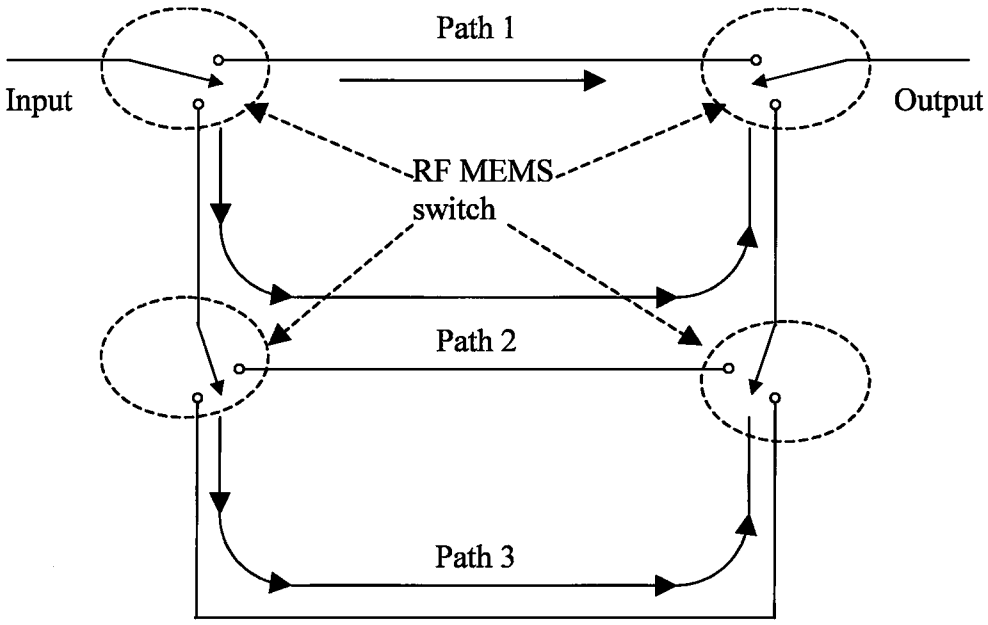

Figure 1.1: Model of the switched line phase shifter.

Single-pole double-throw switch is a capacitive series switch, which performs switching action by changing its capacitance significantly. As seen in Figure 1.2, when the beam is up there is a low capacitance between beam and signal line making the switch off, and when it is down this capacitance increases significantly making the switch on. The beam is pulled down by the electrostatic force due to the voltage applied between the beam and the specific signal line.

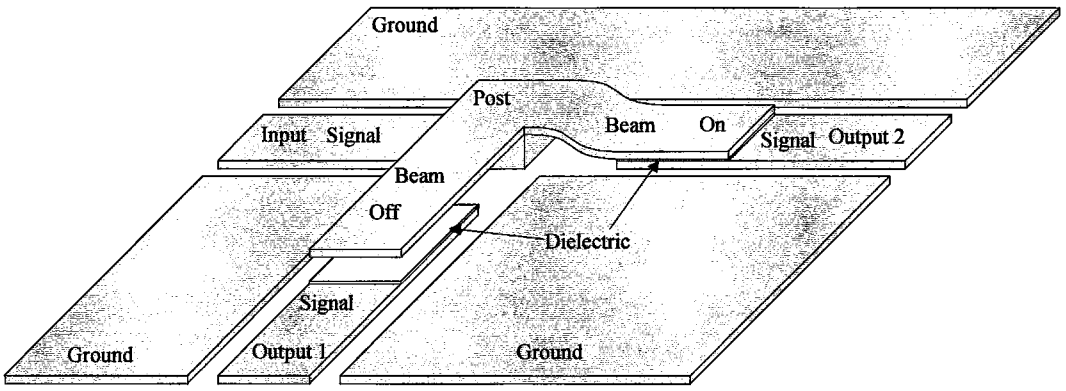

Figure 1.2: Three dimensional model of the single-pole double-throw switch.

The second phase shifter developed in the scope of this research is the loaded line phase shifter, which is based on the capacitance change. As seen in Figure 1.3, it uses shunt switches that are periodically placed over a transmission line as tunable capacitive loads. As the capacitance of these switches are varied by electrostatic force, phase velocity in the transmission line changes leading to phase shift. As the amount of this variation in the loading capacitance is increased magnitude of available phase shift is also increased.

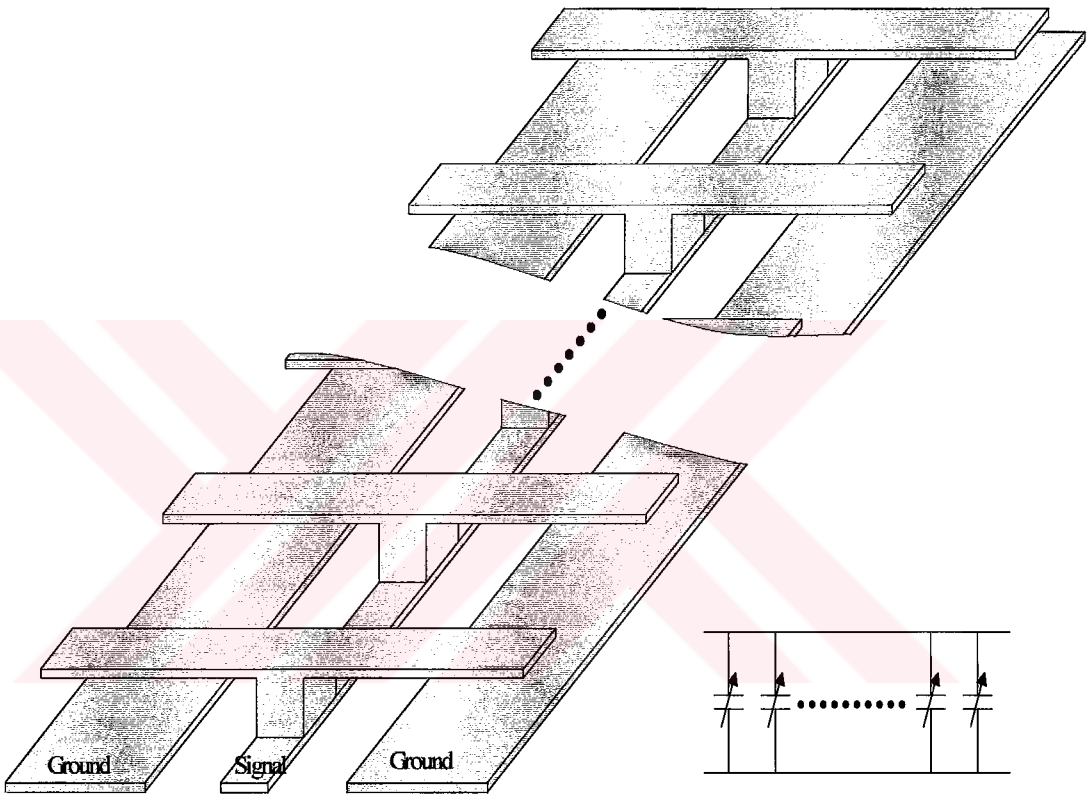

Figure 1.3: Three dimensional model and corresponding circuit model for the loaded line phase shifter.

In order to increase the amount of tunable capacitance hence the available phase shift, a new RF MEMS switch structure, which is seen in Figure 1.4, is developed in the scope of this study. This switch uses the area on the ground plane as the loading capacitance area contrary to the other switches that use the area over

the signal line for this purpose. Since the area over the ground plane is larger than the area over the signal line, this switch has a larger tunable capacitance.

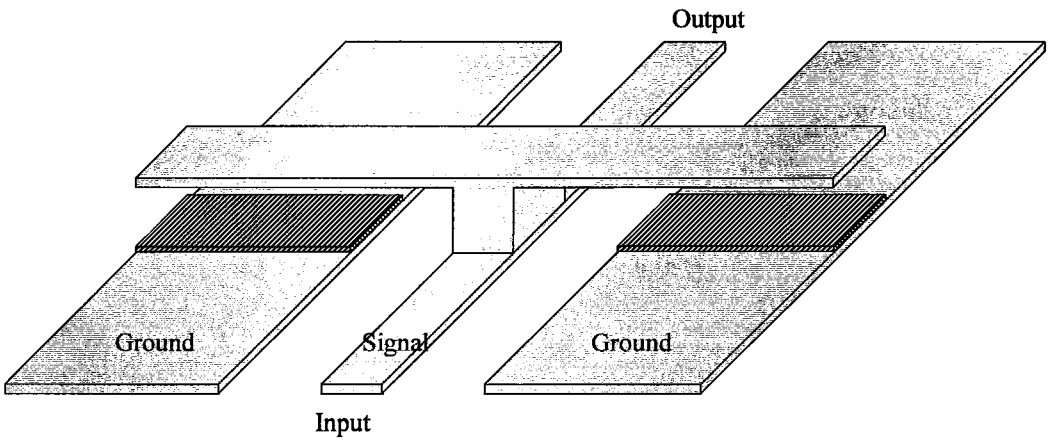

Figure 1.4: Three-dimensional model of the T-wing type switch.

1.4 Objectives and Organization of the Thesis

As the first study on RF MEMS technology in Turkey, this research aims to construct a knowledge and experience database that will guide the following research in Turkey on this subject. In order to gain the required knowledge and experience the specific objectives stated below are taken as the targets to be achieved in the scope of this research.

- Development of a custom fabrication process all steps of which can be performed using the capabilities of the devices available at the microelectronics facilities at METU. Such a process makes it possible to implement the designs easily and in a short time, which reduces the total design time significantly. The process is developed, and is continuously being improved in order to achieve high yield and repeatability.

- Design of new RF MEMS switches. Since switches are building blocks for most of the RF MEMS structures, a good switch design would be helpful for

the design of other RF MEMS structures. Also the experience obtained from switch design is very valuable for an RF MEMS designer. Two different switch structures are developed in the course of this research in order to gain this experience.

- Design of phase shifters that employ the new switch structures. These phase shifters are designed to be integrated with a phased array to demonstrate the applicability of the RF MEMS structures. Continuous and discrete phase shifters that employ the new switch structures are designed.

The study started with a literature survey to investigate current RF MEMS structures. Then new structures were proposed and evaluated. After the evaluation of the structures, the process to realize these structures was developed. As the next step the structures were designed according to this process, and their RF and mechanical simulations were done. Then their layouts were drawn, and mask sets for these layouts were obtained, and the designs were fabricated using the micromachining facilities at METU. Finally, the fabricated structures were tested. The rest of the thesis, which explains these steps in detail, is organized in the following order.

Chapter II gives the theoretical background that is required to understand the basics and operation principles of the designed RF MEMS structures.

Chapter III gives the design criteria that is used to evaluate the performance of a design and the design procedure, which includes some design tips and the critical points in a design, to make a good design to meet the specifications on the design criteria. The simulation results of the structures designed following the given procedure are also presented.

Chapter IV gives the fabrication process and critical points in fabrication that should be considered carefully to obtain error free and high quality products.

Chapter V shows the fabricated structures, and gives the test results for these structures. Also comparison of these results with simulations is made, and possible causes of discrepancies are explained in this chapter.

Chapter VII summarizes the work done in this research, and makes suggestions on future research.

CHAPTER 2

THEORY OF COPLANAR WAVEGUIDES, RF MEMS SWITCHES, AND PHASE SHIFTERS

This chapter presents the theoretical information, which forms a background for understanding the operation of the devices that are subject of this thesis. However, before going through the theory of the structures, one should have a notion about the coplanar waveguides (CPW), since all of the structures are built on CPWs. Therefore, the theory of CPWs will be given in Section 2.1. Section 2.2 explains theory of RF MEMS switches, which are the basic building blocks of all the other RF MEMS devices. Section 2.3 gives the theoretical information governing the operation of the continuous and discrete phase shifters that are constructed using the RF MEMS switches. After presenting the basic equations governing the RF operation of these devices, general mechanical information, which explains the mechanical operation of all devices, is given in Section 2.4.

2.1 Coplanar Waveguides (CPW)

A conventional CPW consists of a center strip conductor with semi-infinite ground planes on either side, all of which are placed on the same side of a dielectric substrate as shown in Figure 2.1. Besides the one seen in Figure 2.1, there are other forms of coplanar waveguides. These variations include lines with extra ground planes on top and bottom or lines whose substrate is intentionally removed for better performance. These types can be broadly classified as follows [28]:

- Conventional CPW
- Conductor backed CPW
- Micromachined CPW

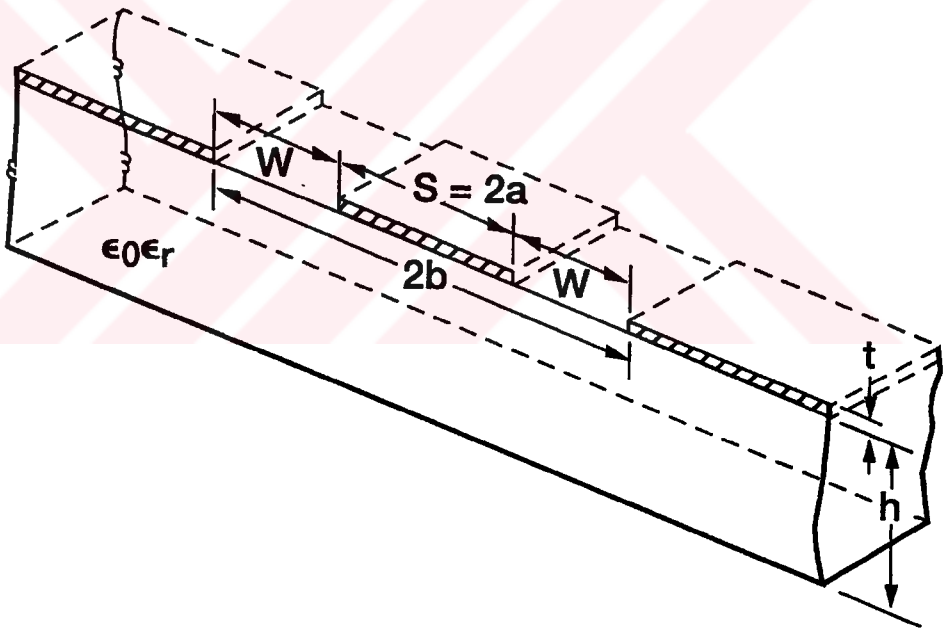

Figure 2.1: 3D drawing of a conventional CPW [28]. Hatched regions are the conductors placed on a dielectric substrate. *S* and *W* are the critical dimensions that determine the properties like the characteristic impedance of the CPW. Also *h* is another parameter, which is included in real designs but taken as infinity for basic calculations.

Only theory of conductor backed CPWs (CBCPW), which is given in Section 2.1.2, is required for understanding the operation of devices designed in this thesis, since the devices are constructed on CBCPWs. However, the theory of conventional CPWs is also given in Section 2.1.1 since theory of CBCPWs is developed from the theory of conventional CPWs.

2.1.1 Conventional Coplanar Waveguides

As theoretical information for the conventional CPW, one should know the electric and magnetic field distributions of the line. This distribution gives an intuition about the properties of the line, and would be helpful in making designs that efficiently use these properties. Therefore, field distributions and related properties are given in Section 2.1.1.1. Besides the field distribution, a designer should be familiar with some parameters such as per unit length capacitance, effective permittivity, and characteristic impedance. Their dependence on the geometry and the substrate type plays an important role in the design of RF MEMS devices that use coplanar waveguides. Detailed information about these parameters is given in Section 2.1.1.2.

2.1.1.1 Field Distribution in Conventional Coplanar Waveguides

Derivation of the field components for a CPW is a well-known information, and can easily be obtained from many microwave books or papers [28-33]. Therefore, they are not included in this section. Using the equations given in [33] one can calculate the field distribution on the line. Figure 2.2 shows an example for the calculated electric field distribution on the $z = 0$ plane. One can see that electric field lines create an elliptic contour across the signal line and the ground planes on either side. The discontinuities in these contours are due to the different permittivity of the substrate region and the air region. In the substrate region phase velocity of the wave is different form the free space velocity. In fact this difference between the phase velocities also lead to discontinuities in the z direction which lead to small

field components in this direction, which is the direction of propagation. This leads to non-TEM mode of operation. However these field components are small compared to the field components in the transverse plane. Therefore, CPW is said to operate in quasi-TEM mode. In fact quasi-TEM mode is an assumption that the structure is operating in TEM mode, but instead of two dielectric regions, it is placed in a single medium with an effective dielectric constant calculated according to the geometry of the structure. However, this dielectric constant is not constant due to dispersion, which can be simply explained by the change in the characteristic parameters, such as the effective permittivity, of the line with frequency. This change in effective permittivity is due to confinement of field in the dielectric region instead of air region as frequency increases. Dispersion is the prime phenomenon, which determines the maximum bandwidth of the signals that can be transmitted through the line. In Figure 2.3 dispersion characteristic for the CPW and the microstrip line can be seen [28]. As seen from the figure CPW has a smoother change in the effective permittivity but the total change is larger than that of a microstrip line. This makes CPWs suitable for applications where longer pulses are used. They present a lower dispersion for this type of pulses compared to microstrip lines. However it is not suitable for short pulse signals since it causes larger dispersion than the microstrip. This is due to the large fringe fields in the CPW, which is also seen in Figure 2.2.

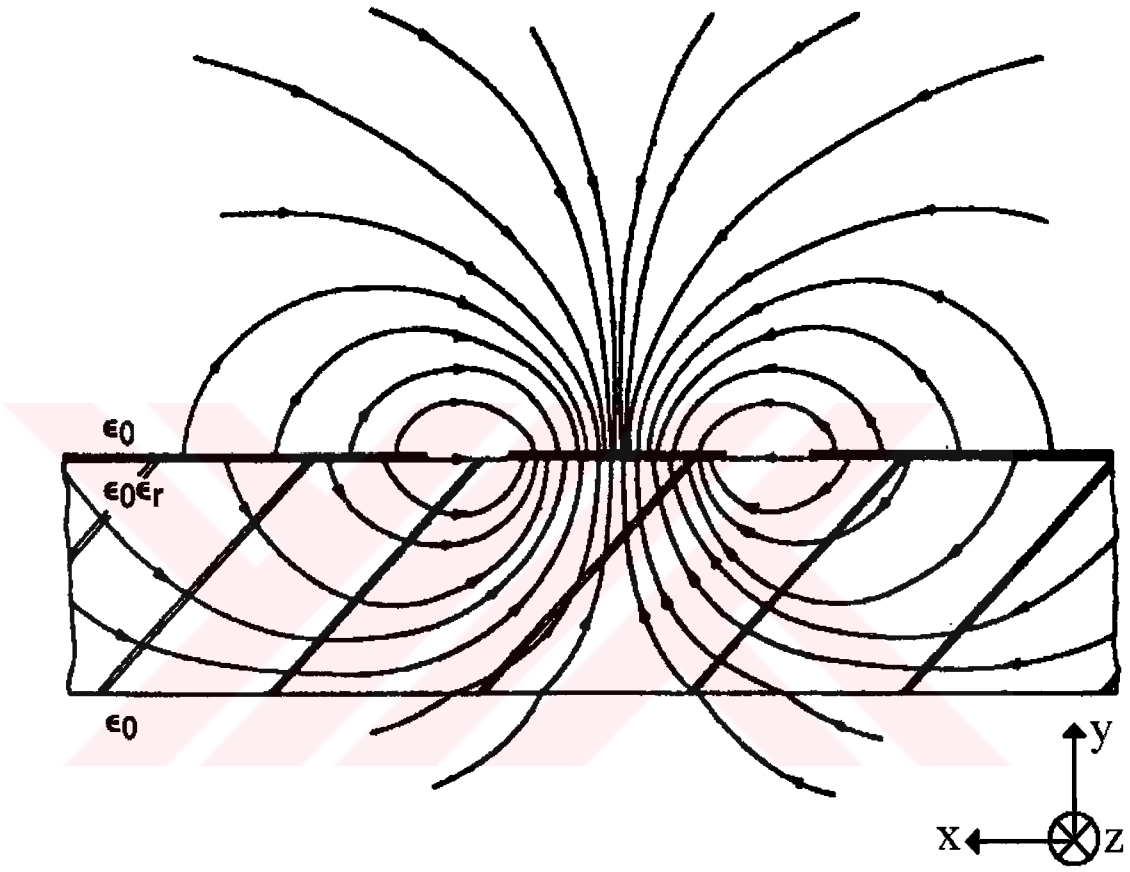

Figure 2.2: Electric field distribution on the $z = 0$ plane. Fields are confined above and below the signal line of the CPW. A small disturbance in this region would cause a large change in the characteristics of the line.

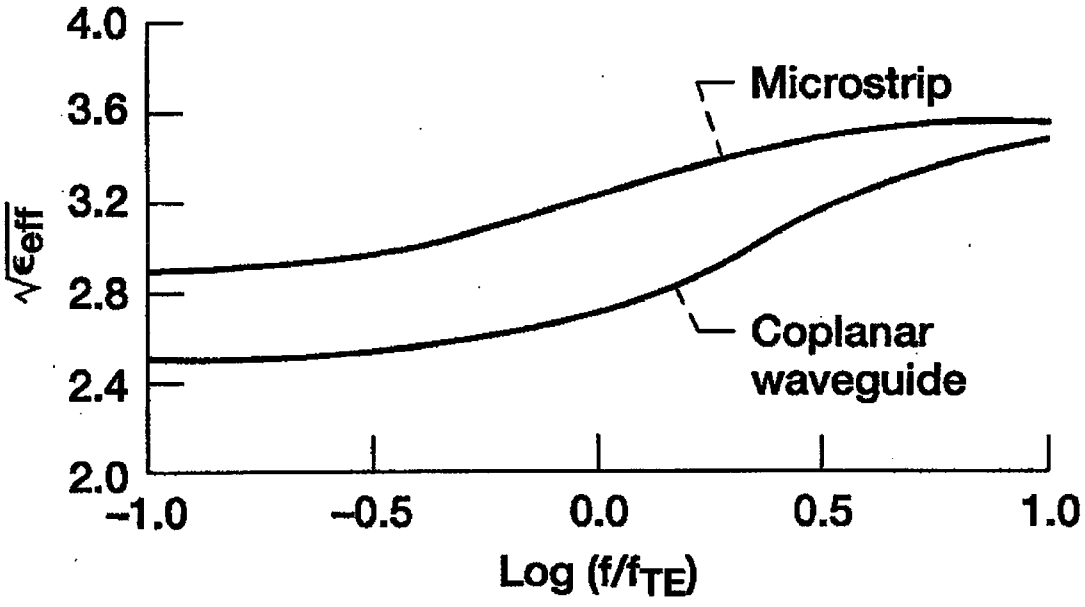

Figure 2.3: Change in the effective permittivity with frequency for a 50 Ω CPW with 85 μm signal line and 50 μm slot width; and microstrip with strip width of 73 μm [28]. Both lines are implemented on GaAs with $\varepsilon_r = 13$ and thickness 100 μm. f_{TE} is the cutoff frequency of the substrate, which is 216.5 GHz. Since CPW starts from a lower effective permittivity, it has a larger dispersion for large bandwidths. However its characteristic is smoother, which makes it suitable for narrow bandwidth signals.

Although there are elliptic fringe field lines that go to the sides of the center conductor, most of the electric field is confined over and under the center conductor similar to the microstrip line. Unlike the electric field lines magnetic field lines are confined in the slot region of the CPW, which can be seen in Figure 2.4. This field distribution makes the center region of the CPW vulnerable to disturbances. In other words placing a dielectric or conductor piece over the center conductor or slots of the CPW would affect the characteristic properties of the CPW. This feature makes CPWs suitable for MEMS applications where moving conductors or dielectric parts are used to alter the characteristic properties of a line.

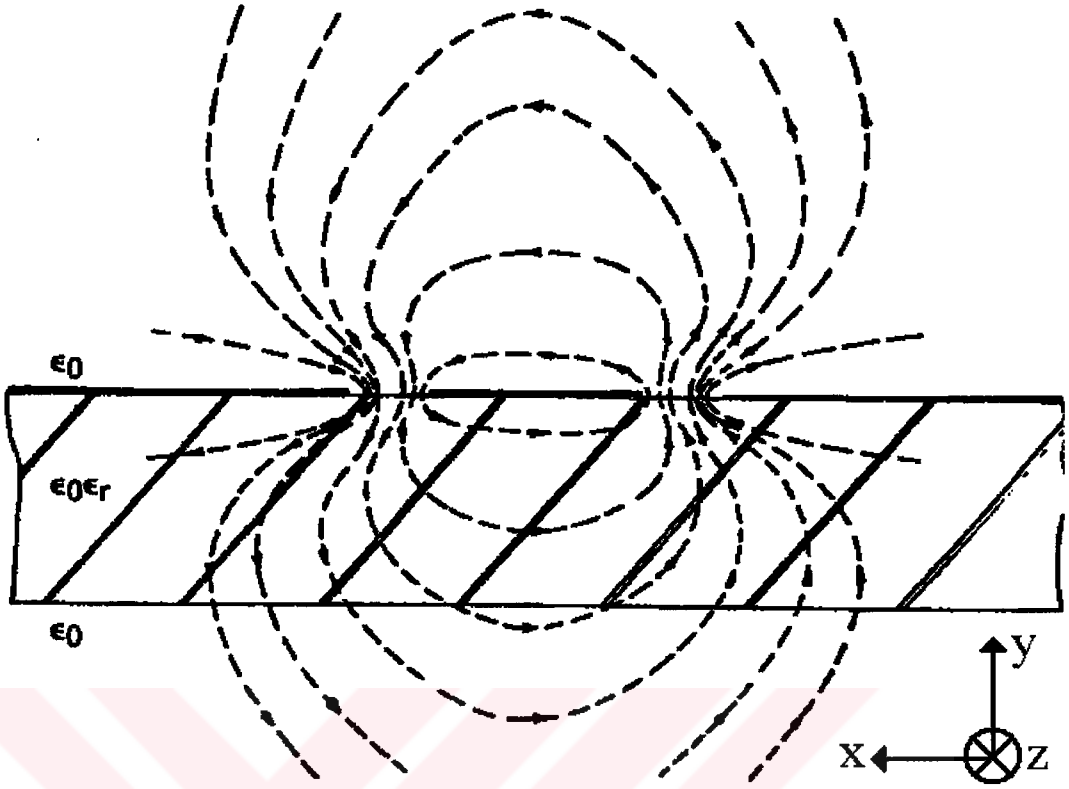

Figure 2.4: Magnetic field distribution on the $x = 0$ plane of the CPW [28]. Fields are confined in the slot regions of the CPW. They create closed loop contours around the center conductor of the CPW.

2.1.1.2 Characteristic Features ε_{eff}, C, Z_c

Characteristic properties of a line and modifying these properties are very important issues in microwave circuit design. For this reason a designer should know the characteristic properties of a CPW and the variables that these properties depend on. Having this knowledge will give the possibility to control these properties and lead to a well-defined and controlled design. Thus, the characteristic properties of a CPW will be given in this section.

In general, the most important property is the effective permittivity of the structure, because it determines the propagation properties of the structure and the characteristic impedance. In order to obtain this parameter, one should find the per unit length capacitance of a CPW, because under quasi-static approximation effective permittivity of a CPW is defined as [30]:

$$\varepsilon_{eff} = \frac{C_{CPW}}{C_{air}}, \tag{2.1}$$

where C_{CPW} is the per unit length capacitance of a CPW with dielectric substrate and C_{air} is the per unit length capacitance of a CPW without dielectric substrate. In order to find these capacitance values for a CPW structure given in Figure 2.5, the CPW is divided into several regions as shown in Figure 2.6 (a)-(c). Then the electric field is assumed to exist only in that region. Capacitance of each region is calculated using conformal mapping technique, and is added to give the total capacitance of the line [28-30].

$$C_{CPW} = C_1 + C_2 + C_{air}. \tag{2.2}$$

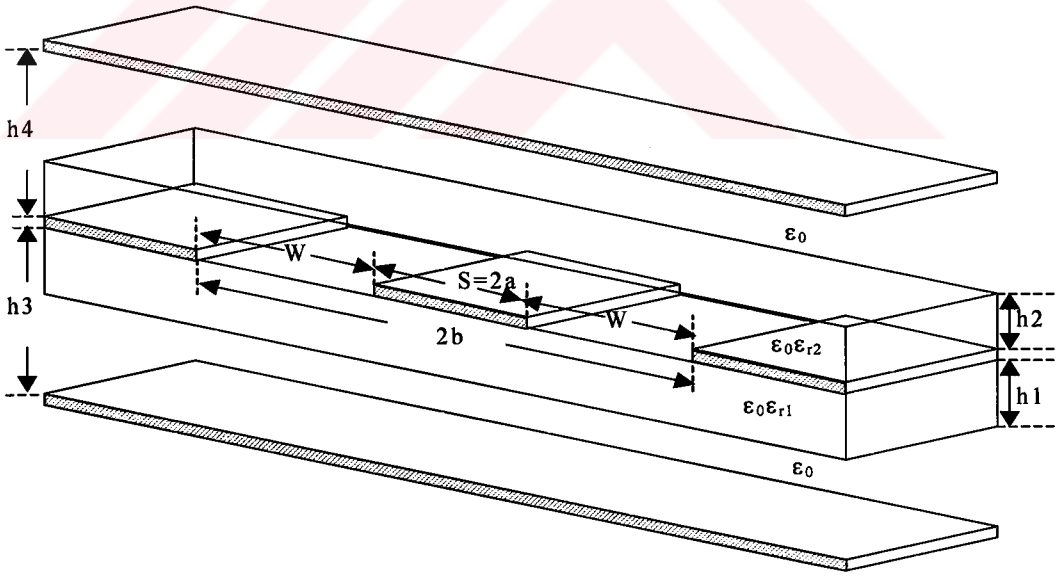

Figure 2.5: A general CPW structure for the calculation of capacitance and other characteristic parameters.

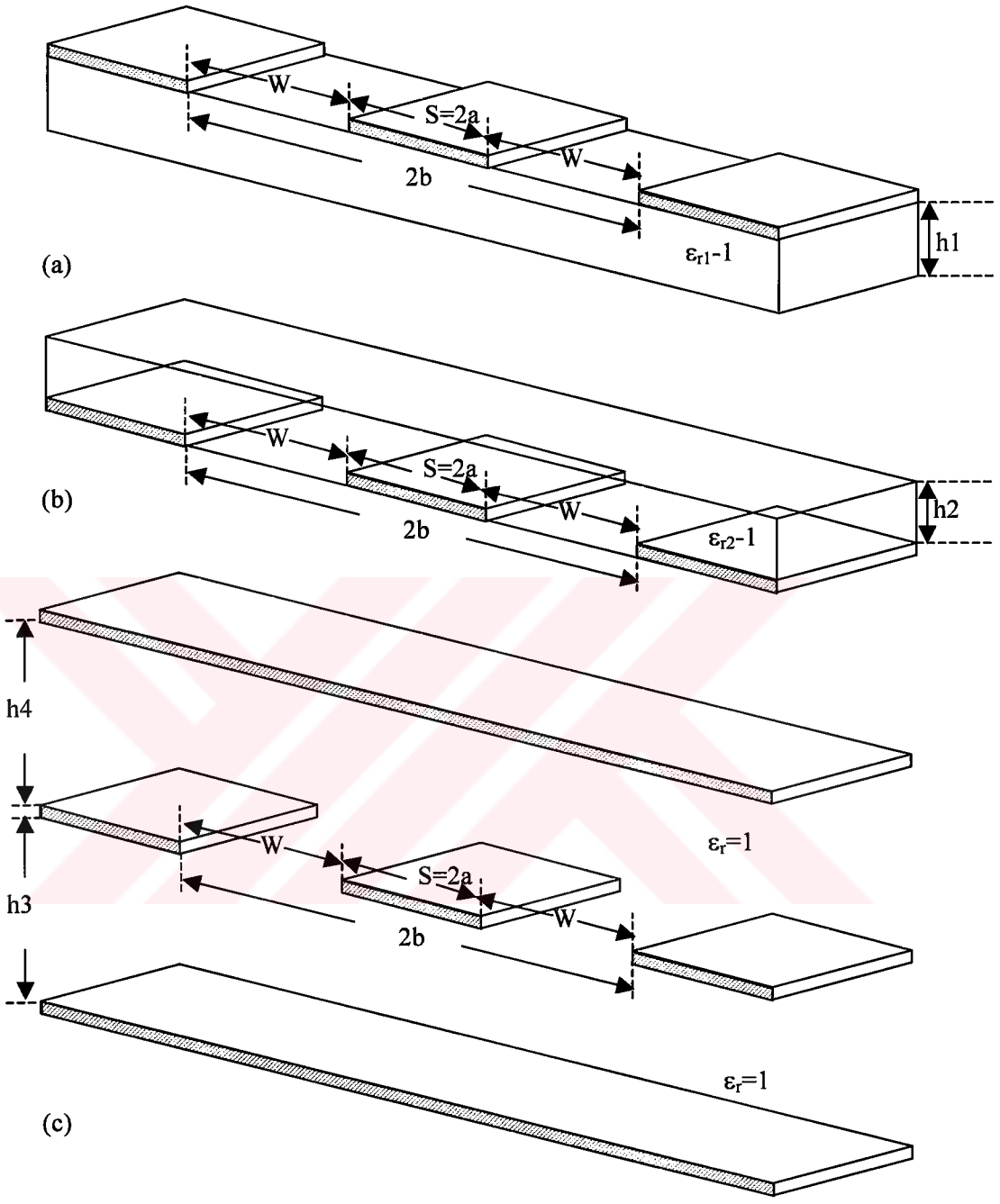

Figure 2.6: Configuration for partial capacitances for a CPW sandwiched between two substrates: (a) C_1 for the capacitance of the lower dielectric layer; (b) C_2 for the capacitance of the upper dielectric layer; (c) C_{air} for the no dielectric case.

The complicated equations stated in [28-30] can be simplified for a CPW with infinitely thick dielectric substrate, and are

$$C_{air} = 4\varepsilon_0 \frac{K(k_0)}{K(k_0')}, \tag{2.3}$$

$$C_{CPW} = 2\varepsilon_0(\varepsilon_{r1}+1)\frac{K(k_0)}{K(k_0')}, \tag{2.4}$$

where K is the complete elliptic integral of the first kind which is also explained in [28, 30], and

$$k_0 = \frac{S}{S+2W}, \tag{2.5}$$

$$k_0' = \sqrt{1-k_0^2}\,. \tag{2.6}$$

Then effective permittivity becomes

$$\varepsilon_{eff} = \frac{1+\varepsilon_{r1}}{2}. \tag{2.7}$$

After obtaining C_{CPW} and C_{air}, hence the effective permittivity, one can easily obtain the phase velocity and characteristic impedance using the following expressions.

$$v_{ph} = \frac{c}{\sqrt{\varepsilon_{eff}}}, \tag{2.8}$$

$$Z_0 = \frac{1}{C_{CPW} v_{ph}}. \tag{2.9}$$

One can understand from the above equations that characteristic properties of a CPW depend on the permittivity of the substrate ε_{r1} and the lateral dimensions of the CPW (S, W). Generally substrates are fixed or common in a design, which makes

ε_{r1} constant. Hence, the designer has S and W as variables to alter the characteristics of a CPW. By changing the *S/W* ratio, designer can change the characteristic impedance without affecting other parameters very much. This gives the designer the flexibility to use wide range of impedances for different applications.

2.1.2 Conductor Backed Coplanar Waveguides (CBCPW)

As a special case of a conventional CPW, conductor backed coplanar waveguides (CBCPW) will be explained in this section since all of the implemented structures are constructed on CBCPWs.

CBCPW has a slightly different field distribution from the conventional CPW. This difference is due to the additional ground plane on the backside of the substrate. The effect of this ground plane on the electric field can be observed on Figure 2.7. As seen from the figure, field distribution in the vicinity of the center conductor and the slots is not affected very much. However field distribution differs from the conventional CPW near the ground plane on the backside. As the thickness of the dielectric substrate *h* is increased this difference is reduced.

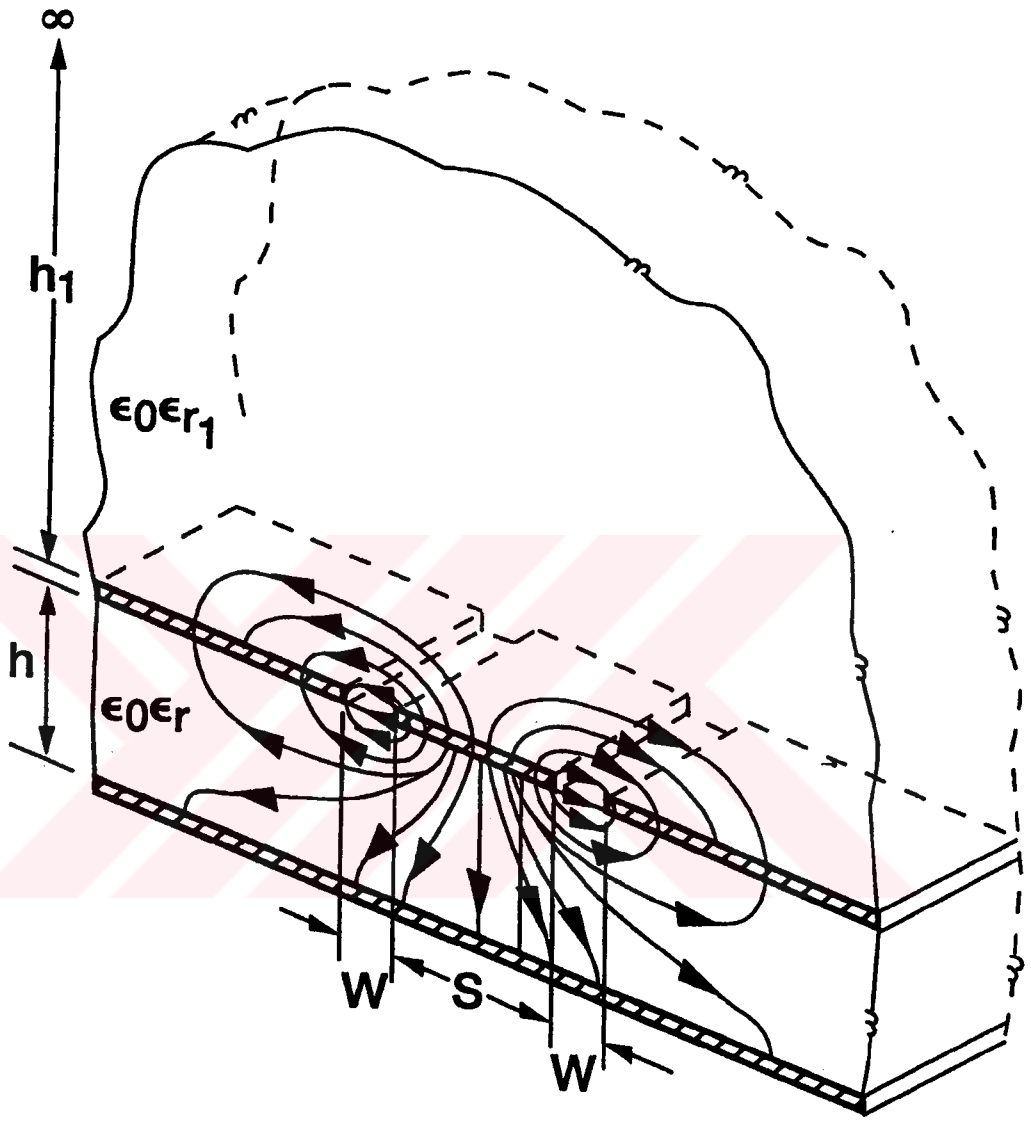

Figure 2.7: Field distribution for CBCPW. The ground plane on the backside of the CPW modifies the field distribution; however field distribution in the vicinity of the center conductor and the slots are not effected much since they are away form the extra ground plane.

The difference in the electric field distribution also affects the characteristic properties of the CPW. Effective permittivity, which is one of the determining characteristic properties of the CPW becomes [28, 30]

$$\varepsilon_{eff} = \frac{1+\varepsilon_r \dfrac{K(k')}{K(k)}\dfrac{K(k_3)}{K(k_3')}}{1+\dfrac{K(k')}{K(k)}\dfrac{K(k_3)}{K(k_3')}}. \tag{2.10}$$

This effective permittivity leads to characteristic impedance given as

$$Z_0 = \frac{60\pi}{\sqrt{\varepsilon_{eff}}} \quad \frac{1}{\dfrac{K(k)}{K(k')}+\dfrac{K(k_3)}{K(k_3')}}, \tag{2.11}$$

where $k = a/b$, $k_3 = \tanh(\pi a/2h)/\tanh(\pi b/2h)$, $k' = \sqrt{1-k^2}$, and $k_3' = \sqrt{1-k_3^2}$.

The variables ε_r, a, b, and h are the substrate permittivity and the dimensions of the CPW given in Figure 2.8, respectively.

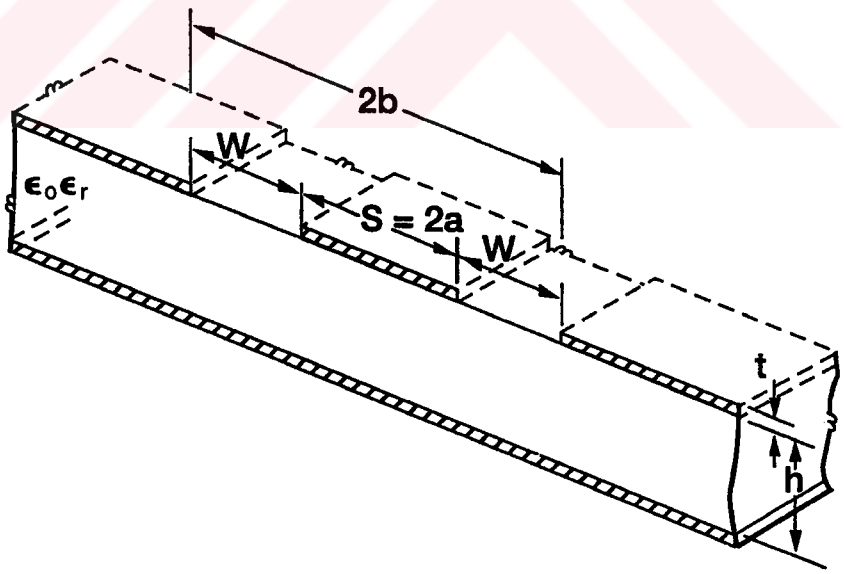

Figure 2.8: CBCPW with a substrate permittivity ε_r and dimensions a, b, and h

Although the effective permittivity of a CBCPW differs from a conventional infinite substrate CPW, it approaches to conventional CPW as the ratio of the height of the substrate to the CPW width is increased. Calculated effective permittivity values for a set of *h/b* values are given in Figure 2.9. From this figure we can see that when *h/b* ratio is greater than 1 we can approximate a CBCPW by a conventional CPW with infinitely thick dielectric substrate. This approximation simplifies the calculation of effective permittivity and the characteristic impedance to a great extent.

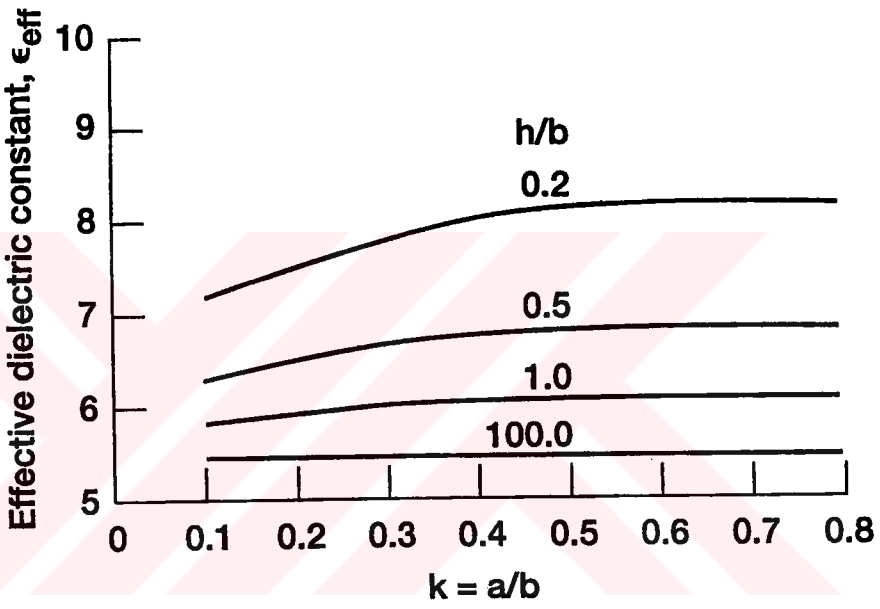

Figure 2.9: Effective permittivity of a conductor backed CPW [28]. Permittivity of the substrate ε_r is 10. As the ratio of *h/b* is increased effective permittivity approaches to that of conventional CPW with infinitely thick dielectric substrate, which is 5.5.

This simplification, which is valid for most of the cases encountered during the realization of the components explained in this thesis, is very valuable since it shortens the design cycle and makes the design procedure very practical.

2.1.3 Summary on the Theory of Coplanar Waveguides

Giving the simplifying assumption for the CBCPW completes theoretical information about the CPWs required for the design of RF MEMS structures in this thesis. The information given can be summarized as the field distributions of conventional CPW and CBCPW, characteristic properties of these CPW types, formulas for the calculation of characteristic parameters, and assumptions and simplifications in this formulation.

Field distribution is confined around the signal line and the slots of the CPW. These regions are the regions that are sensitive to disturbances, and disturbances created in these regions are used to make RF MEMS switches or phase shifters.

The information given in this section will be used in the following sections where the theoretical information on RF MEMS switches and phase shifters will be given.

2.2 Switch

In this section theory of switches will be given starting from the general theory of switches. Then application of this theory to RF MEMS switches, and modeling of RF MEMS switches will be given.

2.2.1 General Switch Theory

A switch is simply a device that controls the signal flow from the input to the output. It either permits the input signal to pass to the output or not. As seen in Figure 2.10 (a) and (b), when the switch is off it disconnects the input from the output, and when it is on it connects the input to the output. When used as a 2-port circuit element a switch can have either series or shunt configuration. Information about each type will be given in the following sections

Figure 2.10: Schematics of a simple switch. (a) The switch is off. Input and output are disconnected. (b) The switch is on. Input and output are connected.

However, before explaining each type, it would be appropriate to give some evaluation criteria that determine the RF performance of a switch. These evaluation criteria are insertion loss, isolation, and reflection coefficient.

Insertion loss is a parameter that is considered when the switch is supposed to transfer the input signal to the output. It is the amount of signal lost during the transfer of the signal. However it should be noted that it is not the actual loss of the signal, which is named as the power loss. Power loss considers the signal reflected from the two port device as a part that is outside the power loss. Therefore, this reflected signal power is subtracted from the insertion loss during the calculation of power loss, which leads to a power loss in terms of S parameters that is given as:

$$power\ loss = |S_{21}|^2 - |S_{11}|^2 . \tag{2.12}$$

Therefore, insertion loss, which includes the reflected power, can be written as:

$$insertion\ loss = |S_{21}|^2 . \tag{2.13}$$

Ideally insertion loss and power loss should be zero in order to transmit the entire signal.

Isolation is a term that is valid when the switch is supposed to block the signal transfer from input to output. It is defined as the amount of signal transferred from input to the output when the switch is open. In other words it is the insertion loss for switch off case. For an ideal switch, it should be zero since no signal leak to the output is desired. It is given as:

$$isolation = |S_{21}|^2 . \tag{2.14}$$

Reflection coefficient is defined for the case where the switch is supposed to transfer the input signal to the output. It is defined as the amount of the signal reflected from the switch due to the impedance mismatch of the switch with the feed line having a reference impedance. There should be no reflection from the switch, hence a perfect match in impedances in the ideal case.

$$reflection\ coefficient = |S_{11}|^2 . \tag{2.15}$$

The evaluation criteria given above can be related with the switch structure easily when the circuit model of the switch is known. Circuit models of series and parallel switches are presented in the following sections.

2.2.1.1 Series Switch

A series switch, which is seen in Figure 2.11, connects the input to the output to permit the signal flow, and disconnects to block signal flow. For the disconnected case, current flow from the input to output is prevented, hence the signal transmission is blocked. This is due to the open circuit created by the switch. However, open circuit is possible only for ideal switches. In real life this open circuit is a large impedance, which can be assumed as open circuit. Therefore, circuit model for a series switch, which is given in Figure 2.12, is just composed of a series impedance.

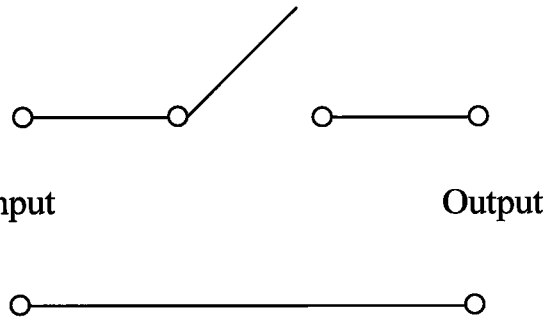

Figure 2.11: Schematic of a series switch. Switching element, which is placed on the upper line, controls the signal flow from the input port to the output port.

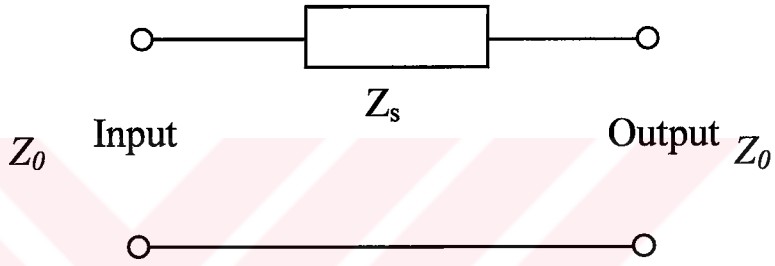

Figure 2.12: Circuit model for the series switch. Z_s is the impedance of the switch, which is altered in order to acquire switching action.

According to this circuit model it is possible to write down the two port S-parameters of a series switch as:

$$\begin{bmatrix} S_{11} & S_{12} \\ S_{21} & S_{22} \end{bmatrix} = \begin{bmatrix} \frac{Z_s}{2Z_0 + Z_s} & \frac{2Z_0}{2Z_0 + Z_s} \\ \frac{2Z_0}{2Z_0 + Z_s} & \frac{Z_s}{2Z_0 + Z_s} \end{bmatrix}, \tag{2.16}$$

where Z_0 is the impedance seen at the ports of the switch, which is the reference impedance.

Using equation (2.12) and (2.15), the performance parameters of a switch can be expressed as:

$$insertion\ loss = \left| \frac{2Z_0}{2Z_0 + Z_{s,on}} \right|^2 . \tag{2.17}$$

As can be observed from the expression, insertion loss increases with $Z_{s,on}$. Because of this keeping Z_s small, when the switch is on, is critical in terms of insertion loss.

$$isolation = \left| \frac{2Z_0}{2Z_0 + Z_{s,off}} \right|^2 . \tag{2.18}$$

As observed from the expression, isolation becomes better as $Z_{s,off}$ increases. Because of this increasing Z_s, when the switch disconnects input from output, is critical in terms of isolation.

$$reflection\ coefficient = \left| \frac{Z_s}{2Z_0 + Z_{s,on}} \right|^2 . \tag{2.19}$$

In order to minimize the amount of reflection, $Z_{s,on}$ should be kept small when the switch is supposed to connect input to the output.

According to the information given above, it is proper to say that Z_s should be small when the switch is on in order to improve the insertion loss and reflection coefficient. It should be large when the switch is off to have a good isolation.

2.2.1.2 Parallel Switch

A parallel switch, seen in Figure 2.13, connects the input to ground to prevent the signal flow to the output, and disconnects the input and ground to permit signal flow. When the input is connected to ground plane, a short circuit is created, which prevents the voltage transfer from the input port to the output port.

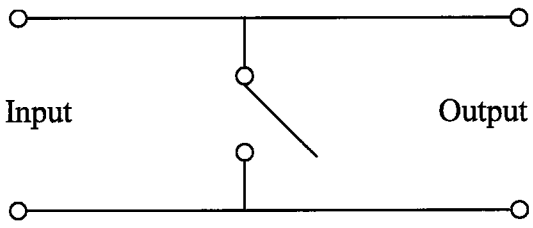

Figure 2.13: Schematic of a parallel switch. Switching element, which is placed between the top line and bottom line, controls the signal flow from the input port to the output port.

A parallel switch, which is the parallel-connected version of a switching element, can be modeled as a parallel impedance as shown in Figure 2.14.

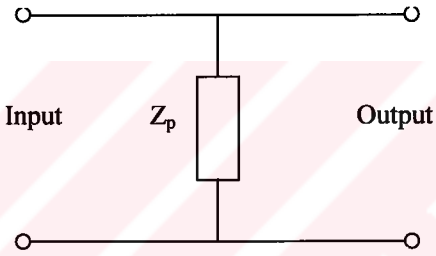

Figure 2.14: Circuit model for parallel switch. Z_p is the impedance of the switch.

According to this circuit model S-parameters can be written as:

$$\begin{bmatrix} S_{11} & S_{12} \\ S_{21} & S_{22} \end{bmatrix} = \begin{bmatrix} \dfrac{Z_0^2/Z_p}{2Z_0 + Z_0^2/Z_p} & \dfrac{Z_0}{2Z_0 + Z_0^2/Z_p} \\ \dfrac{Z_0}{2Z_0 + Z_0^2/Z_p} & \dfrac{Z_0^2/Z_p}{2Z_0 + Z_0^2/Z_p} \end{bmatrix}. \tag{2.20}$$

Then the evaluation criteria can be given as:

$$insertion\ loss = \left| \frac{Z_0}{2Z_0 + Z_0^2/Z_{p,off}} \right|^2, \tag{2.21}$$

$$isolation = \left| \frac{Z_0}{2Z_0 + Z_0^2 / Z_{p,on}} \right|^2, \tag{2.22}$$

$$reflection\ coefficient = \left| \frac{Z_0^2 / Z_{p,off}}{2Z_0 + Z_0^2 / Z_{p,off}} \right|^2. \tag{2.23}$$

One can see from the above equations that $Z_{p,on}$ should be small when the switch is on, hence signal flow from the input to the output is prevented. In this case decreasing $Z_{p,on}$ improves isolation, which is a desired effect. However, for the other case, where the switch is off and signal is to be transmitted from input to output, $Z_{p,off}$ should be large. Because increasing $Z_{p,off}$ would improve the insertion loss and reflection coefficient for this case.

2.2.2 RF MEMS Switches

Different types of switches can realize the impedances stated in the general switch theory section. Some of these switches are PIN diode, FET, and MEMS switches. PIN diode and FET switches have detailed impedance models given in many microwave books [34]. Therefore, they will not be explained in here. However, modeling of RF MEMS switches will be given since the switches implemented in this thesis are of this type. RF MEMS switches are classified in two groups, which are series switches and shunt switches. They are also separated among themselves as capacitive and resistive contact type switches. These types are explained in the following sections.

2.2.2.1 Series RF MEMS Switch Model

A general series RF MEMS switch has a beam, which is connected to input as shown in Figure 2.15. This beam is disconnected from the output, but it forms a parallel plate capacitance with the CPW signal line that is connected to the output. When the switch is off, it is suspended in the air, which introduces an air gap

between the beam and the signal line. When it is on, beam is pulled down on the signal line by an electrostatic force due to the voltage applied between two actuation pads. In this case there is no air gap between the beam and the signal line. When the switch is on, there are two alternatives. In the first alternative, beam directly touches to the signal line, and actuation voltage is applied from an actuation pad different from the signal line to prevent DC short. This type of switch is called resistive contact switch. In the second alternative, beam does not directly touch to the signal line, but it touches a dielectric layer that covers the signal line. This type of switch is called capacitive contact switch. It does not require a separate actuation pad since the dielectric layer prevents DC short in the on state.

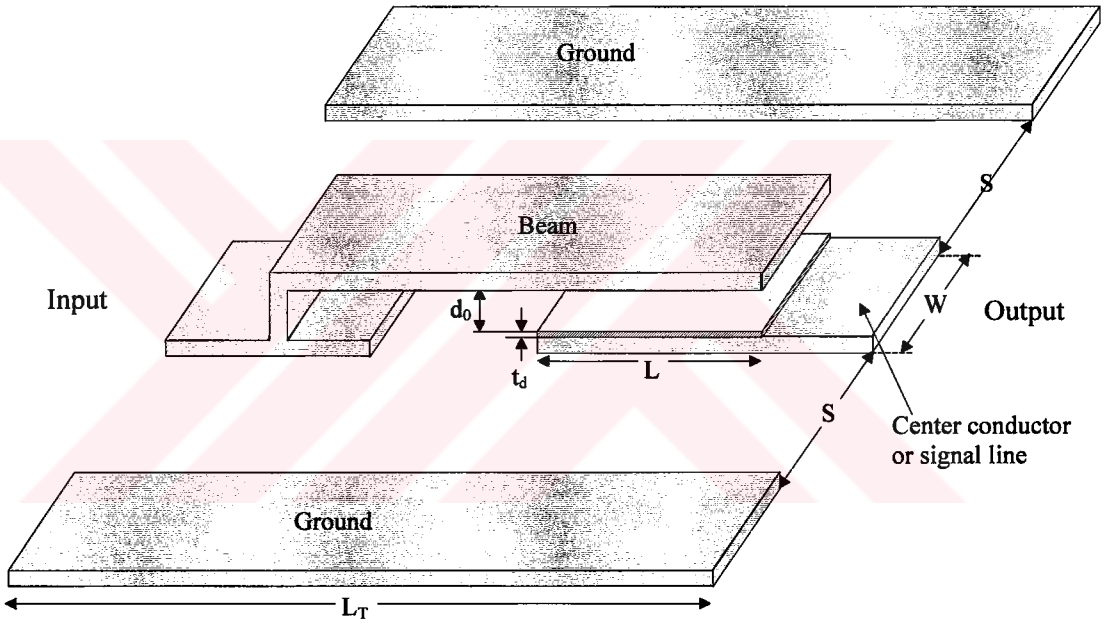

Figure 2.15: Three-dimensional model of series switch.

Whether capacitive contact or resistive contact, switches are modeled as combination of capacitances inductances, and resistances. The models do not contain controlled current sources or voltage sources since the devices are not active or semiconductor based. The number of components in the model of a switch

increases as more accurate models are desired. Such an accurate model, which takes into account most of the parasitic effects coming from substrate and packages, is presented in [35]. However, a simpler model, which is suitable for most design applications, is an RLC circuit [8, 22] given in Figure 2.16.

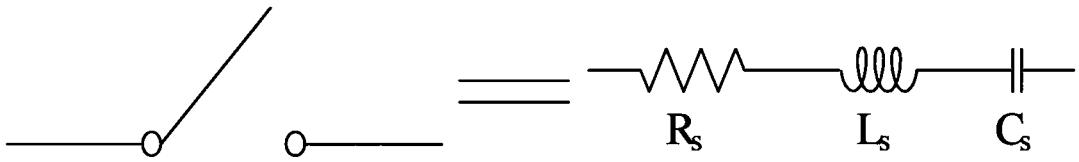

Figure 2.16: Circuit model for an RF MEMS switch.

According to this model switch impedance can be written as [8]:

$$Z_s = R_s + j\omega L_s + \frac{1}{j\omega C_s}. \tag{2.24}$$

R_s, L_s, and C_s attain different values according to the type and state of the switch. For capacitive switches R_s simply represents the resistive losses in the switch due to finite conductivity of the signal line and the beam. Since these structures are generally short in length they have very small resistances, which are generally less than 1-2 Ω [12, 21, 36]. Therefore, they are generally neglected in most of the calculations leading to a series LC circuit as the switch model. In this model L_s is a small inductance, which is generally extracted from the frequency response of the switches for both on and off state. It has different values for on and off states, however the difference between the values for different states is not so significant. Therefore, L_s can be assumed to have a value which is the average of the on and off state values for practical calculations. However for C_s it is not possible to make such an approximation, since C_s changes significantly from off state to on state. It is the capacitance between the beam and the signal line given in Figure 2.17. When the switch is off, there is an air gap between the beam and the signal line. This air gap reduces the value of C_s to a great extent, which increases the value of Z_s significantly

as seen in equation 2.24. This leads to a better isolation according to equation 2.18. Value of C_s can be approximated by a parallel plate capacitance between beam and signal line as:

$$C_s = \frac{\varepsilon_0 LW}{d_0 + \frac{t_d}{\varepsilon_r}}, \tag{2.25}$$

where L, W, d_0, and t_d are the dimensions, and ε_r is the relative permittivity of the isolation dielectric of the switch shown in Figure 2.15.

However, this approximation may not be valid since the effects of the fringing fields due to large air gap between beam and signal line can introduce a significant capacitance that may not be negligible [8]. This fringe field capacitance may be neglected when the switch is on [8]. Because when the switch is on, beam sticks on the dielectric that covers the signal line as seen in Figure 2.17, hence there is no air gap, and total distance between beam and signal line is reduced significantly. This leads to small fringe fields hence small fringe capacitances. Also value of parallel plate capacitance is increased significantly since the distance between the beam and signal line is reduced. This large on state capacitance helps to reduce $Z_{s,on}$, hence it improves insertion loss and reflection coefficient.

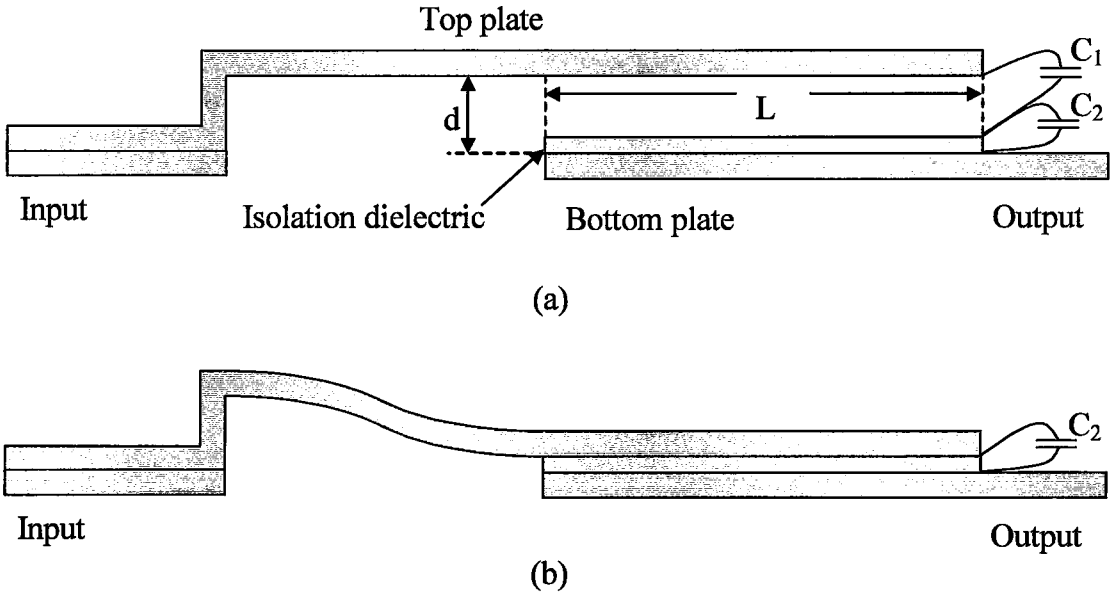

Figure 2.17: Cross-section of a capacitive RF MEMS switch. (a) Off state where total capacitance is equal to the series connection of C_1 and C_2. (b) On state where the total capacitance is just C_2.

In order to further reduce $Z_{s,on}$, resistive contact switches are used. These switches do not have an isolation dielectric on the signal line as seen in Figure 2.18. Hence, there is a short circuit between beam and signal line. This eliminates the effect of on state capacitance. In fact, on state model is just an RL circuit. In this model, value of R_s becomes important since it introduces an impedance component, which is constant with frequency. It acts as an offset in the impedance vs. frequency characteristic of the on state switch. It is higher than the standard R_s, which is the resistance of the beam and the signal line, because the value of contact resistance is added to these two resistance components. Contact resistance is the resistance due to the contact surface between the beam and the signal line. Value of this resistance may significantly change due to the roughness of the surface of the signal line and the beam, because this roughness determines the amount of surface that a successful contact is achieved. Therefore, there is not a standard value or range for this

resistance. However it is possible to say that it introduces an effect, which is larger than the signal line and beam resistance. Hence, implementation of a smooth surface is very important for the resistive switch contact resistance, since it reduces $Z_{s,on}$ significantly. However even a rough surface results in lower $Z_{s,on}$ for resistive switches compared to capacitive switches since the effect of capacitance, which introduces an additional impedance component is eliminated in the resistive contact switches. This is the most important difference between the capacitive and resistive switch.

Their behavior is almost the same for the off state. Only difference is the higher $C_{s,off}$ values of resistive switch. This increase is due to the lack of the series capacitance introduced by the isolation layer of the capacitive switch, which is seen in Figure 2.17.

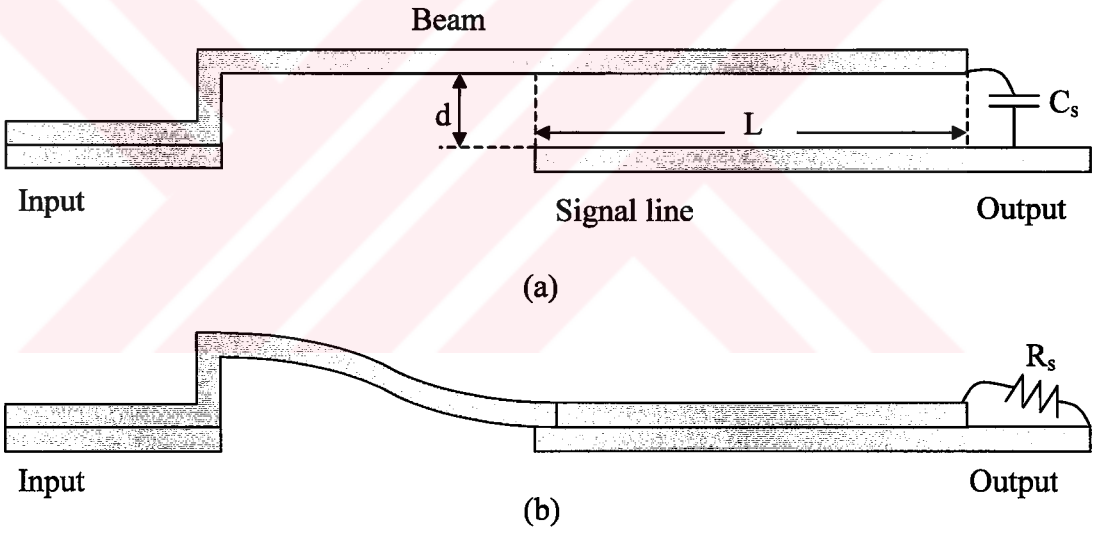

Figure 2.18: Cross-section of a series resistive switch. (a) Off state where the beam does not touch the signal line. (b) On state where the beam is connected to the signal line.

2.2.2.2 Shunt RF MEMS Switch Model

Shunt RF MEMS switch, which is given in Figure 2.19, is composed of a bridge placed over the signal line with two posts on the ground lines. When this bridge is up, meaning there is an air gap between the bridge and the signal line, switch is in the off state. As explained in Section 2.2.1.2, off state shunt switches permit signal flow from the input to the output. Therefore, when the bridge is up, signal flow is permitted. When the bridge is down meaning it sticks on the signal line, switch is on hence signal flow is prevented. Z_p attains different values for these two states in order to insure proper operation. The structure and the dimensions of the switch determine values of Z_p for the on and off states.

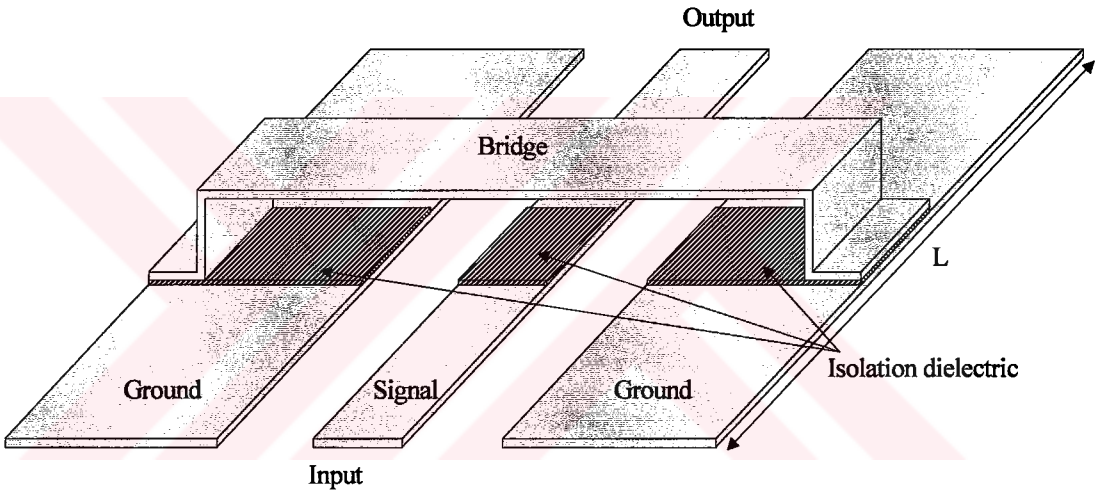

Figure 2.19: Three-dimensional model of the parallel capacitive bridge type switch is given. In order to actuate the bridge, a DC voltage, namely actuation voltage is applied between the bridge and the ground planes. Dielectric layers prevent DC short but do not prevent RF short.

The switch structure can be modeled as an RLC circuit similar to the series switch case. However, this model is not enough for the design of parallel switches, because this model only considers the effect of the bridge. A more appropriate

model would be the one given in Figure 2.20. This model considers the transmission lines at the ends of the bridges as a part of the switch, and includes them in the model. Including the transmission lines on both ends to the model enables an appropriate design for the off state. When the switch is off, it has a shunt impedance which loads the CPW. This loading effect changes the impedance seen from the ports of the switch depending on the length and characteristic impedance of the CPW. In order to minimize reflection coefficient, this loading effect must be compensated with the characteristic impedance of the CPW to match the reference impedance. For this reason, the compensation for the switch impedance must be calculated by including the CPWs in the model.

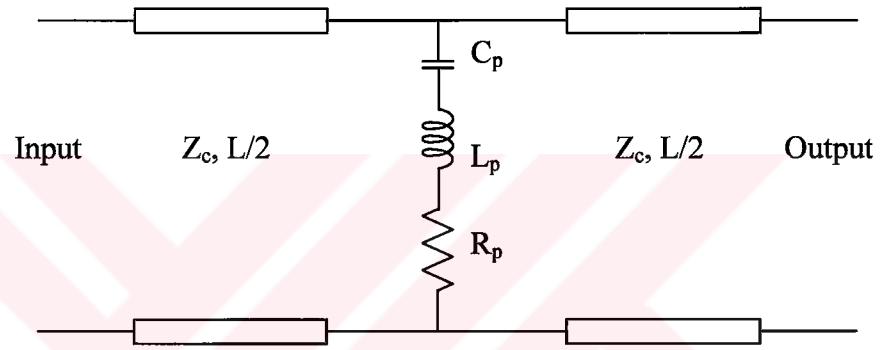

Figure 2.20: Circuit model of the shunt RF MEMS switch.

According to this model RLC resonator can be taken as the shunt switch, and the transmission lines can be taken as the matching components that match off state switch impedance Z_p to the reference impedance. Then it is possible to state that Z_p is composed of R_p, L_p, and C_p, values of which are determined by the switch structure and dimensions.

When the switch is off, R_p has a very small value for both capacitive and resistive switches. It is only composed of the resistance introduced by the bridge itself. For most cases this resistance is less than 0.5-1 Ω, which makes it negligible for most of the calculations [4, 8, 37]. When it is neglected, remaining model of Z_p is

an LC resonance circuit. The resonance frequency of this circuit should be out of the region of operation, because at this resonance frequency Z_p reduces to R_p, which is a very small value. Hence, it heavily loads the CPW and prevents signal flow from input to output where the switch was supposed to transmit signal from the input to the output. In order to prevent such a situation $L_{p,off}$ and $C_{p,off}$ should be kept as small as possible to increase the resonance frequency. When the resonance frequency is above the frequency of operation Z_p can be assumed to be composed of only C_p [8]. Since typical resonance frequencies of the switches are above 300 GHz [8], it is possible to say that Z_p is taken as a capacitance for the off state. However for the on state, it is not possible to say the same thing. First of all capacitive and resistive switches have different Z_p models for the on state.

Resistive switches do not have a capacitance in the on state model since the bridge directly contacts with the signal line. Therefore, resistive switch $Z_{p,on}$ is composed of $L_{p,on}$ and $R_{p,on}$. $R_{p,on}$ is different from the $R_{p,off}$ since it has a contact resistance which is added to $R_{p,off}$. This contact resistance changes according to the roughness of the contact surfaces. Hence, it cannot be determined exactly. However it is generally large compared to $R_{p,off}$.

Capacitive switches have $R_{p,on}$, $L_{p,on}$, and $C_{p,on}$ in the model, where $R_{p,on}$ and $L_{p,on}$ are same as $R_{p,off}$ and $L_{p,off}$. However $C_{p,on}$ is significantly higher than $C_{p,off}$ since the bridge directly touches to the isolation layer on the signal line. This significant increase in the capacitance decreases the resonance frequency very much. In fact, typical resonance frequencies are around a few tens of GHz. Therefore, effect of resonance can be observed in the operation. As the operation frequency approaches resonance frequency Z_p reduces to the value of R_p hence isolation of the switch increases. A design that uses this phenomenon can improve its isolation 10-20 dB at resonance depending on the design dimensions [7, 9].

2.3 Phase Shifter

Phase shifter is a device whose insertion phase can be altered in order to change the phase of an input signal in a controllable manner. However, before going to the details of this definition and phase shifters, it is appropriate to state the definitions of phase, insertion phase of a device, and phase shift.

First of all, phase is a parameter defined for periodic signals in frequency domain. It is the information indicating where a point stands on the time axis according to a reference time origin. So it is simply the time difference between that point and the origin. If phases of two signals are different from each other, this means one of the signals is delayed in time compared to the other signal. This time difference between two signals is named as phase difference between these two signals.

Phase difference between the input and output signals of a two-port device is named as the insertion phase of the device. It is proportional to the time delay introduced by this device. In fact, insertion phase of a device is the remainder of the division of the time delay with the period of the signal. If insertion phase of a device can be controlled to attain two different values, then the difference between them is the phase shift created by this device. If expressed in time domain, it is the difference between two time delays created by this device.

All circuit elements have an insertion phase since they have some physical length that the signal has to travel in some time. However, their insertion phase may not be controlled. A device whose insertion phase can be controlled can be used as a phase shifter. If the phase of the output signal for a specific state is taken as zero, then the phase of the output signal for other states directly gives the phase shift of the phase shifter.

Phase shift of a phase shifter can be either constant with frequency meaning it is dispersive or linearly increasing with frequency meaning nondispersive [38, 39].

Dispersive phase shifters are also named as constant phase phase shifters since they introduce constant phase shift with frequency. Nondispersive phase shifters are named as constant time delay phase shifters, because when divided with the signal period, constant time delay introduces increasing phase with increasing frequency. In fact, this relation between time delay and phase, makes dispersive phase shifters, which give constant phase shift for all frequency range, theoretically impossible. Because when we pass to negative frequencies the time delay associated with the phase shift becomes a time advance, which leads to non-causal systems. Since non-causal systems are not physically realizable it is not possible to make constant phase phase shifters that operate in all the frequency range. However, it is still possible to make dispersive phase shifter for a specified band of operation.

Both dispersive and nondispersive phase shifters have various types such as ferrite phase shifters, switched line phase shifters, reflection type phase shifters, and loaded line phase shifters. Among these types, switched line phase shifters, reflection type phase shifters, and loaded line phase shifters can be constructed using RF MEMS components [16-20]. These phase shifters commonly use transmission lines as the phase shifting element. A transmission line has an insertion phase given by the following expression:

$$\theta = \frac{2\pi}{\lambda} \times v_{ph} \times d \,, \tag{2.26}$$

where θ is the amount of insertion phase or electrical length, v_{ph} is the phase velocity, and d is the physical length of the transmission line. According to the above expression, only changing its physical length or phase velocity can change insertion phase of a transmission line. Phase shifters stated above either change the phase velocity or the physical length of a transmission line in order to obtain a controlled phase shift. Reflection type phase shifters and switched line phase shifters that change the physical length of the transmission line, whereas a loaded line phase shifter changes the phase velocity of a transmission line. Their operation and theory will be given in the following sections.

2.3.1 Phase Shifters That Change Physical Length

This type of phase shifters simply changes the length of the transmission line. However, they do not add a section of line at the end of the transmission line or cut a part of it. Instead, they route the input signal through lines of different lengths. Routing occurs in two different ways. In the first method, switches are used to change the signal path to a different line. This type of phase shifters are called switched line phase shifters since they switch the normal path with a different length one [38, 39]. Second method is to use a directional device that separates the incident and reflected signal, and the reflection phenomenon in order to create different length lines [38, 39].

2.3.1.1 Switched Line Phase Shifters

Switched line phase shifters change the path of the signal in order to change the length of the transmission line. General model for this type of phase shifters is given in Figure 2.21. According to this model, phase shift for any path chosen can be given as:

$$\theta_i = (2\pi/\lambda) \times v_{ph} \times (l_i - l_1). \tag{2.27}$$

Since there is a step difference between the line lengths, this type of phase shifters can only give phase shifts in discrete steps.

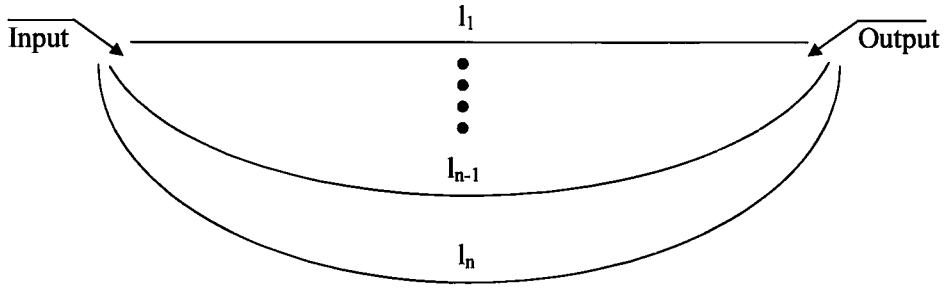

Figure 2.21: General model for the switched line phase shifters. Different length lines are chosen by two synchronously working switches.

2.3.1.2 Reflection Type Phase Shifters

Reflection type phase shifters use reflection and directional devices such as circulators or 90° hybrids. Models for this type of phase shifters are given in Figure 2.22.

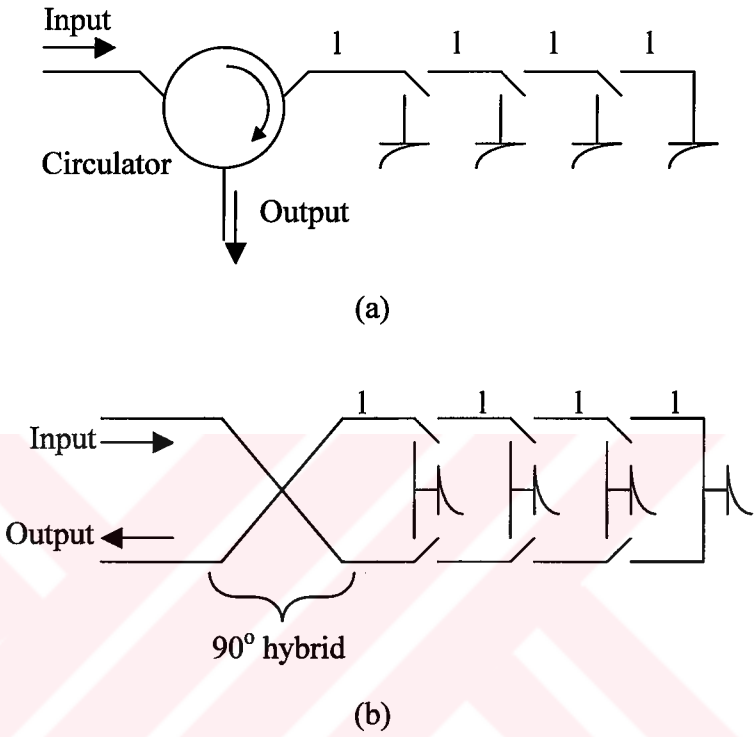

Figure 2.22: Circuit models for reflection type phase shifters.

According to the models given in Figure 2.22 operation principle is as follows: Input signal is transferred to a different port than the output. This port is connected to a transmission line on which some switches are placed. These switches are either connected to ground or to the following transmission line. When they are connected to ground, full reflection occurs at that point. If they are connected to the following line, full reflection occurs at a different line length. Then the fully reflected signal is directed to the output port by the directional device. Signal at the output travels a different length for different switch configurations. When the length

difference between two switch configurations is l, the length difference for the signal is $2xl$, since the signal travels twice, once forward and once backward on the length l. This introduces an efficient use of the available area by using the same line length twice, which makes reflection type phase shifters advantageous in terms of area economy.

2.3.2 Phase Shifters That Change Phase Velocity

Phase shifters that change phase velocity just modify the characteristic property of a transmission line, which is given by

$$v_{ph} = \frac{1}{\sqrt{LC}}, \tag{2.28}$$

where L and C are the per unit length inductance and capacitance of a transmission line. They are generally related with the geometry of the line and the dielectric materials used in the line. In order to change these characteristic properties, the transmission line can be loaded with reactive loads [38, 39]. These loads can be inductances or capacitances or both of them. When they are placed periodically over a transmission line they would change per unit length capacitance or inductance of a transmission line. For a load distribution given in Figure 2.23 per unit length capacitance would become

$$C_{new} = \frac{l \times C_{old} + 3 \times C}{l}, \tag{2.29}$$

where C_{old} is the original per unit length capacitance of the line, C is the loading capacitance, l is the total length of line, and C_{new} is the resulting per unit length capacitance of the line.

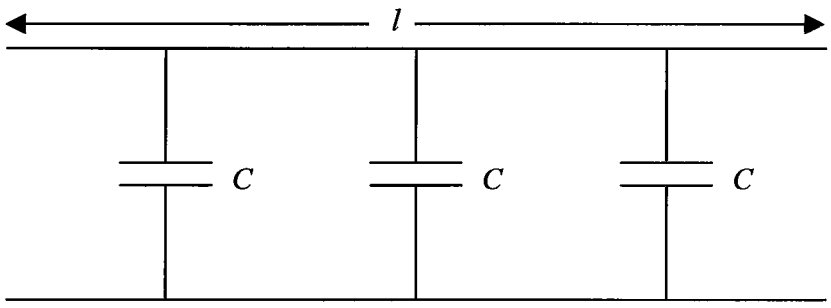

Figure 2.23: Circuit model for a capacitively loaded transmission line. Line length is *l*, and it is loaded with three identical capacitances, which are periodically spaced.

Above equation can be generalized for a periodically loaded line as [16, 38, 39]:

$$C_{total} = \frac{s \times C + C_L}{s}, \tag{2.30}$$

where s is the periodic spacing between two adjacent capacitance, C_L is the value of each loading capacitance, C is the per unit length capacitance of the transmission line, and C_{total} is the per unit length capacitance of the loaded line.

Using equations 2.27 and 2.29 phase dependence on loading capacitance is given as [16, 38, 39]:

$$v_{ph} = \frac{1}{\sqrt{L\frac{s \times C + C_L}{s}}}. \tag{2.31}$$

Hence, when loading capacitance is varied it is possible to obtain phase shift. Loaded line phase shifters use this approach to change their insertion phase. They either add discrete amounts of capacitances from a capacitor bank or they change the value of load capacitance continuously, which is the case for RF MEMS phase shifters [16, 22].

The load capacitances in the RF MEMS phase shifters are formed by capacitive switches that are shunt connected to the line. Such a phase shifter configuration is given in Figure 2.24. These periodic bridges behave as capacitances whose value can be adjusted by a control voltage. Since these bridges are placed periodically over the line, they cause a phenomenon known as Bragg reflection, which limits the upper frequency of operation [16] that occurs at

$$f_{Bragg} = \frac{1}{\pi s \sqrt{L(C + C_L/s)}}. \tag{2.32}$$

For a good design, Bragg frequency should be much higher than the frequency of operation.

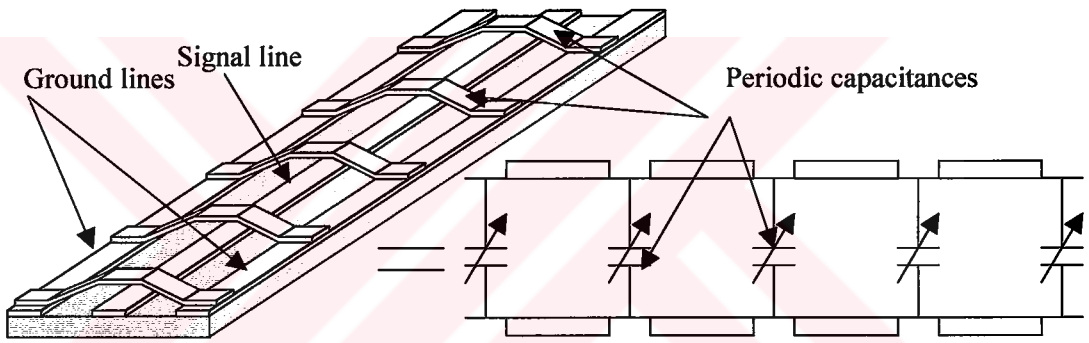

Figure 2.24: Three-dimensional view of a loaded line MEMS phase shifter, and the corresponding approximate circuit model.

2.4 Mechanical Theory

Mechanical theory forms the other side of the design for the RF MEMS structures. Mechanical behavior of designs is important for all MEMS devices, since MEMS means a moving mechanical structure. Knowing the basic rules of these structures is mostly helpful and sometimes critical for estimating the device performance. Therefore, mechanical theory will be explained briefly in this section.

Firstly, most of the RF MEMS structures use the switches as the mechanically active or moving part. Therefore, mechanical properties of switches become important. Most of the switches used in the designs can be classified as beam type mechanical structures. An example for such a beam structure is given in Figure 2.25.

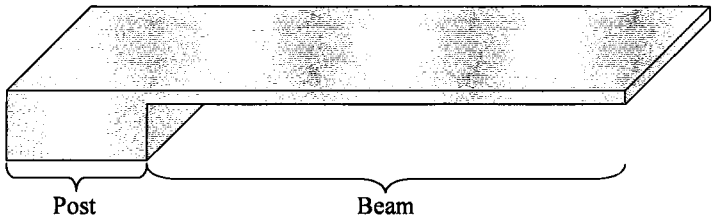

Figure 2.25: Three-dimensional view of a beam with a single post. Post side of the beam is rigid since it is directly connected to the substrate by the post, however other side can be bended by an applied force.

Beam structures are generally formed of a mechanical post and a beam supported by this post. Generally, a force is applied to a point or some points on the beam to bend it. The response of the beam to an applied force is given by the following differential equation [40].

$$M\ddot{z} + D\dot{z} + Kz = F\,, \tag{2.33}$$

where M is the mass of the beam, D is the damping coefficient of the beam, and K is the spring constant of the beam. Dot denotes derivation with respect to time, and F is the applied force, and z is the direction of motion. This equation, also named as the differential equation of motion of a single-degree-of-freedom system, assumes that the beam can move only in the z direction. First and second terms of the equation give information about how fast the beam moves in response to an applied force. Third term determines the equilibrium distance supplied by the pull back spring force of the beam. The coefficient of the second order derivative of displacement is the mass of the beam, which implies that the beam can move faster if

the mass of the beam is reduced. The coefficient of the first order derivative of displacement is the viscosity of the beam. If the medium were vacuum, in other words if there were no gas, air or any material in the medium, then there would be no damping, making the beam faster. Spring coefficient is mainly determined by the stiffness of the cantilever. It is affected by the stiffness of the material used in the design and the thickness of the beam. As the beam becomes stiffer, it becomes harder to move.

The force applied to the beam can have many sources but in our case this force is an electrostatic force. This force is applied on the beam by accumulating charged particles on the two plates as shown in Figure 2.26. Charge accumulation on these plates is achieved by creating a potential difference between two plates hence charging them as a capacitor.

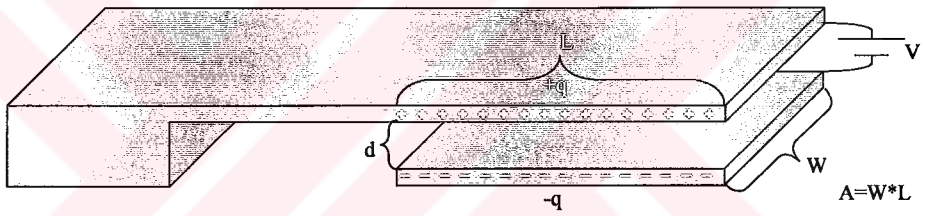

Figure 2.26: Three-dimensional view of an actuated beam. Actuation pad and the section of beam over the actuation pad are forming a parallel plate capacitor.

According to this capacitive plates approach, electrostatic force due to the acquired charge can be given as [40]:

$$F = \frac{1}{4\pi\varepsilon}\frac{q^2}{d^2}, \tag{2.34}$$

where q is the accumulated charge due to an applied potential, and d is the spacing between plates. This equation can be written as a function of the applied voltage as:

$$F = \frac{\varepsilon A}{2d^2}V^2. \tag{2.35}$$

When this equation is substituted in equation 2.32 it is possible to find the z point where the spring force becomes equal to electrostatic force. This point is the critical point of pull down where the maximum value of electrostatic force without pull down is reached. When electrostatic force is increased system becomes unstable, and beam collapses on the actuation pad. Point of pull down, which can be derived using equation 2.32 and 2.34, is $2d_0/3$ for a general beam structure [3, 16, 42], which leads to a pull down voltage equation that is stated below [3, 16, 42].

$$V_p = \sqrt{\frac{8k}{27\varepsilon A} d_0^3}\,, \tag{2.36}$$

where d_0 is the initial height of the beam. When this voltage is reached, beam is no longer stable and collapses on the actuation pad. This can be observed in Figure 2.27, where the unstable point is the sharp edge in the graph. As can be understood from Figure 2.27 only a portion of the total gap height can be manipulated in a controlled manner. In this controllable region gap height changes almost linearly with voltage, and there is no hysteresis. However below the pull down region there is hysteresis. In other words after the pull down voltage is applied and pull down had occurred, beam is not pulled back although the voltage is reduced below the pull down voltage. The reason for this hysteresis is that electrostatic force is inversely proportional to the square of the distance. Although the voltage is kept constant, force increases drastically when the gap height decreases due to pull down. Therefore, voltage must be reduced to reduce the electrostatic force below pull down force.

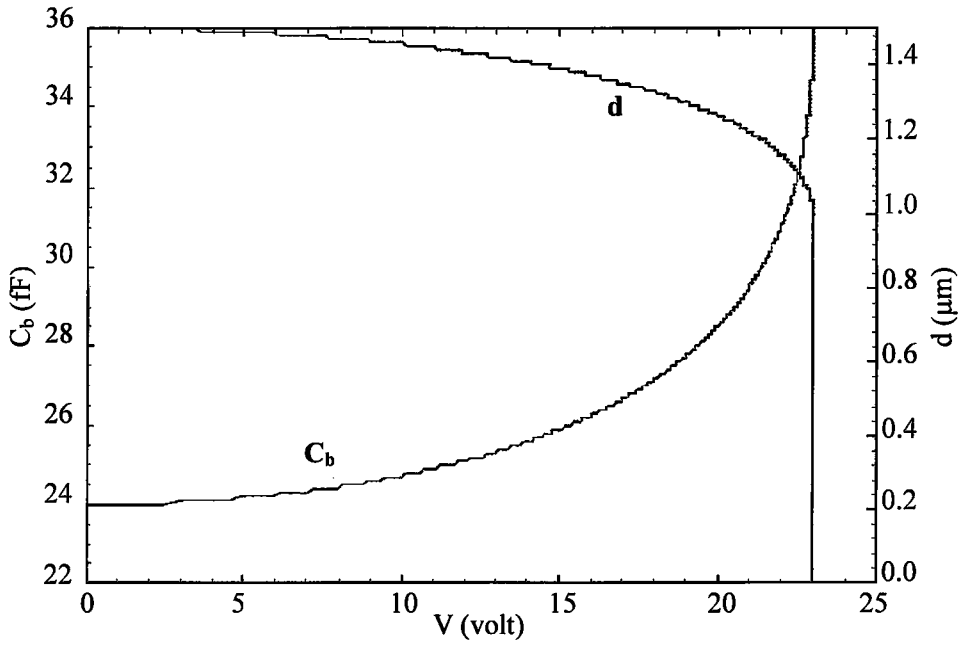

Figure 2.27: Gap height versus actuation voltage graphics for a sample beam. Also capacitance of the beam is given as C_b.

2.5 Summary

This chapter gives the theoretical background on the RF MEMS components developed in this study. First brief information on CPWs, which includes field distributions and characteristic properties, is given in Section 2.1. Then switches are explained in Section 2.2, where operation principles of a general switch are given, and this operation is applied to RF MEMS switches through their models. Then theory of phase shifters, including the models for RF MEMS phase shifters, is explained in Section 2.3. Finally mechanical theory, which explains the mechanical behavior of the devices, is given in Section 2.4.

Next chapter explains the design cycle of the RF MEMS components developed in the scope of this study using the theoretical information given throughout this chapter.

CHAPTER 3

DESIGN OF RF MEMS SWITCHES AND PHASE SHIFTERS

This chapter explains the design of RF MEMS switches and phase shifters. In Section 3.1 the design of RF MEMS switches will be explained. Section 3.2 will explain the design of RF MEMS phase shifters that employ these switches.

3.1 RF MEMS Switch

In this section design methodology of RF MEMS switches will be explained in detail. As the first item, general design criteria for evaluating the performance of a switch will be given in Section 3.1.1 before going through the specific structures. Then series switch design will be explained in Section 3.1.2, and parallel switch design will be given in Section 3.1.3.

3.1.1 Design Criteria

Before designing a switch the designer should know about the parameters of a switch, which determine its performance. Therefore, this section is dedicated to listing the design criteria of a switch in general. While explaining design criteria, their dependence on switch structure and parameters are also given.

Design criteria for a switch can be listed as:

- *Insertion loss*: The amount of signal lost when the switch is inserted in the signal path when it is on. Insertion loss should ideally be zero. However in real life it has a finite value due to the loss created by nonideal factors. One of these factors is the finite conductivity of the conductors used in the switch structure. This loss cannot be eliminated totally but can be reduced by increasing the conductivity of the conductors used in the switch structure. The other factor is the non-ideal switch impedance which is created by finite or nonzero impedance values which are desired to be infinite or zero for the ideal case. This impedance generally causes reflection from the switch due to impedance mismatch hence the reflected signal is lost and added to the insertion loss. This impedance is determined by the type and structure of the switch. It will be explained for each switch structure in the following sections.

- *Isolation*: The amount of signal transmitted to the output when the switch is off. It can also be considered as the signal that is not reflected from the switch, since RF MEMS switches reflect most of the signal when the switch is off. Therefore, in order to improve isolation, a designer should increase the amount of reflection from the switch. Since reflection is due to the impedance mismatch between the switch and the reference impedance, switch impedance should be either increased to ideally infinity or decreased to ideally zero. Since these values cannot be achieved for real life designs, there is a finite isolation in the switches. The switch type and the structure of the switch generally determine this finite isolation. In the following sections, dependence of isolation on switch structures will be explained in detail.

- *Reflection coefficient*: The amount of signal reflected back to the input when the switch is on. As explained in the insertion loss definition, the finite or nonzero impedance of the switch in the on state causes impedance mismatch, which leads to a reflection back to the input port.

- *Bandwidth*: The bandwidth of a signal, which can be transmitted without distortion. Distortion has mainly two reasons. First reason is the dispersion created by the transmission line, which is not a property of the switch itself, but observed in all systems that employ strip type lines. This is explained in Section 2.1.1.1, which explains the theory of coplanar waveguides. Second reason is the frequency dependent characteristics of the on state switch impedance. Since the switch impedance changes with frequency, it affects insertion loss, which causes different attenuation values for different frequency components of the signal, hence distorting the waveform of the signal.

- *Band of operation*: The frequency range that a switch can operate within the specifications of other performance criteria. As explained in bandwidth definition, switch impedance for on and off state changes with frequency leading to changes in insertion loss, isolation, and reflection coefficient values with frequency. For this reason there is a finite frequency band over which the switch can operate for specified insertion loss, isolation, and reflection coefficient values. This frequency band is named as the band of operation. It changes according to the type of switch and the specifications for performance criteria.

- *Response time*: The time required for the switch to change its state from on to off and off to on. This state change is generally related to the deflection of the beam that makes the switching action. This beam is pulled down by electrostatic force, and pulled up by the spring force of the beam as explained in Section 2.4. The time required for the beam to be pulled down or up is generally related with the structural parameters such as mass, damping coefficient, and spring constant of the beam.

- *Lifetime*: Number of times that a switch can perform switching operation while meeting the required performance criteria or without failure of

switching. Generally failure of switching or loss of performance is caused by the wear or crack growth in the materials constructing the switch.

- *Power handling capacity*: The amount of power that can be switched without destructing the switch or distorting the signal. This parameter is generally important for the on state of switches, since all of the signal is passing over the switching element in this case. This signal can cause excessive heating, which can damage the device, or residual charge on the dielectrics used causing degradation of the device performance.

In order to design a good switch, these performance criteria should be improved by optimization of the switch structure. However, it is not usually possible to improve all of the parameters due to the trade offs among some of these performance criteria. For this reason, design specifications for each parameter must be defined. These design specifications are generally determined by the application that a switch will be used. For some applications fast switching is required, and for some other good RF performance is required.

The switches designed in the scope of this thesis were not designed for a specific application. Therefore, they do not have strict specifications on design criteria. The primary motivation in the design was to demonstrate the functionality of RF MEMS switches. Hence, initial designs were aimed to have moderate performance values. Then, they were improved to have better RF performance rather than better mechanical performance. The switches designed according to this scheme are presented in the following sections.

3.1.2 Series Switch

Series switches have switching elements which are connected in series between the input and output port as explained in Sub-Section 2.2.1.1. They have two types. First one is the resistive contact switch, and the second one is the capacitive contact switch. The series switches designed in the scope of this thesis are

all capacitive contact type. There are two capacitive contact series switches. First one is a single-pole single-throw (SPST) switch, and the second one is a single-pole double-throw (SPDT) switch. They are explained in 3.1.2.1 and 3.1.2.2 respectively.

3.1.2.1 Single-Pole Single-Throw Series Capacitive Switch

The three dimensional view of the single-pole single-throw capacitive switch is shown in Figure 3.1. As seen from the figure, the switch is constructed on a CPW. It is formed of a cantilever beam, which is placed inline over the center conductor of the CPW. Post of the cantilever is placed on the center conductor of the CPW closer to the input port. Post is directly connected to the center conductor. Beam is laid over the center conductor of the CPW closer to the output port. Beam and the center conductor of the CPW form a parallel plate capacitance, value of which is changed by the height of the beam.

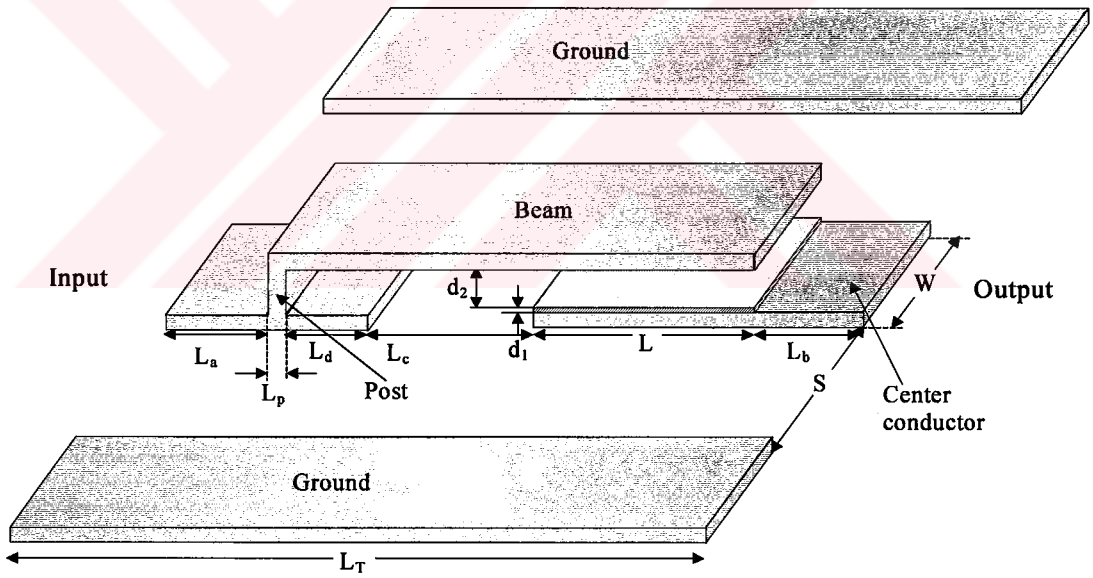

Figure 3.1: Three-dimensional view of a series capacitive contact switch. It is composed of a cantilever beam, which is connected in series with the signal line of a CPW. It acts as a series capacitance between input and output value of which is changed by the electrostatic force between the beam and the center line due to the voltage applied between them.

Operation of this structure can be divided into two parts. The first part is the mechanical operation, and the second part is the RF operation. These two parts will be explained separately.

First part, which is the mechanical operation, is governed by equation 2.32 stated in Section 2.4. According to this equation, an amount of force would displace the beam by an amount determined by the spring constant of the beam, in a time determined by the damping coefficient and the mass of the beam. As the amount of force is increased, the displacement value and the speed of displacement increase. In our case, there are two states of the system corresponding to two different applied forces. In the first state, an electrostatic force due to an applied voltage between beam and the center conductor pulls down the beam. This force increases quadratically with the amount of displacement. In the second case, the beam is pulled up to the equilibrium condition by the spring force of the beam, which determines the speed of displacement. This results in a constant pull up time for the beam, which is determined by the physical structure of the beam. However when the voltage is applied, the electrostatic force affects displacement velocity and pull down time. Since the applied voltage can change the electrostatic force, it is possible to change the pull down time. As the switching time of a switch is desired to be as short as possible, pull down voltage is kept as high as possible to reduce the pull down time. Typical pull down and pull up times are around 1 μsec and 10 μsec respectively [21, 22, 43]. The relatively high difference is due to the weak spring force of the beam compared to electrostatic force. For this reason, a designer should increase the spring constant of the beam as much as possible to reduce the total switching time. However, this increase has a limit. When the spring constant is increased, pull down voltage increases. This pull down voltage causes significant electric field in the dielectric material used for isolation when the switch is pulled down. This field can cause a breakdown in the dielectric causing a serious damage to the structure. For this reason spring constant is limited by the pull down voltage that does not cause breakdown. Also one other thing to note is that a safety margin should be left between the pull down voltage and the breakdown voltage, because the

breakdown voltage of the dielectric may change due to the production errors. Pull down voltage may also be affected from the production errors. Therefore, the spring constant of the beam should be determined to obtain a pull down voltage lower than the breakdown voltage.

After the ideal spring constant is determined, the remaining thing is the mass and the damping coefficient of the switch. In order to have a fast switch, mass and damping coefficient should be reduced. Mass is directly related with the total volume of the beam, hence the dimensions of the beam. As the dimensions change, spring constant also changes. Therefore, mass is generally determined while designing the switch for optimum spring constant. Damping coefficient is related with air damping which is due to the air under the beam, which resists the movement of the switch. Sealing the switch in a vacuum package can eliminate it. If vacuum packaging is not possible, small holes can be opened in the beam, which permit airflow. These holes can reduce both the damping coefficient and the mass of the switch. However they also affect the spring constant. For this reason, sizes of the holes should be kept small, and the spacing between them should be kept large.

A design, which considers all the critical points stated above, can be assumed as a good mechanical design. However, a good mechanical design is not always a good design, because there is also another side of the design. This is the RF side, which deals with the signal transmission. A good design should also have a good RF performance.

As explained in Section 3.1.1, design criteria that determines the RF performance can be listed as insertion loss, isolation, reflection coefficient, bandwidth, and band of operation. For a series switch these parameters all depend on the series impedance Z_s of the switch as explained in Section 2.2.1.1. In order to have a good series capacitive switch Z_s should be very large, ideally infinity, for the off state, and very small, ideally zero, for the on state. However in real life, Z_s has finite and nonzero values. This nonideal behavior of Z_s affects the performance parameters. In order to have a good design, these effects should be predicted and

reduced as much as possible. Because of this, behavior of Z_s should be modeled. A model for Z_s is given in Section 2.2.2.1. According to this model, Z_s is dominated by the capacitance of the switch. Therefore, it is proper to state that a good series capacitive switch design mostly depends on the on and off state capacitances of the switch. Off state capacitance mainly determines isolation behavior. If it is low, then the switch can give sufficient isolation at higher frequencies. As it is a capacitive load, its impedance decreases with increasing frequency leading to a degraded isolation. For this reason, off state capacitance determines the upper limit for the band of operation for a specified isolation. On state capacitance and inductance determine the insertion loss of the switch. If capacitance is high, then the impedance introduced by it is low leading to a better insertion loss. Since it is an LC circuit, the impedance has a minimum at the resonance frequency, and increases with decreasing frequency. This means an increasing insertion loss with decreasing frequency. Since L is almost constant for most designs, on state capacitance determines the lower limit for the band of operation when an insertion loss is specified. The on state capacitance also determines the magnitude of reflection coefficient. When it is large, reflection coefficient is small.

As the effect of capacitance on performance criteria is considered, it is proper to state that on state capacitance should be as large as possible, and off state capacitance should be as small as possible. The parameters affecting these capacitances are W, L, d_1, and d_2. For a large on state capacitance W and L should be large, while d_1 should be small. However, for a small off state capacitance, d_2 should be large and d_1, W, and L should be small. Although these two requirements conflict with each other, a designer can obtain a very large on capacitance and very small off capacitance by making d_1 very small and d_2 very large. However this has two adverse effects on mechanical operation. If d_2 is large leading to a small off state capacitance, then pull in voltage will become extremely large. If d_1 is very small then breakdown voltage of the dielectric will become very small. These two effects both lead to a beam, which cannot be pulled down because of breakdown. Therefore,

the designer should consider both mechanical and RF characteristics simultaneously during the design.

Up to now design rules for a good series capacitive switch were explained. From this point on, the simulation results and the comments on these results for a switch will be given. These results and comments are helpful in understanding the design procedure of a switch. The results will follow the order in the previous paragraphs. First results of mechanical simulations, then results of RF simulation will be given. Before giving the simulation data, it is proper to give the dimensions of the switch that these simulation data is obtained for.

The dimensions of the switch structure given in Figure 3.1 are:

L_a= 103 μm, L_b= 110 μm, L_c= 50 μm, L_d= 105 μm, L_p = 2 μm, L_T= 845 μm, L= 475 μm, W= 120 μm, S= 20 μm, d_1= 0.1 μm, d_2= 5 μm.

The mechanical simulations of this design is made using Coventorware, which is a MEMS design software. According to these simulations, off state capacitance is 97.5 fF, which is close to the value of 100.6 fF, which is theoretically calculated using standard parallel plate capacitance formula. This capacitance changes when the bridge bends down due to the applied voltage. Capacitance vs. actuation voltage is given in Figure 3.2. As it is observed in the figure, capacitance changes nonlinearly with actuation voltage. This also means that spacing between the beam and the center line changes nonlinearly with voltage. Spacing vs. voltage graphics is given in Figure 3.3. It can be observed that spacing decreases nonlinearly with increasing actuation voltage

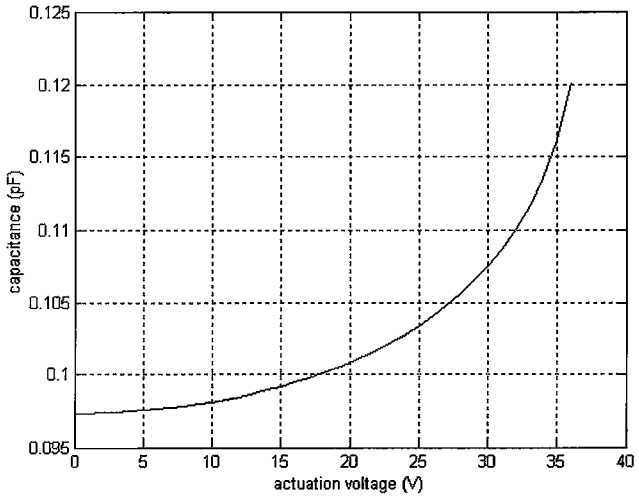

Figure 3.2: Capacitance between the beam and the signal line of a series switch vs. actuation voltage obtained using Coventorware simulations. After 36 volts capacitance abruptly changes to a very high value, which is not shown in the figure. This change is due to the pull in phenomenon, which is the instability in the mechanical state of the beam leading to collapse of the beam on to the signal line.

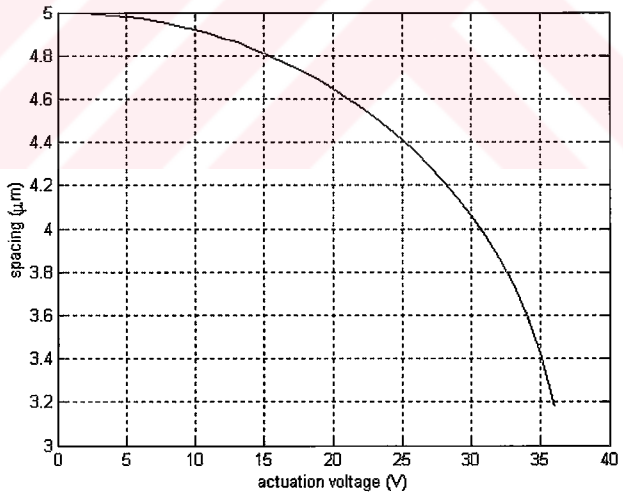

Figure 3.3: Spacing between beam and signal line vs. actuation voltage. The spacing changes nonlinearly with actuation voltage, and has an abrupt change around 36 volts. This voltage is the pull in voltage, after which spacing suddenly drops to zero due to mechanical instability of the system.

Both results in Figure 3.2 and Figure 3.3 are up to 36 volts. After that voltage pull in occurs. According to Coventorware simulations pull in voltage is between 36.25 and 37.5 volts. The spacing where pull in occurs is 3.09 μm, which is close to $2d_2/3$=3.3 μm.

RF simulations of the above mentioned structure are accomplished using Ansoft's HFSS (High Frequency Structure Simulator). The program uses finite element method to analyze three-dimensional structures. The simulations made using HFSS were performed for on and off states by drawing two different geometries for these two states. Off state geometry is a simple cantilever beam. On state geometry should be a bended version of this beam. Therefore, it should have a smooth curvature from the post to the signal line. However, both creating and simulating this curvature takes too much time. In order to simplify the problem and reduce the problem size, on state geometry is drawn as if the beam was totally lowered to the level of signal line. Two other parameters that affect the simplicity or the size of the problem are the size of the air box and substrate box seen in Figure 3.4. These two boxes are required in order to correctly model the CPW. The thickness of substrate is fixed by the actual thickness of the substrate, which is 500 μm. Size of air box should be infinity or very large for the actual case. However, this would create an unsolvable problem size therefore, it should be limited. In our case it is limited to 1000 μm, which is a moderate value for the problem size that does not affect the simulation results much.

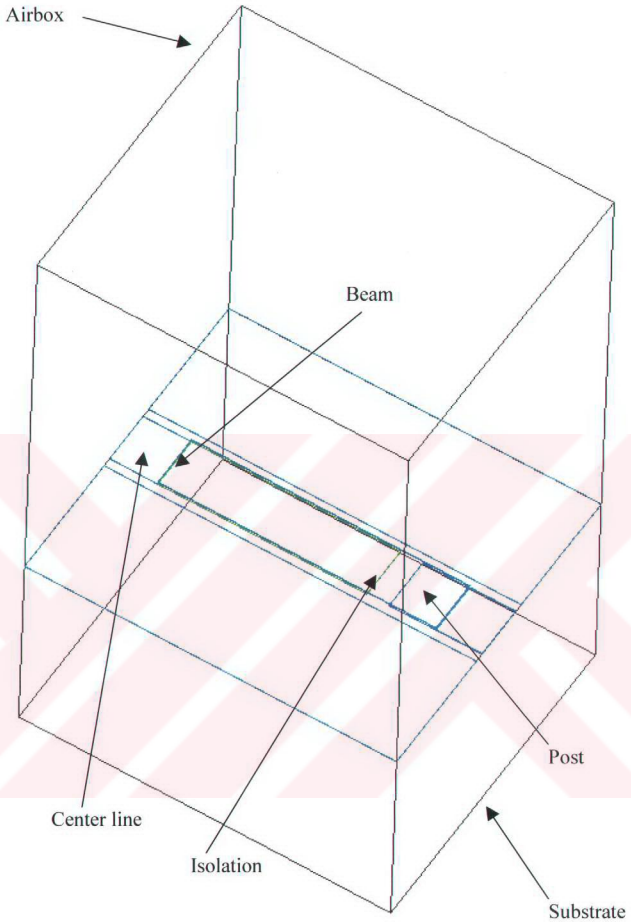

Figure 3.4: Three-dimensional model of the series switch used by HFSS for RF simulations. Size of air box and substrate box affects the problem size hence the solution time directly. Input and output ends of the CPW are defined as port boundaries at HFSS. Remaining boundaries were taken as infinite conductors.

Simulation results of the model given in Figure 3.4 are shown in the figures below. The results are for three different beam dimensions. Specifically, blue lines are for L= 475 μm, red lines are for L= 245 μm, and black lines are for L= 45 μm. These beam length values change on state capacitance, off state capacitance, and actuation capacitance by the same ratio. Effects of this decrease in capacitance on RF performance can be observed from the following figures.

As observed from Figure 3.5, decreasing L leads to a better isolation. Although isolation improves generally, behavior of isolation with frequency does not change significantly. It is shifted by a constant value at all frequencies. These characteristics lead to a series impedance given in Figure 3.6, which is calculated using equation 2.17. This impedance shows $1/f$ characteristics with frequency, which is a property of capacitive loads. This result confirms the assumption that a series capacitive switch in its off state can be modeled as a capacitance.

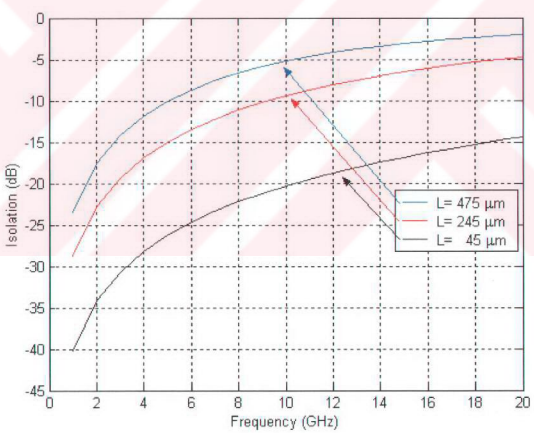

Figure 3.5: Isolation of series capacitive switches for three different beam lengths. As the beam length decreases isolation becomes better due to the decreased series capacitance between input and output.

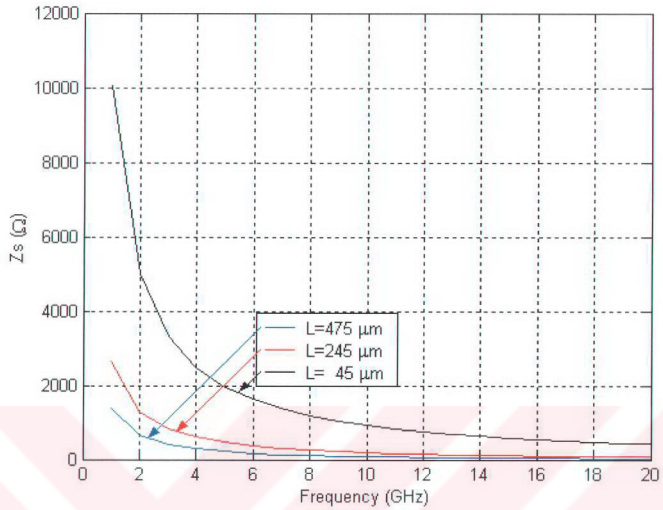

Figure 3.6: Series impedance of the series capacitive switch for the off state. It is extracted using the isolation vs. frequency data. As the beam length decreases impedance increases due to decreasing capacitance.

Figure 3.7 shows the insertion loss vs. frequency. As observed from the figure, insertion loss makes a minimum at different frequencies for different beam lengths. This is due to the fact that effect of on state capacitance becomes comparable with the effect of on state inductance. Hence, the switch behaves as a series LC resonant circuit. Also, as series on capacitance decreases, insertion loss increases generally, because decreased capacitance increases on state impedance, which results in higher insertion loss.

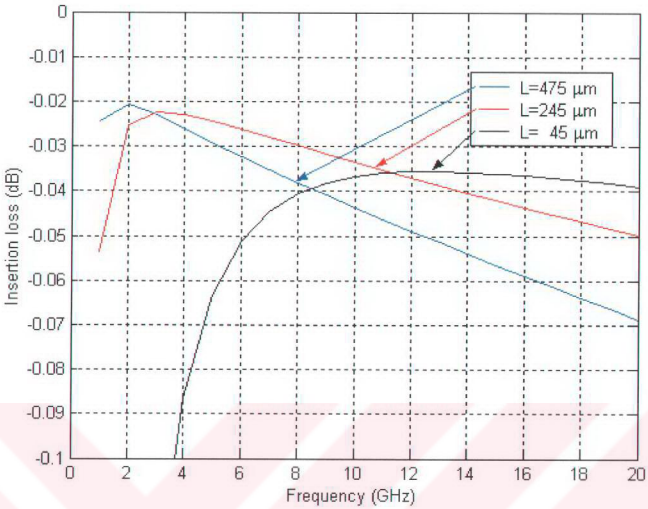

Figure 3.7: Insertion loss vs. frequency plot of series capacitive switch. Effect of inductance on the insertion loss is increased for higher capacitance values at longer beam lengths.

3.1.2.2 Single-Pole Double-Throw Series Capacitive Switch

This switch is similar to the series switch explained in the previous section except that it has two output ports. Three-dimensional model of the switch can be seen in Figure 3.8. It is formed of two series switch beams with a common post. This structure leads to a model given in Figure 3.9.

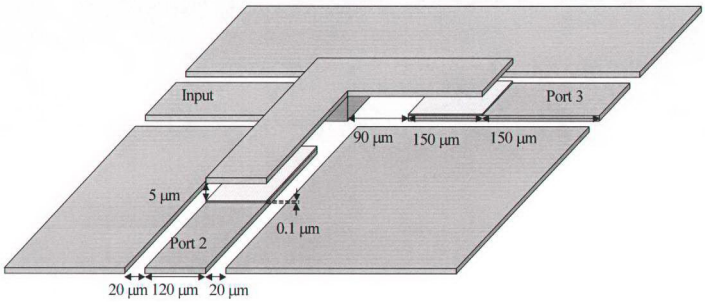

Figure 3.8: Three-dimensional model of the switch.

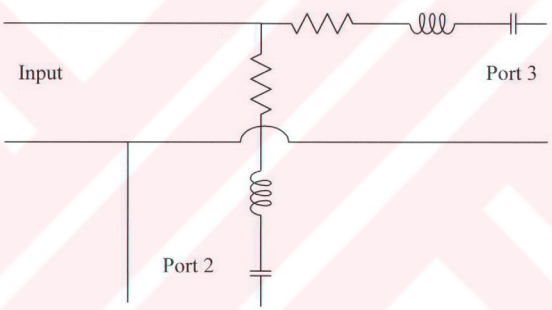

Figure 3.9: Circuit model of the SPDT switch. Each beam is modeled as a series RLC circuit.

Mechanical design of the switch given in Figure 3.8 is same as the single-pole single-throw version, because SPDT switch is formed of two beams that share a common post. Therefore, while making mechanical simulations, SPDT switch is modeled as a single-beam switch. The simulations were performed for the structure given in Figure 3.8. According to these simulations, off state capacitance was

40.4 fF, which is close to 31.8 fF that is calculated using the parallel plate capacitance formula. The change of this capacitance with applied voltage is given in Figure 3.10. The capacitance curve is same as the series switch beam. Also spacing vs. actuation voltage curve, which is given in Figure 3.11, is same as the series switch beam. However in this case, simulation results are given up to 95 volts, i.e. the lower limit of the pull in voltage, which is found to be between 95 and 97.5 volts. This increase in pull in voltage is expected since we have a shorter beam resulting in higher spring constant and lower capacitance, hence lower electrostatic force for an applied voltage. Pull in voltage and the capacitance values are the differences of SPDT switch given in Figure 3.8 from the series switch given in the previous section.

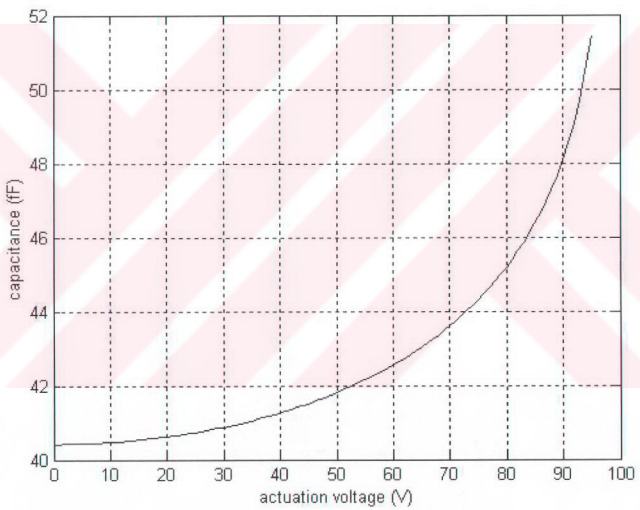

Figure 3.10: Beam capacitance vs. actuation voltage graphics of one of the beams of the single-pole double-throw switch.

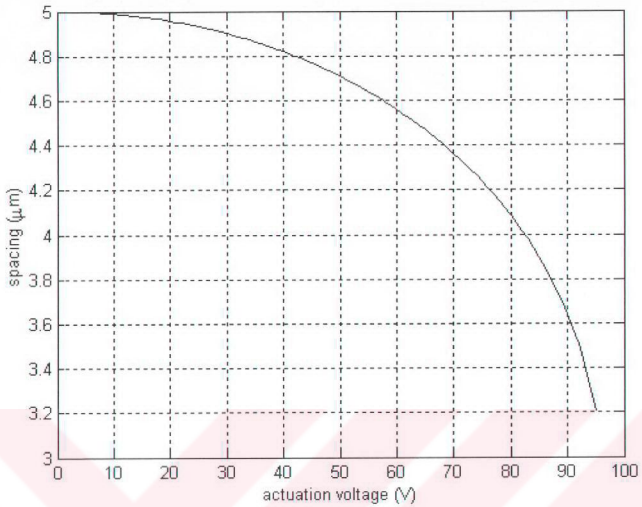

Figure 3.11: Spacing between the beam and the center line vs. actuation voltage for a single-pole double-throw switch.

The model given in Figure 3.9 leads to an RF design slightly different from the series capacitive switch. When one of the switches is on, the other one is off. This means high impedance for one of the ports and low impedance for the other. If high impedance port is treated as an open circuit, then the model turns into a simple series capacitive switch, design of which is explained in the previous section. However, since the off impedance of the switch is not infinity, its effect should be added for precise calculations. The shunt impedance increases insertion loss and reflection coefficient, degrading the performance, and increases isolation improving performance. These effects can be observed in the following figures.

Figure 3.12 gives the insertion loss vs. frequency plot obtained using HFSS. Blue line presents the state when switch on port 2 is on, and switch on port 3 is off. Red line is for the reverse case, and black line is for a single-pole single-throw switch with same beam dimensions. As can be observed from Figure 3.12, insertion loss of the single-pole single-throw switch is the least. The difference increases at higher frequencies since the shunt impedance, which is mainly a capacitive load, decreases with frequency, draining more signal by power division between two ports. As observed from Figure 3.12, this power division is not equal. In other words, insertion loss of port 3 is lower. This is due to the geometry of the line, which is seen in Figure 3.8. Port 3 has a straight connection with input, but port 2 has a 90^{o}-bend, which introduces additional loss.

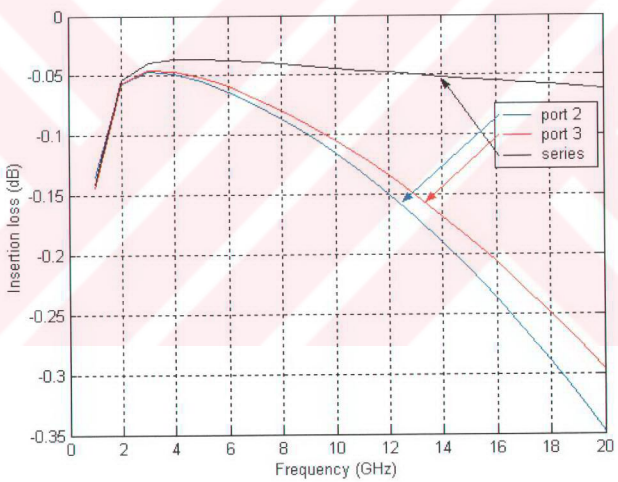

Figure 3.12: Insertion loss vs. frequency plot for the single-pole double-throw switch. Port 2 means that the signal is routed to port 2 by turning the port 2 switch on and port 3 switch off. Port 3 means the reverse case. Series means single-pole single-throw switch with the same beam dimensions.

Figure 3.13, which gives reflection coefficient vs. frequency plot, shows that series switch has the least reflection coefficient, and the difference increases with increasing frequency. In this case the shunt impedance of the off switch reduces as frequency increases. This leads to lower total impedance causing more reflection. Also, reflection coefficient for two cases has a significant difference. This difference is due to the 90°-bend of port 2. This bend introduces impedance mismatch, which adds to the reflection coefficient. This increased reflection coefficient also causes an increase in insertion loss.

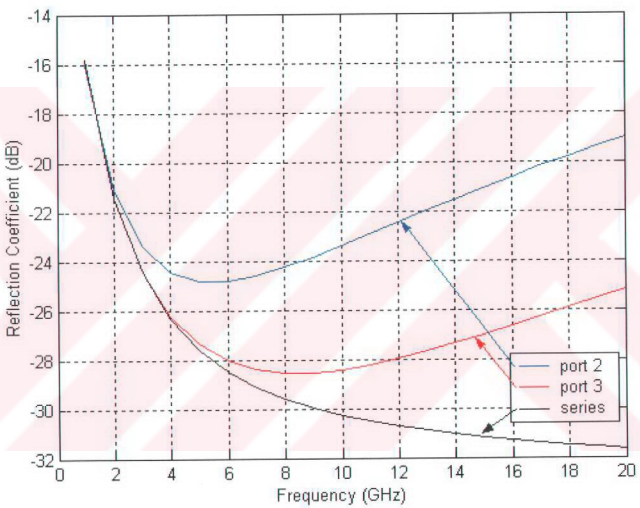

Figure 3.13: Reflection coefficient vs. frequency plot for the single-pole double-throw switch. Port 2 means that the signal is routed to port 2 by turning the port 2 switch on and port 3 switch off. Port 3 means the reverse case. Series means single-pole single-throw switch with same beam dimensions.

Figure 3.14, which shows isolation vs. frequency, illustrates that isolation becomes better for the single-pole double-throw switch. The data is obtained for three different cases. In the first case port 2 of the switch is on, and isolation of port 3 is obtained. Second case is the reverse of first case, and third case is the isolation value for a series switch. Isolation is the only parameter that is improved. The reason is that any signal that is lost during transmission means a better isolation, and any additional shunt or series impedance means a signal loss. Therefore, shunt connection of the other ports switch impedance improves isolation.

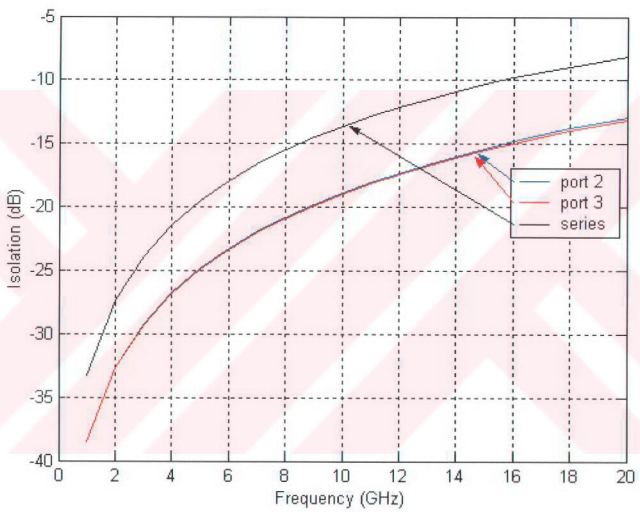

Figure 3.14: Isolation vs. frequency plot for the single-pole double-throw switch. Port 2 means that the signal is routed to port 2 by turning the port 2 switch on and port 3 switch off. Port 3 means the reverse case. Series means single-pole single-throw switch with same beam dimensions.

3.1.3 Parallel Switch

In this section design of parallel switch will be explained. There are two different geometries for the parallel switch. First geometry, which is a bridge that has two posts on ground planes, will be explained in Section 3.1.3.2. Second geometry, which is a T shaped wing structure that has a single post on the center line, will be explained in Section 3.1.3.3. General design issues will be explained in 3.1.3.1 before going through different geometries.

3.1.3.1 General Design Issues for Parallel Switch

As explained in Section 3.1.2, switches have two design aspects: the mechanical design and the RF design. Mechanical design of parallel switches is mostly the same as the series switches. Therefore, they will not be explained in this section. However RF design is different from the series switches. For this reason it is explained in the following paragraphs.

A parallel switch is the parallel connected switching element between input and output. The circuit model for parallel switch is given in Figure 2.20. However, this model is not enough for designing a parallel switch. As seen in Figure 2.19 and Figure 3.24, the switch is not only composed of a switching element, but also two transmission lines added to both ends. The effects of these transmission lines should be taken into account. For this reason, an accurate switch model is the one given in Figure 3.15.

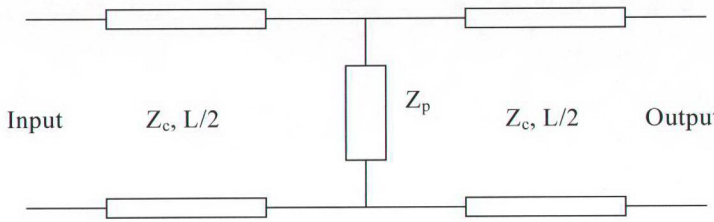

Figure 3.15: Circuit model for the parallel switch. *Zp* denotes switch impedance. Transmission lines with a length of half the total switch length are added to both ends to accurately model the actual switch structure.

According to this model, when the switch is off, Z_p is very high acting like an open circuit hence introducing minimum load on the line. However, this finite load affects the reflection coefficient of the two port. Since this load is capacitive in nature, it acts like a parasitic capacitance, which reduces the characteristic impedance of the line segments at the two ends. In order to cancel this effect, designer should increase the impedance of these line segments to a higher value than the reference impedance. For example a characteristic impedance of 75 Ω is required to have a switch, which has minimum reflection coefficient for 50 Ω port impedance. In order to achieve this, width of the center line can be decreased or spacing between the center line and the ground lines can be increased. First method may result in very thin center lines, which might be impractical for production and testing. Second method means an increase in the total area of the switch, hence should be limited. Another way to cancel this loading effect is to increase the line lengths. By this way the amount of per unit length loading capacitance is decreased though the total loading capacitance remains same. This method reduces the demand for high line impedance for the off state of the switch.

When the switch is on, Z_p should be small acting as a short circuit. If $Z_p = 0$, all the signal is reflected back to the input, and none is transmitted to the output. In this case, value of Z_p is important for the isolation characteristics. Since Z_p is modeled as a series RLC circuit it attains the minimum value at the resonance frequency of the LC resonator. At resonance it is only the resistance in the RLC. Therefore, if very good isolation is desired, resonance frequency of the LC resonator should be set to the operating frequency of the device. However, this would require an inductive tuning for the switch for most operating frequencies. This inductive tuning can affect the general operation of the switch. Also it may result in a more complex structure, which would generally require more device area. Therefore, the designer should determine the specifications on the isolation characteristics, and then decide to use inductive tuning or not.

Other than the issues stated in the previous paragraphs, design of the parallel switch is similar to the series switch that is explained in Section 3.1.2.1 in detail. The design generally addresses two important issues. Up state capacitance should be adjusted so that it would not create reflection, and also would not result in high actuation voltages. Down state capacitance should be adjusted to give the best isolation, but not result in very high breakdown voltages. Considering these issues, and the ones stated in this section, would result in good switch designs. In the following sections simulation results for two different parallel switches, which are done considering these issues, will be given.

3.1.3.2 Bridge Type Capacitive Parallel Switch

Bridge type parallel capacitive switch has a bridge, which is fixed from two ends by means of two posts, as seen in Figure 2.19. This structure makes the bridge very stiff, which results in higher actuation voltages than a beam. Actuation voltage is applied between the bridge and the two ground planes. Dielectric under the ground planes prevents the DC short. According to this actuation scheme, Coventorware simulations give a pull in voltage of 130 volts. From zero actuation to

the pull in voltage, spacing between bridge and the center line changes according to the characteristic curve given in Figure 3.17. This curve is same as the spacing curve of the beam, which is given in Figure 3.1. Also capacitance curve, which is given in Figure 3.18, is same as the capacitance curve of the beam given in Figure 3.2.

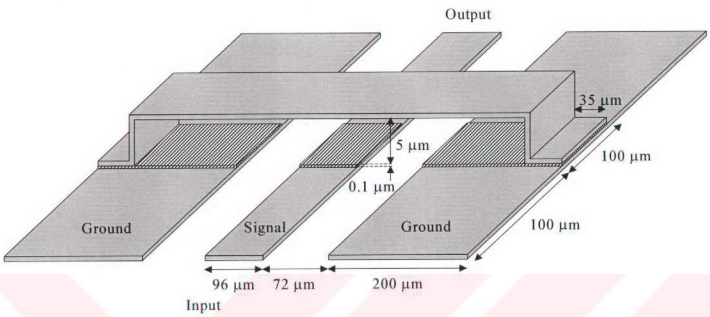

Figure 3.16: Three-dimensional model of the parallel capacitive bridge type switch. Actuation voltage is applied between the bridge and the ground planes. Dielectrics prevent DC short, but do not prevent RF short.

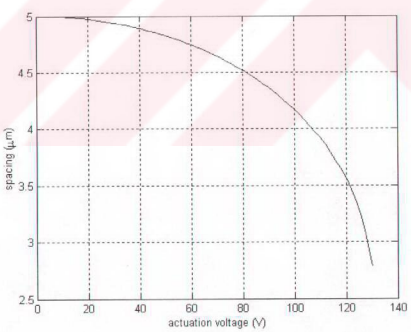

Figure 3.17: Spacing between the bridge and the center line vs. actuation voltage for parallel bridge switch. At 130 volts where spacing becomes approximately 2.75 µm pull in occurs leading to immediate collapse of bridge on to the signal line.

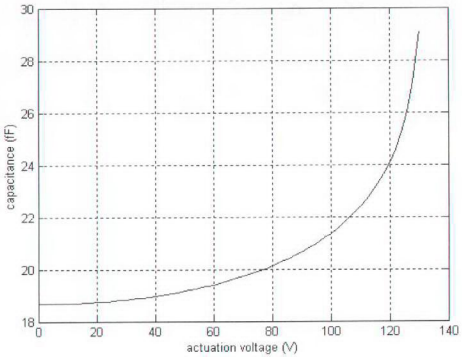

Figure 3.18: Capacitance between the bridge and the center line vs. actuation voltage for parallel capacitive bridge type switch.

As seen from the above figures, mechanical behavior of the bridge is similar to the beam. RF behavior is also similar to the series switch. However, when the bridge is up meaning switch is off, signal transmission from input to output is permitted and when it is down, meaning switch is on signal transmission is prevented, which is the reverse case of the series switch. In the following figures, behavior of the parallel switch for the on and off states will be given.

Insertion loss and the reflection coefficient are the two important parameters for the off state. Insertion loss vs. frequency is given in Figure 3.19. As seen from the figure, insertion loss is degraded with frequency. Reflection coefficient vs. frequency is given in Figure 3.20. This figure shows that reflection coefficient is degraded with increasing frequency. These two results mean that Z_p is decreasing with frequency, hence departing from the open circuit condition. In fact behavior of Z_p for the off state is given in Figure 3.21. This behavior is obtained using the model given in Figure 3.15. Since the S-matrix of the total system is known, it is possible to obtain ABCD matrix of the system. If one knows the ABCD matrix of the

transmission lines, then it is possible to obtain the ABCD matrix of the two port defined by the parallel impedance Z_p. Therefore, in order to find Z_p, simulations for the line segments of the parallel switch were made. Using the simulation data for the transmission lines and the total switch, Z_p is obtained by matrix calculations made in Matlab. Resulting Z_p behavior is presented in Figure 3.21. This behavior is similar to $1/x$ behavior, which is typical for capacitive loads. Therefore, it is possible to say that Z_p is dominated by the capacitance of the bridge. Impedance curve for a capacitance of 21.86 fF is also presented in Figure 3.21. It perfectly matches with the Z_p curve. Therefore, it is possible to say that parallel switch is formed of a capacitance whose value is 21.86 fF in the off state. The capacitance of this structure calculated according to the parallel plate capacitance formula is 16.88 fF. Actual capacitance is 30% larger than the parallel plate capacitance, which is due to the fringing field capacitance between the bridge and the signal line [8]. The amount of this capacitance is the key factor affecting the off state parameters, which are the insertion loss and the reflection coefficient, of the parallel switch.

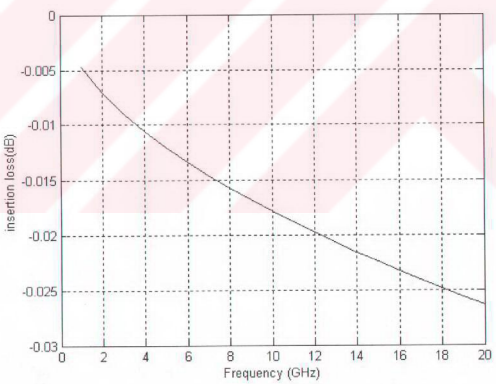

Figure 3.19: Insertion loss vs. frequency plot of the parallel capacitive bridge type switch. It increases with frequency since impedance of the switch decreases with frequency due to the capacitive nature of the impedance.

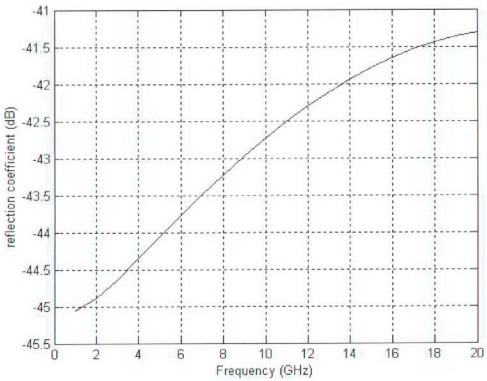

Figure 3.20: Reflection coefficient of the parallel capacitive bridge type switch.

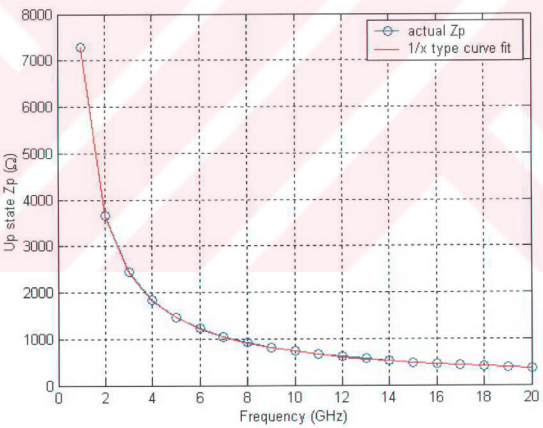

Figure 3.21: Off state impedance of the parallel capacitive bridge type switch and the curve fit for this impedance. Curve fit perfectly matches the actual data. Therefore, off state impedance is dominated by the capacitance of the switch making impedance and resistance terms negligible.

Off state parameter is the isolation for a parallel switch. Isolation is improved with increasing frequency as seen in Figure 3.22. This means a decrease in Z_p approaching to short circuit with increasing frequency. Behavior of Z_p is given in Figure 3.23. It is decreasing with increasing frequency close to $1/x$ behavior, which is also presented with the red line in Figure 3.23. In fact this fitting leads to a capacitance of 5.07 pF for the on state. Parallel plate capacitance for this case is 4.8 pF. Actual capacitance is 5.6% higher than the parallel plate capacitance. The difference between actual and parallel plate capacitances is less compared to the off state because the amount of fringing field is reduced as the bridge approaches the signal line [8].

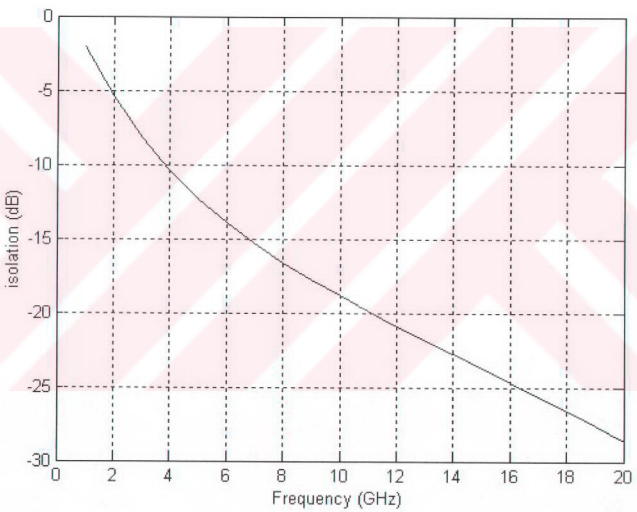

Figure 3.22: Isolation vs. frequency plot of the parallel capacitive bridge type switch. It increases with frequency meaning decreasing impedance with frequency.

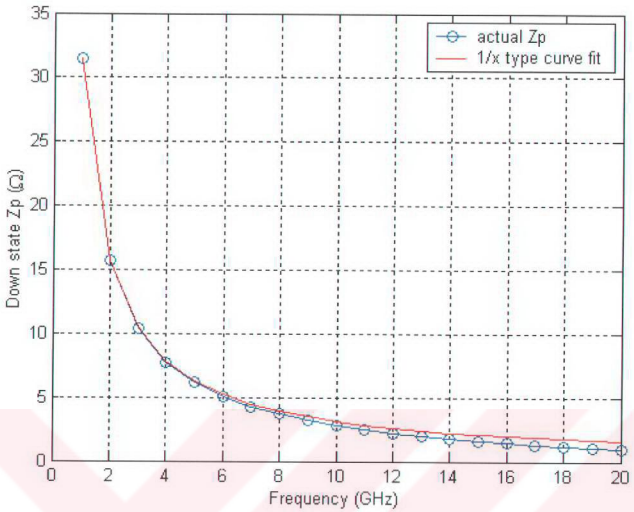

Figure 3.23: On state impedance of the parallel capacitive bridge type switch and the fitted curve. Curve fit mostly matches the actual data. This means switch impedance is dominated by capacitive effects.

3.1.3.3 T-Wing Type Capacitive Parallel Switch

As seen in Figure 3.24, T-wing type switch has a single post on the center line and two beams, which lie over the ground planes. This structure can be interpreted as two beams that share the same post in terms of mechanical considerations. Since both beams have identical structures, simulation of single beam would be sufficient to define the system mechanically.

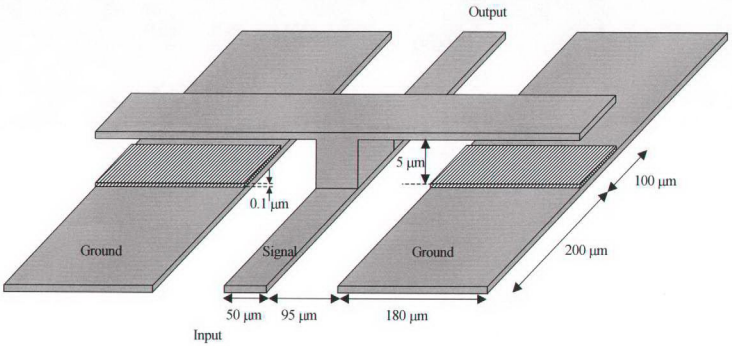

Figure 3.24: T-wing type capacitive switch. A DC voltage is applied between the signal line and the ground lines to pull down the wings of the switch. By this way capacitance between the signal and ground is increased leading to a very small impedance between ground and signal which causes signal reflection.

Simulation of a single beam gives pull in voltage of 130 volts and up state capacitance of 47.1 fF. The capacitance vs. actuation voltage plot is given in Figure 3.25, and beam to ground spacing vs. actuation voltage plot is given in Figure 3.26. As can be seen from these figures, T-wing beams show the same characteristic with series switch beams. Only difference is that actuation voltage is applied between the beam and the ground plane. Since there is more area on the ground plane, it is possible to extend the beam over the ground plane and increase the actuation capacitance without changing the dimensions of the switch very much. This introduces flexibility in the mechanical design of the switch.

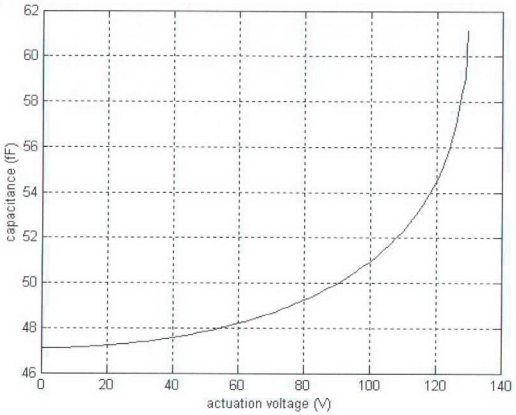

Figure 3.25: Capacitance of the beam vs. actuation voltage for the T-wing type parallel capacitive switch.

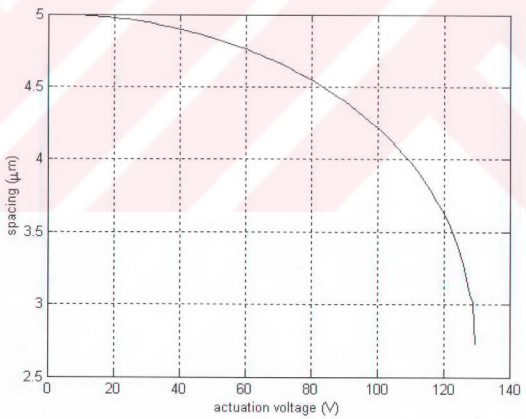

Figure 3.26: Spacing between the wing and the ground plane vs. actuation voltage for the T-wing type parallel capacitive switch.

This design flexibility is also valid for the RF design of the switch. Extending the beams over the ground plane makes it possible to adjust the up and down state capacitance of the switch easily, which are important in RF performance. In a bridge type design, capacitance is limited by the width of the center line. There is only one variable, which is the width of the bridge that can be changed to adjust the capacitance. However in the T-wing case, width of the ground plane can extend as much as desired hence capacitance can be adjusted in two dimensions. This gives the chance to increase the up or down state capacitance as much as desired. Also the up and down state capacitance is doubled compared to bridge case because there are two beams that extend over the ground planes, which introduce two equal and parallel capacitances. This increase in capacitance is helpful in obtaining high isolation values in the on state, however it has a negative effect on insertion loss and reflection coefficient for the off state. Insertion loss, isolation, and reflection coefficient characteristics of the T- wing type switch, whose dimensions are given in Figure 3.24, are explained in the following paragraphs.

As seen in Figure 3.27 insertion loss is degraded with increasing frequency. Figure 3.28 shows that reflection coefficient is also degraded with increasing frequency. These two results imply a Z_p that decreases with increasing frequency. This decreasing Z_p behavior is seen in Figure 3.29. The fitted data in Figure 3.29 corresponds to the impedance of a capacitance of 83.24 fF, which is 31% larger than the parallel plate capacitance of 63.54 fF.

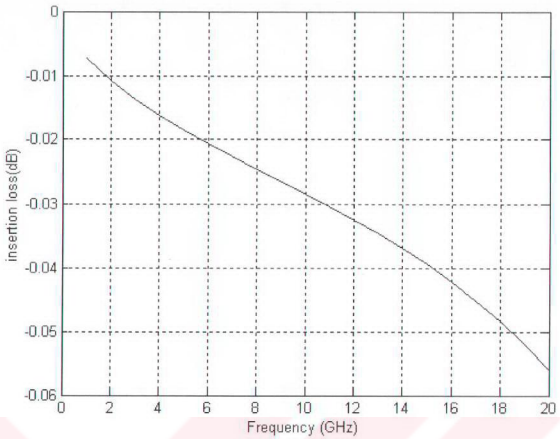

Figure 3.27: Insertion loss vs. frequency plot of the T-wing type parallel switch.

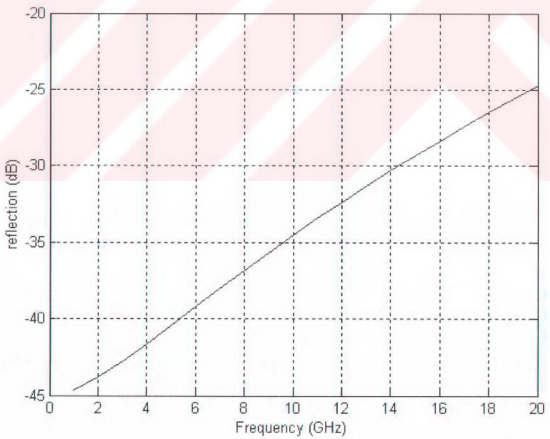

Figure 3.28: Reflection coefficient vs. frequency plot of T-wing switch.

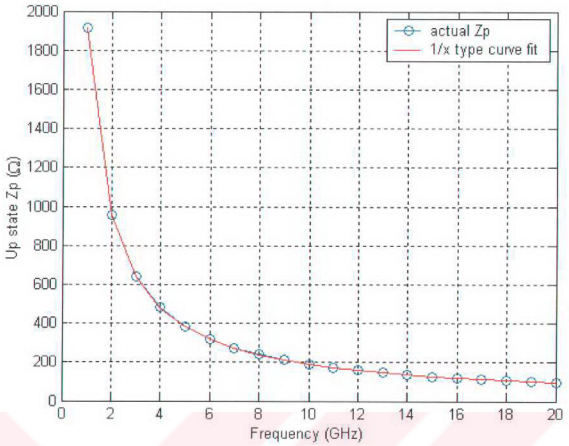

Figure 3.29: Up state impedance vs. frequency of a T-wing parallel switch and the fitted curve is presented. Fitted curve is the impedance curve of a capacitive load.

As seen in Figure 3.30, isolation of a T-wing switch makes a minima around 11 GHz. In fact this minima is the resonance point of the series LC resonator. At this point Z_p has a minimum value, which can also be observed in Figure 3.31. This means that capacitance of the bridge is so large that resonance frequency becomes small enough to be observed in the simulated frequency range. This Z_p characteristic leads to a capacitance of 27 pF, where parallel plate capacitance is 22.3 pF, and inductance of 7.1 pH. These L and C values lead to a resonance frequency of 11.44 GHz, which is also observed in Figure 3.30 and Figure 3.31. Obtaining the resonance within the operation frequency significantly increases the amount of isolation, which can be observed in Figure 3.30. At resonance isolation can go down to -55 dB. However for the off resonance case, it can go up to -30 dB. Therefore, for applications demanding high isolation, resonance frequency of the switch should be pulled into the operating frequency range.

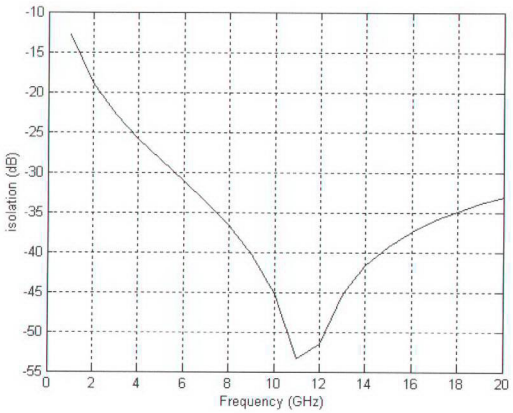

Figure 3.30: Isolation vs. frequency plot for the T-wing switch. Isolation makes a dip around 11 GHz meaning a resonant structure with resonance at this frequency.

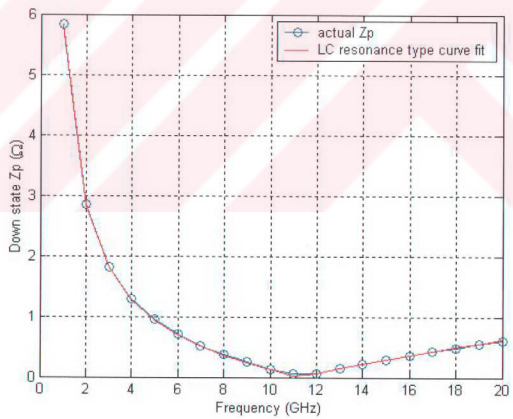

Figure 3.31: On state Z_p and the curve fit for T-wing switch. This impedance is modeled as a series LC circuit whose impedance curve is fitted on the actual data.

There is a conclusion that can be drawn when the results of bridge type switch and T-wing type switch are compared. First of all insertion loss of bridge type switch is better, and it also has a better reflection coefficient. This can be explained by the lower off state capacitance of the bridge, which is almost 1/5 of the T-wing type switch. Also on state capacitance of the T-wing switch is significantly higher than the bridge type switch. It is 5 times the capacitance of the bridge type switch. This high on capacitance brings the advantage of high isolation. Therefore, as a conclusion, T-wing type switches generally have larger on and off state capacitances leading to degradation in the off state performance and improvement in the on state performance.

3.2 Phase Shifter

In this section, design of RF MEMS phase shifter will be explained. Design criteria and specification of these criteria for application specific designs will be explained in Section 3.2.1. Then, design of continuous phase shifter will be explained in Section 3.2.2, and design of discrete phase shifter will be explained in Section 3.2.3.

3.2.1 Design Criteria for RF MEMS Phase Shifters

Design criteria for RF MEMS phase shifters can be grouped into two categories. First one is the mechanical design criteria, and second one is the RF design criteria.

Mechanical design criteria can be listed as follows

- *Response time*: It is the time that is required to obtain a desired amount of phase shift from a phase shifter. This time depends on the type of the phase shifter very much. For discrete phase shifters, this time is the switching time of the switches used in the phase shifter. However, for continuous phase shifters it is the time required to pull the bridges down to a certain height.

Since these bridges do not make a full-scale deflection, in other words pull in, their response time is smaller than the discrete phase shifter switches response time. For a specific type of phase shifter, structure of the switch is the main component that determines the response time. If the switch has a stiff structure, then the switching time is shorter; hence the response time is shorter. However, having a very stiff switch would cause high pull in voltages, which might cause breakdown that damages the switch structure. For this reason, the designer should make the designs considering this trade off between response time and pull in voltage.

- *Lifetime*: It is the time that the phase shifter can operate without failure to meet the performance criteria. It depends on the type of phase shifter very much. Discrete phase shifters have shorter lifetimes compared to continuous phase shifters. The switches used in the discrete phase shifters are deformed more, since they are pulled down on to the bottom plate. Every time the switches are pulled down, fatigue occurs due to bending of the beams, and wear on the contact surfaces occur due to the crushing force during touch down. Since the bridges in the continuous phase shifter are not pulled down that much, they have longer lifetimes.

RF design criteria are:

- *Loss per degree*: It is the insertion loss for one degree of phase shift. It is simply found by dividing the total insertion loss of the phase shifter to the total phase shift. This is the most important parameter that determines the RF performance of a phase shifter.

- *Bandwidth*: It is the maximum bandwidth of the signal that can be transmitted without distortion. It is generally related with the frequency dependent insertion loss behavior of the phase shifter. If this behavior is flat or relatively constant, then bandwidth is large. If it varies much with the frequency then bandwidth is small.

- *Band of operation*: It is the frequency band defined by the maximum and minimum frequency of operation. These frequencies are determined according to the specification of loss per degree. Since insertion loss changes with frequency, loss per degree stays below the specified value only for a range of frequency, which is the band of operation.

Above stated design criteria can be used to determine the performance of a phase shifter. Each of these parameters can be improved independently. However all of them cannot be improved at the same time. Depending on the type and structure of the phase shifters, there are trade offs between design criteria. Therefore, before starting a design, specifications on these criteria should be stated clearly according to the requirements of the application that this design will be used. However, in our case these phase shifters are not designed for a specific application, and there are no specifications to be met. Therefore, rather than improving a specific criteria to a specified value, our design goal was to realize some design ideas. Hence, while designing the phase shifters obtaining moderate performance values were the primary motivation. After obtaining moderate values, design was improved to have better RF performance rather than having better mechanical performance. The resulting designs are explained in the following sections.

3.2.2 Continuous phase shifter

As explained in Section 2.3.2, continuous phase shifters are based on loaded line phase shifting principle. Capacitive switches form the capacitances that load the line. Two types of capacitive switches were used in the continuous phase shifters that are designed in this thesis. First one is the bridge type capacitive switch, which is explained in Section 3.1.3.2, and second one is the T-wing type capacitive switch, which is explained in Section 3.1.3.3.

Bridge type switches were used in loaded line phase shifters by some researchers [16, 17]. Therefore, our designs are same in structure with their designs. However, dimensions of our designs are different from their designs. In designing bridge type

phase shifters, goal was to observe the effect of device dimensions on the device performance. For this reason many designs with different dimensions were made. These dimensions are listed in Table 3.1. The numbers given in Table 3.1 define the dimensions of the phase shifter shown in Figure 3.32.

Table 3.1: Dimensions of the various loaded line phase shifters that are loaded with bridge type capacitances.

Name	S (μm)	W (μm)	L_1 (μm)	L_2 (μm)	L_T (μm)	Number of bridges	Z_c Ω
Phase shifter 1	74	83	100	100	22300	111	83
Phase shifter 2	96	72	100	200	22200	74	74
Phase shifter 3	122	59	100	400	22000	44	44

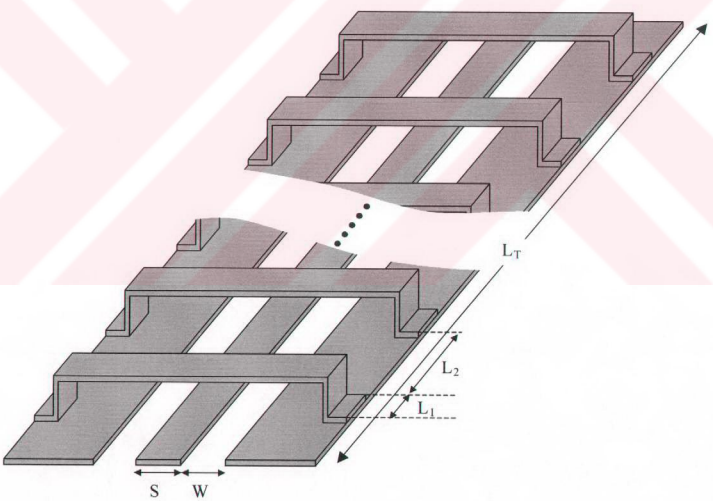

Figure 3.32: Three-dimensional view of a loaded line phase shifter that use bridge type switches as loading capacitance.

As observed from Table 3.1, spacing between the bridges are varied in each design. Since total length of the phase shifter is fixed, this changes the total number of bridges. This changes the magnitude of the total loading capacitance, which implies a change in the unloaded capacitance of the CPW. Therefore, the signal width and signal to ground spacing is changed. Changing the spacing between the bridges changes the magnitude of capacitance that can load the line in a tuned manner, which directly affects the magnitude of phase shift that can be obtained from a unit length. Also different spacing values result in different Bragg reflection frequencies, which is explained in Section 2.3.2. In order to observe the effect of Bragg reflection on device operation, changing the spacing values is helpful.

It is not possible to observe these effects by means of simulations, because the phase shifter structure is a long line with many bridges over it. Simulating this structure creates a significant problem size, which is not possible to simulate with available computer resource. So, only a portion of the phase shifter is simulated, and then phase shift data is scaled to obtain the results for the real design. However this small portion of the phase shifter introduces a very small phase shift value, and numerical errors may constitute a considerable part of this value. Hence, the accuracy of the result obtained for the real design might not be very good. Therefore, it is required to implement the real long phase shifter and make tests on it to observe the above stated effects. Therefore, phase shifters with different dimensions are designed and implemented to observe these effects. Their simulations were made for only a small portion. These simulations are used to ensure small reflection coefficient and small insertion loss. The results of these simulations for a small portion of phase shifter 1 are given below. In fact the simulated model has 4 bridges instead of 111 bridges in phase shifter 1. Its length is 0.8 mm. Therefore, while analyzing the simulation results, they should be scaled by the ratio of the original length to simulated length. By this way, results such as total insertion loss and total phase shift can be obtained for the original structure. These results are given in the following paragraphs.

Figure 3.33, which shows the reflection coefficient vs. frequency plot, reveals that the reflection coefficient of the phase shifter is below -25 dB. This means that the loading effect of the capacitive bridges is balanced with high characteristic impedance of the unloaded line to give loaded line characteristic impedance close to reference impedance. In fact loaded line characteristic impedance is designed as to be 51 Ω, because when the bridge height is reduced to give phase shift, magnitude of loading capacitance would increase leading to a decrease in the characteristic impedance of the loaded line making it approach to reference impedance. For example when bridge height is reduced to 4 μm from 5 μm, characteristic impedance reduces to 48 Ω from 51 Ω. The reflection coefficient vs. frequency plot for this case is also seen in Figure 3.33.

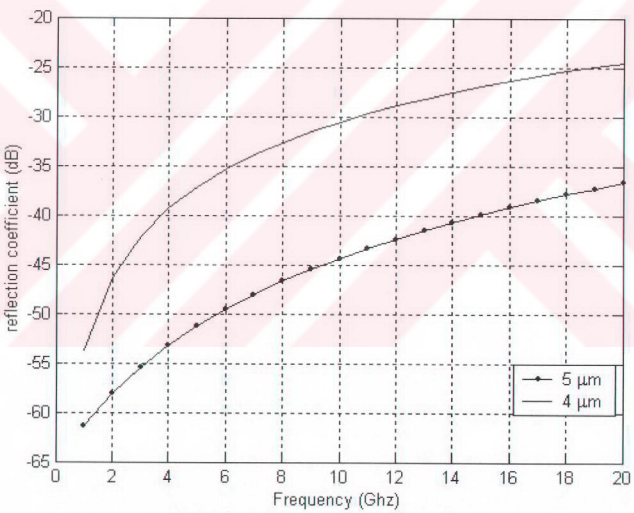

Figure 3.33: Reflection coefficient vs. frequency plot for bridge type loaded line phase shifter.

Insertion loss vs. frequency plots for these cases are presented in Figure 3.34. Insertion loss of the 4 μm high bridge case is more since it has worse reflection coefficient. Therefore, it is possible to say that having a phase shifter with good reflection coefficient would mean having a phase shifter with better insertion loss leading to a design with better insertion loss per degree. However, these insertion loss values are for a 0.8 mm length of line. For the actual length of line they should be multiplied by 27.875, which is the ratio of original line length to simulated line length. For example insertion loss of the simulated phase shifter for a bridge height of 4 μm at 10 GHz is approximately 0.07 dB. Then insertion loss of the original phase shifter is 1.95 dB. However, there is one thing to note. Generally, insertion loss is due to the reflection from the phase shifter, and reflection coefficient does not change with line length very much. What is increasing with line length is the per unit length loss of the CPW. Therefore, it is expected to have lower insertion loss value for the original phase shifter.

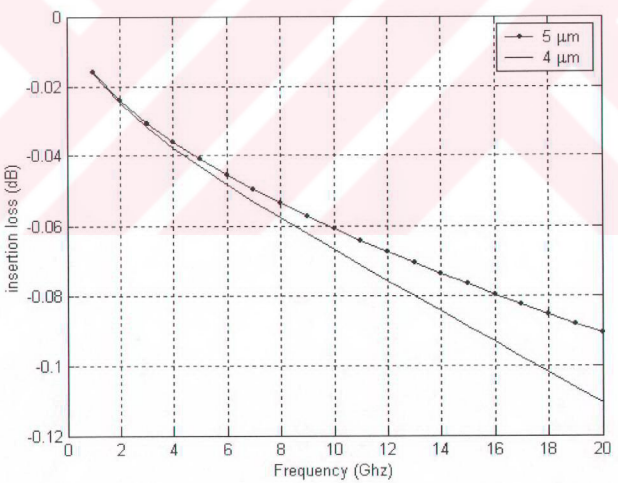

Figure 3.34: Insertion loss vs. frequency plot for bridge type loaded phase shifters.

As given in Section 3.2.1, insertion loss per degree is obtained by dividing the total insertion loss to the total phase shift. Total phase shift, which is given in Figure 3.36, is obtained by subtracting the insertion phase at 4 μm from the insertion phase at 5 μm. Their magnitude is linearly increasing with frequency as seen in Figure 3.35. Also magnitude of phase shift is increasing linearly with frequency. However the values given in Figure 3.36 are for 0.8 mm length of phase shifter. For the original case they should be multiplied with 27.875, which is the ratio of original line length to simulated line length. This leads to a phase shift of 34.8° at 10 GHz corresponding to 1.25° simulated phase shift. In order to increase this total phase shift value, the magnitude of load capacitance that can be added in a tunable manner should be increased. To achieve this an alternative capacitance loading structure is proposed, which is explained in the following paragraphs.

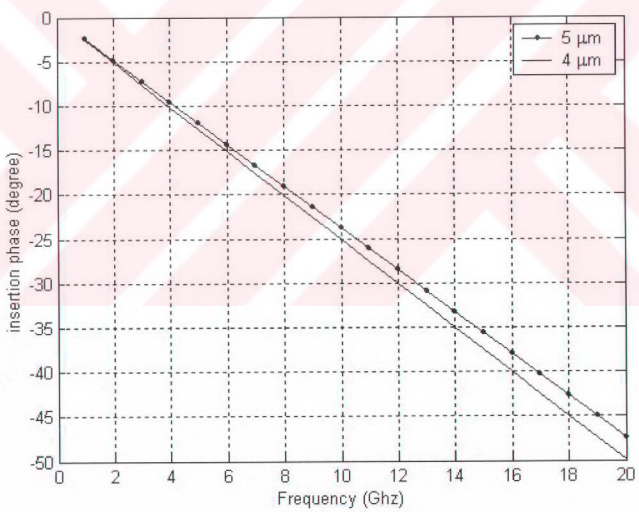

Figure 3.35: Insertion phase vs. frequency plot for bridge type loaded line phase shifter.

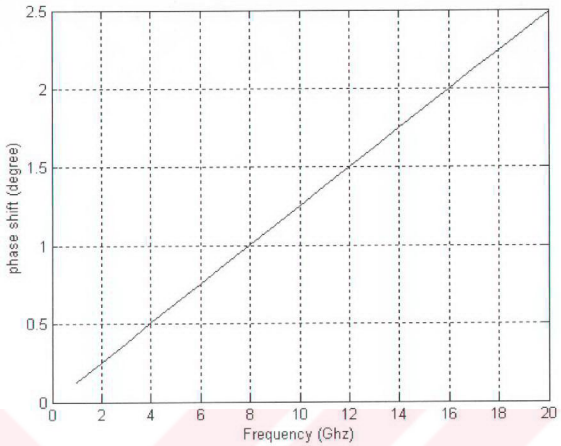

Figure 3.36: Phase shift for bridge type loaded line phase shifter. Bridge height changes from 5 microns to 4 microns. Phase shift data is obtained for a line of 2 mm length. Actual phase shifter is 20 mm in length so the actual phase shift is 11 times the simulated phase shift.

In order to increase the amount of tunable loading capacitance a new switch structure was designed for the first time in the literature. This structure, which is named as T-wing switch due to its T shape, was proposed as an alternative loading capacitance to the standard bridges, because loading the CPW with a large load capacitance using bridges was not easy. When CPW is loaded with large capacitance, signal line has to be narrowed in order to increase the unloaded characteristic impedance to compensate for the capacitive loading. Since the capacitance is between the bridge and the signal line for bridge type switches, narrowing signal line leads to a decrease in loading capacitance. However, T-wing switches have capacitances between the wings and the ground planes, which are

independent of the signal line width. Hence, narrowing signal line width is not a problem in terms of loading capacitance for T-wing type switches. Therefore, it is possible to load the CPW with larger capacitance using T-wing switch without being affected by a narrow signal line.

Although it is possible to load the line with large capacitances by using a narrower signal line, signal line cannot be narrowed below a certain limit. Limiting issues for the signal line width are practical issues such as implementation and testing. When the signal line is narrow it becomes very difficult to implement it in an error free and repeatable fashion. Any error on the line width causes large variations in the characteristic impedance leading to degradation in performance. Also narrow signal line is hard to get a connection for testing. Therefore, signal line should have a width that is large enough to be tested and implemented. Three-dimensional model and dimensions of the phase shifter structure for such a signal line width is given in Figure 3.37.

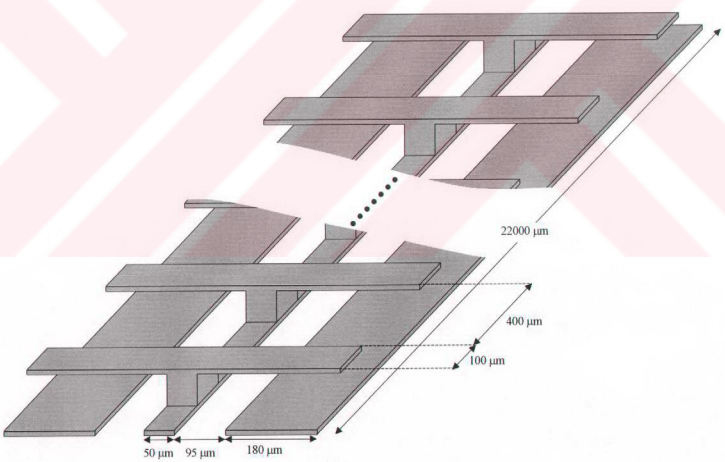

Figure 3.37: Three-dimensional view of the loaded line phase shifter that uses T-wing switches for capacitive loading.

Simulation results for a small portion of this structure are given in the figures below. This small portion of phase shifter contains 4 T-wing switches instead of 44 switches. Its length is 2 mm instead of 22 mm. Therefore, the scaling factor is 11. While considering the results for the whole phase shifter, this scaling factor should be taken into account.

Reflection coefficient vs. frequency plot of the phase shifter given in Figure 3.37 is shown in Figure 3.38. As seen from Figure 3.38 when the bridge height is decreased, reflection coefficient is increased. Effect of this increase in reflected signal can also be observed in the insertion loss vs. frequency plot given in Figure 3.39. As reflection coefficient increases, insertion loss increases. This degradation in performance is due to the decrease in characteristic impedance due to capacitive loading. As explained in the bridge loaded phase shifters, the designer should make the initial state of the phase shifter matched to an impedance slightly greater than reference impedance so that reflection coefficient does not vary so much with loading capacitance.

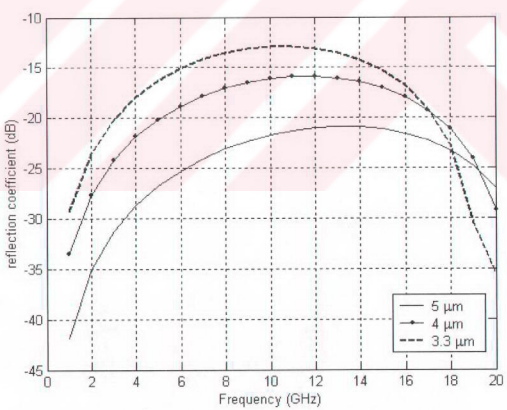

Figure 3.38: Reflection coefficient vs. frequency plots for the T-wing type loaded line phase shifter.

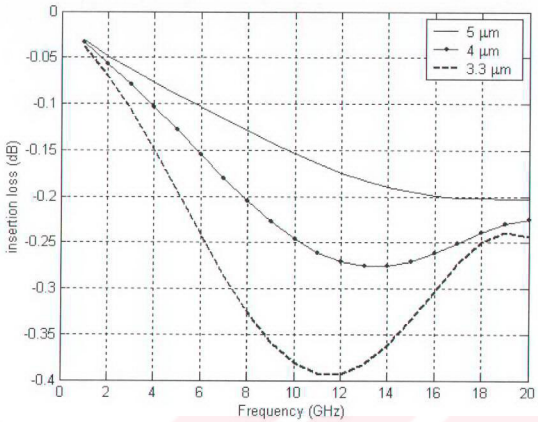

Figure 3.39: Insertion loss vs. frequency plots for T-wing loaded line phase shifter.

Insertion phase vs. frequency plots for three different wing heights are given in Figure 3.40. Resulting Phase shift plots are given in Figure 3.41. As seen from these figures, phase shift is almost linearly increasing with frequency, which means that the device is non-dispersive. Also one other thing to note is that magnitude of phase shift is changing nonlinearly with the change in wing height. When the change in wing height is 1 μm, phase shift at 20 GHz is 11.9 degrees. When it is 1.7 μm, phase shift at 20 GHz is 24.3 degrees. Therefore, if the height of the bridge is decreased more, phase shift can increase significantly. However 3.3 μm is the final point that the wing height can go down, because below this value pull in occurs. This means that the designer should calculate the maximum available phase shift for a height that is above the pull in height. If this height is taken as 4 μm then the maximum available phase shift for the simulated phase shifter at 10 GHz is approximately 6^{o}. When this number is multiplied by 11, which is the scaling factor between the simulated and the original phase shifter, total phase shift is found as 66^{o}.

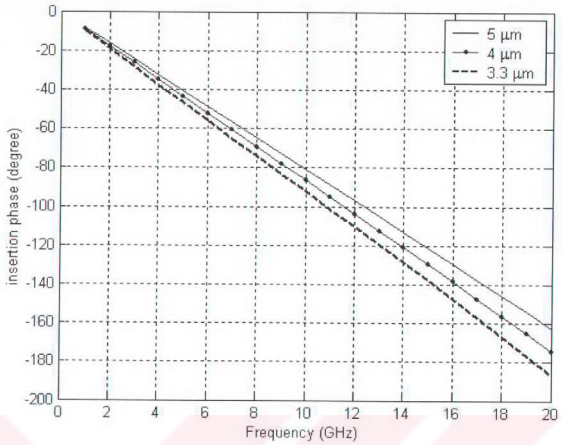

Figure 3.40: Insertion phase of the T-wing type loaded line phase shifter.

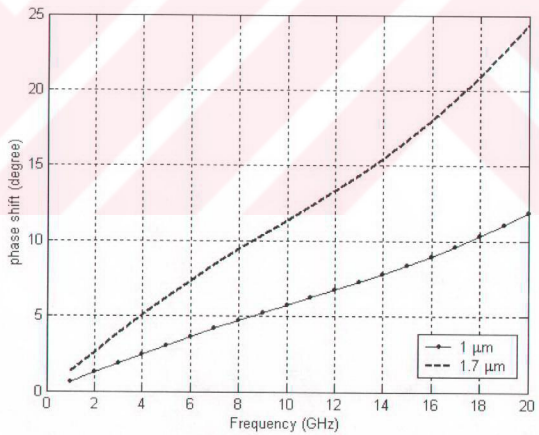

Figure 3.41: Phase shift for T-wing type loaded line phase shifter.

When the simulation results for the bridge type capacitance loaded and T-wing type capacitance loaded phase shifters are compared, it is observed that T-wing type phase shifter has more insertion loss, but it can give twice the phase shift of bridge type phase shifter. In fact insertion loss in the T-wing type phase shifter is mostly due to reflection coefficient. This means that when reflection coefficient is decreased by a better design insertion loss in the T-wing type phase shifters can have as low a value as that of bridge type phase shifters. However bridge phase shifters cannot give as much phase shift as that of T-wing type phase shifters for a unit length. Therefore, T-wing type phase shifters can be assumed to have better performance than the bridge type phase shifters especially in terms of maximum available phase shift. Maximum available phase shift of T-wing type loaded line phase shifter is 66^{o} at 10 GHz for 1 μm displacement, but it is only 34.8^{o} for the bridge type loaded line phase shifter.

However these values are only a portion of the whole cycle, which is 360^{o}. In order to obtain the whole cycle, length of the phase shifter should be increased to 120 mm for T-wing type phase shifter or 200 mm for the bridge type phase shifter. However these lengths are impractical. Therefore, there is a need for phase shifters that can give large phase shifts in small areas. Discrete phase shifters, which are explained in 3.2.3, are a solution to this problem.

3.2.3 Discrete Phase Shifter

Discrete phase shifters can give large phase shifts in relatively small areas. This is the reason for the need of a discrete phase shifter. In order to satisfy this need discrete phase shifters are designed and implemented in the course of this thesis. Design of these phase shifters will be explained in this section. First, design goals and methodology will be given. Then, the structure of the designed phase shifter will be given, and its operation will be explained. Then, parameters that affect the device performance and how these parameters affect the performance, will be explained. Finally, simulation results for the designed structure will be given.

Discrete phase shifter was designed to be used with a continuous phase shifter. By this way, it is possible to extend the performance of continuous phase shifter to a wider phase shift range. For example if a continuous phase shifter can give a maximum of 30° phase shift, then a discrete phase shifter with 30° steps can be used in combination with this continuous phase shifter to obtain large phase shifts in a continuous manner. This combination can be used to obtain a phase shifter that can scan the whole phase cycle continuously and that has a small area. In order to demonstrate the hybrid use, this discrete phase shifter was designed.

While designing the phase shifter, goal in the beginning was to make a phase shifter that has moderate performance values. Therefore, as a first step a functional phase shifter structure was proposed. The lengths of lines were adjusted to give 30° phase shift at 15 GHz. Then, in the limited time period this design was optimized. While optimizing the design, primary concern was to improve the RF performance rather than the mechanical performance. In order to achieve this, reflection coefficient was minimized. This is done by designing better switches, because most of the reflection is due to the switches. This concept is better understood in the following paragraphs where structure and operation of discrete phase shifter is explained.

Operation principle of discrete phase shifter is based on the switched line phase shifter explained in Section 2.3.1.1. It can be briefly explained as: signal path from input to output is switched through different length lines by means of switches in order to give desired phase shift. Important thing about this discrete phase shifter is how these lines are switched. In order to explain this, three-dimensional model of the discrete phase shifter is shown in Figure 3.42. As seen from the model, there are single-pole double-throw switches, which are explained in Section 3.1.2.2, placed symmetrically between input and output. These switches operate in pairs to ensure desired operation. Therefore, they are labeled as pairs on the model. When pair 1 is on, signal is transmitted through path 1. When pair 2 is on, signal is transmitted to the sideway. In this case if pair 3 is on, then signal is transmitted through path 2 and

if pair 4 is on, signal is transmitted through path 3. The length difference between each path is same and equal to 2*(90+480) μm. This difference can be adjusted to give desired phase shift steps. In fact this structure is a ladder type structure, and it can be repeated as much as desired to obtain as many steps as required. However increasing the number of steps degrades the performance of the phase shifter, which is explained in the following paragraphs.

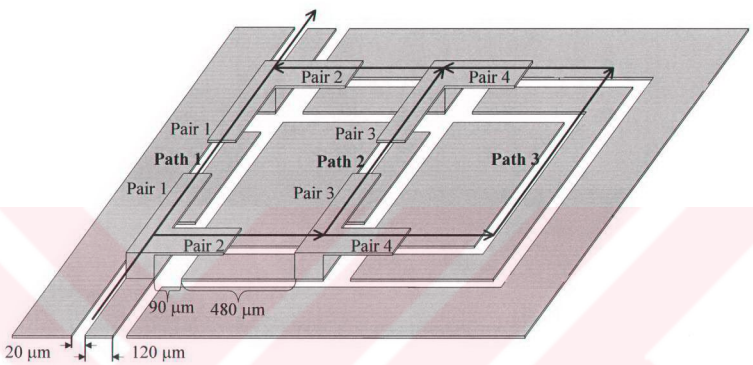

Figure 3.42: Three-dimensional view of the discrete phase shifter. Red lines represent the alternative signal paths. Difference between two paths is 2*(480+90) μm.

The switches mainly determine RF performance of the phase shifter, because remaining part is the CPWs, which do not have significant insertion loss or reflection coefficient values compared to switches. Therefore, reflection coefficient, isolation, and insertion loss optimization of the switches constitute most of the design.

Reflection coefficient of the switch directly determines the reflection coefficient of the phase shifter. In fact, total reflection coefficient can be approximated as the sum of two terms. First term is the reflection from the switch at

the input. Second term is the reflection from the output switch reduced by the amount of insertion loss of the input switch. This term also has a phase component relative to the first component due to the insertion phase of the input switch and the CPW between two switches. In fact, if this phase component is adjusted properly, it can make a canceling effect reducing the reflection coefficient.

Isolation of the switch is important in terms of multipath effect. The signal that leaks to the other port of the switch travels through the alternative path and reaches to the output with a different phase from the original path signal. These two signals are added at the output resulting in a signal with different phase from the original path signal. This effect can be named as the multipath effect. It means a changing output phase with the isolation of the switch. Since isolation of the switch changes with frequency, it creates an insertion phase that is nonlinearly changing with frequency.

Insertion loss of the switch directly adds to the insertion loss of the phase shifter. Since CPWs do not have significant losses, it can be assumed that insertion loss of the phase shifter is equal to the sum of the insertion losses of the switches used. It is twice the insertion loss of a switch for path 1 in Figure 3.42. However, it is 4 times the insertion loss of a switch for path 2. For every additional step 2 switches are added to the path increasing the insertion loss. For this reason, having many steps degrades the performance of the phase shifter.

In order to observe the above stated effects of switch performance on the device, performance simulations of the discrete phase shifter was made. Simulated model, which is given in Figure 3.43, is a simpler version of the discrete phase shifter. Path 2 is directly completed by a CPW instead of a switch to simplify the simulation. The results for this simplified model are given in the following paragraphs and figures.

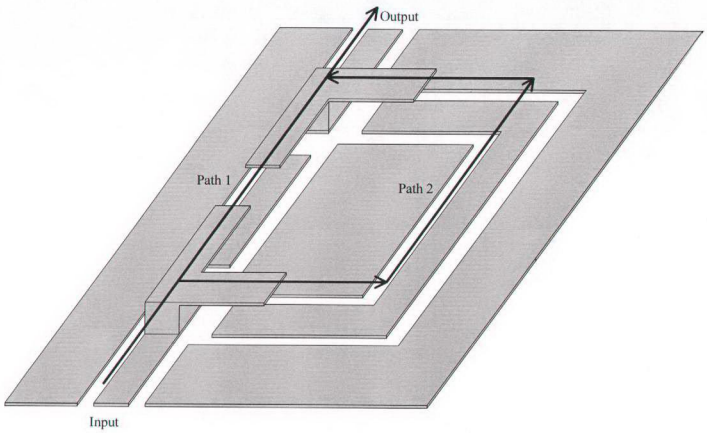

Figure 3.43: Simulated discrete phase shifter structure. Only one step of phase shift is simulated to simplify the problem hence reduce the problem size.

Reflection from the phase shifter for path 1 and path 2 is given in Figure 3.44. When the signal travels through path 2, reflection coefficient makes a dip around 9 GHz. This is due to the canceling effect of the reflection from path 1 due to the negative phase of this reflection term. When this canceling effect turns into an additive effect, reflection coefficient becomes larger than the path 1 reflection coefficient, which is observed above 15 GHz.

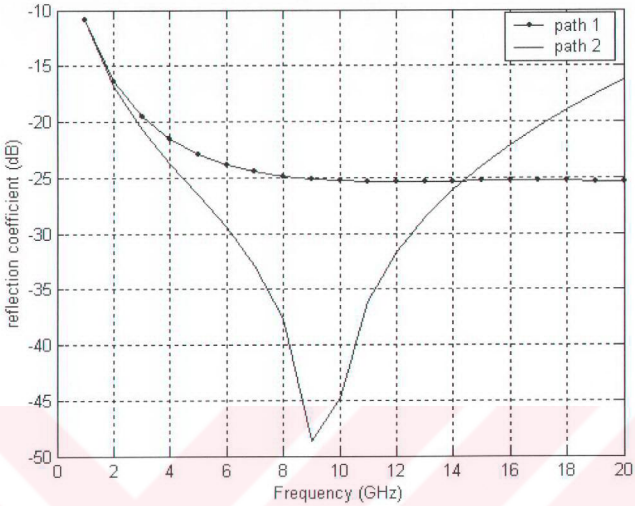

Figure 3.44: Reflection coefficient vs. frequency plot for discrete phase shifter. Dot marked line is the reflection coefficient when the signal flows from path 1, which is the shorter path in the phase shifter. Continuous line is for path 2.

Insertion loss of path 2 is larger than the insertion loss of path 1 which is given in Figure 3.45. This difference between two insertion losses is due to two terms. First term is the different insertion loss values of the switch for direct port and 90^{o} rotated port, which is given in Figure 3.12. Second term is the loss due to 90^{o} corners on path 2. In the actual case there are switches in these corners, and their insertion loss is taken as the second term.

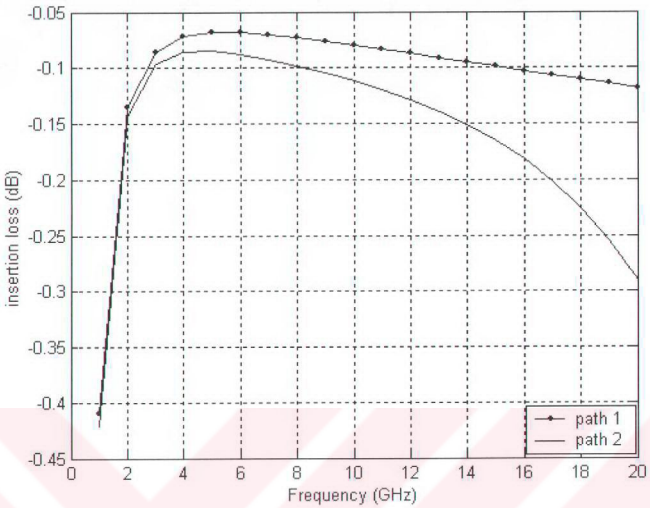

Figure 3.45: Insertion loss vs. frequency plot for discrete phase shifter.

Insertion phase for both of the paths show a nonlinear behavior at low frequencies as can be observed in Figure 3.46. This nonlinear behavior is due to the multipath effect caused by the isolation of the switch as was explained previously in this section. Since isolation of the switch, which is given in Figure 3.14, becomes small at low frequencies and rapidly increases as frequency increases, multipath effect rapidly decreases with frequency leading to a nonlinear insertion phase. However since multipath effect is equal for both paths the difference between these two insertion phases is not affected from this nonlinear behavior. It can be observed in Figure 3.47 that the difference between two insertion phases is linearly increasing with frequency.

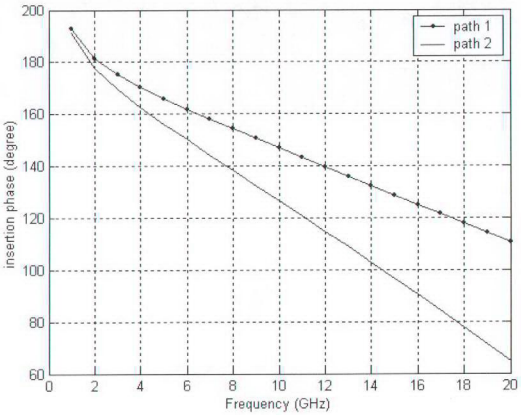

Figure 3.46: Insertion phase vs. frequency plot for discrete phase shifter. Data is obtained at integer frequencies. For this reason nonlinear behavior in the insertion phase is observed as a sharp edge at 2 GHz.

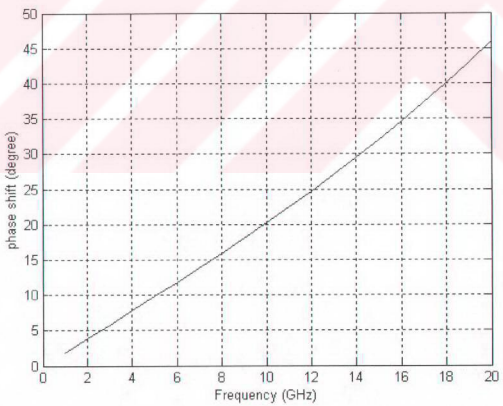

Figure 3.47: Phase shift vs. frequency plot for discrete phase shifter.

It can also be observed in Figure 3.47 that the phase shift is very large compared to continuous phase shifters. Since this was the primary goal in designing a discrete phase shifter, it is possible to say that primary design goal is reached. In the following section, design goals and methodology for all of the RF MEMS structures will be summarized.

3.3 Summary

Design information given in this chapter can be classified in four different groups. These groups are series switches, parallel switches, continuous phase shifters, and discrete phase shifters. Summarized information about each group is given in the following paragraphs.

1. Series switches have large impedances at the off state mostly composed of a capacitance. This capacitance depends on the width and length of the overlapping area of the beam and the signal line of the output port. Decreasing capacitance improves the RF performance of the switch. However it also degrades the mechanical performance by increasing the pull in voltage. On state impedance has a very small value, which is mainly determined by the on state capacitance. Increasing this capacitance improves RF and mechanical performance but causes degradation in the off state RF performance. It can also lead to breakdown, which may damage the switch. Therefore, the designer cannot improve all aspects of performance at the same time due to these design trade offs. He should make a compromise between these trade offs.

2. Similarly, increasing on capacitance improves the on state RF performance but degrades off state RF performance, and decreasing off state capacitance increases off state RF performance but degrades on state RF performance and mechanical performance for the parallel switch. Hence, these trade offs should be balanced according to the design requirements.

3. Continuous phase shifters use loaded line principle to supply phase shift. Periodically spaced capacitive switches give this capacitance. Off state capacitance of these switches make an initial loading on the CPW reducing its capacitance. To cancel this initial loading effect CPW impedance should be designed to be larger than the desired impedance value. Also this desired impedance value should be a bit larger than the reference impedance. Since the loading capacitance increases as the amount of phase shift increases, impedance of CPW will decrease and become closer to the reference impedance as the phase shift increases.

4. Switch design is the most important issue in the discrete phase shifter design, because most of the performance criteria is determined by the performance of the switches. After a good switch design, line lengths of the discrete phase shifter paths can be altered to reduce the reflection coefficient using phase cancellation effect.

Many useful design information is given in this chapter in addition to those summarized in the previous paragraphs. Also simulation results for the designed structures are given to give the reader an intuition about the device behavior and performance.

In the following chapter fabrication of these structures will be explained in detail.

CHAPTER 4

FABRICATION OF RF MEMS SWITCHES AND PHASE SHIFTERS

This chapter describes the fabrication process of the RF MEMS switches and phase shifters. Section 4.1 gives brief information about the general device structure and a brief flow of the fabrication process for the implementation of the structures. Section 4.2 gives information about the deposition and patterning of first metal and the isolation layer and the specifications on these steps for a successful device fabrication. Section 4.3 describes the sacrificial layer formation, the second metal layer deposition using electroplating process, and release of the structures by removing the sacrificial layer. This section also explains the critical points in these steps that are important in terms of the performance of the resulting structures. Section 4.4 summarizes the information given in this chapter.

4.1 General Device Structure

All of the devices presented in this thesis are formed of two metal layers and an isolation layer. They are all produced on the same substrate, which is Corning 7740 glass (Pyrex). These layers are presented for a sample structure, cross section of which is given in Figure 4.1.

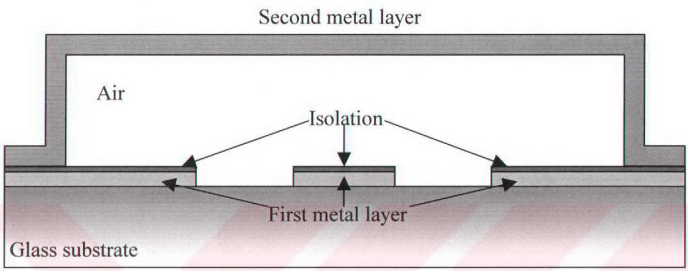

Figure 4.1: Cross section of a sample structure. Region defined as air is initially filled with a sacrificial layer, which is removed at the end of the process.

In order to obtain such a structure, the process, whose general steps are given in Figure 4.2, is used. First Metal 1 layer is deposited using evaporation and patterned using lift off. Then Isolation layer is deposited wit PECVD technique and patterned using etching. Then sacrificial layer is deposited and patterned. After sacrificial layer second metal layer is deposited and patterned. As the final step sacrificial layer is removed and the structures are released.

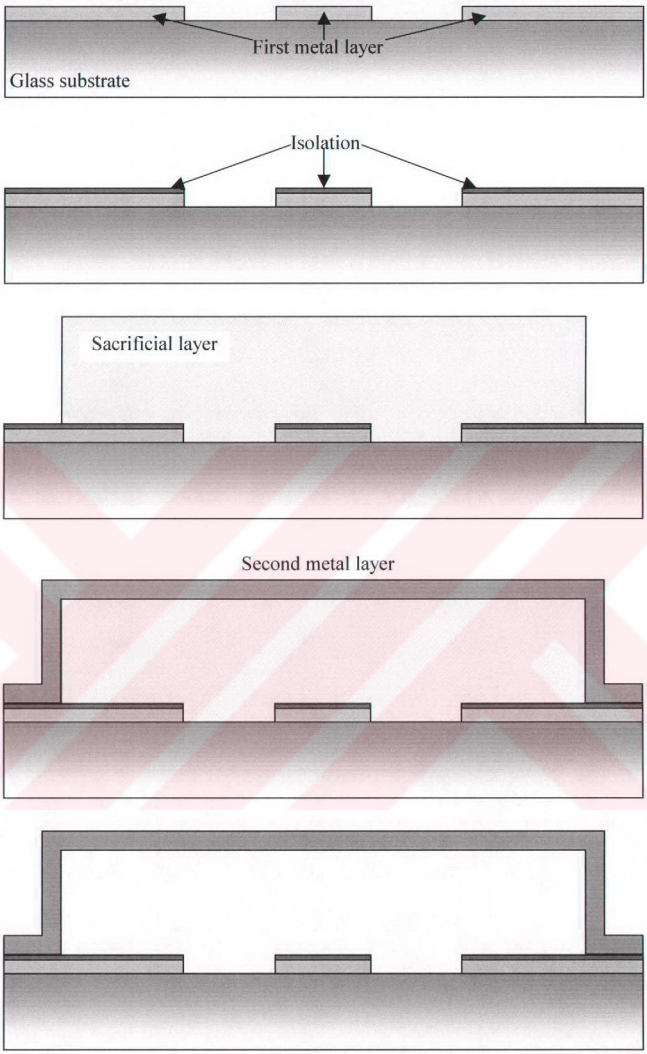

Figure 4.2: General process flow for the fabrication of RF MEMS devices.

First metal layer is mainly used for defining the CPWs. Its conductivity and thickness is important in terms of resistive losses in the CPW. It should have a high conductivity and also sufficient thickness, which is larger than the skin depth for the operation frequency. This layer is also used for defining the routings for DC actuation and the pads to which these routings are connected. These pads are used to make connection to the external world.

Isolation layer is used for DC isolation between the upper metal plate and lower metal plate, which are used for electrostatic actuation. Its dielectric constant is important since it directly affects the on state capacitance for the switches hence the RF performance. Also thickness of this layer affects the value of this capacitance and the maximum applicable DC voltage together with the breakdown voltage of the dielectric.

Second metal layer is used to form the bridges, beams, and wings, which are the movable parts of the system and, which make the switching action by bending from an up state to a down state. It is also named as the structural layer. This layer mainly affects the mechanical properties of the devices. Its thickness and stiffness directly affects the value of pull in voltage.

Besides the above stated layers there is an additional layer, which is used during processing, and then removed at the end. It is named as the sacrificial layer. It is used to support the structural layer during processing. Then it is removed and replaced by air at the end of the processing. It is the air region below the bridge in Figure 4.1. Its thickness and uniformity directly affects the off state capacitance hence the RF performance of the switches.

4.2 First metal layer and isolation layer

First metal layer is the layer, which CPWs are made of. Most of the signal transmission is preformed on this layer. Therefore, its resistive losses should be minimized to increase device performance. In order to achieve this, its conductance

should be chosen high, and its thickness should be kept large so that its sheet resistance is decreased. First specification limits the types of metals to good conducting ones such as copper, gold, silver or aluminum. Among these metals gold is the only one that is not oxidized. Since oxidation changes the resistance very much, gold is preferred for the first metal layer.

Gold is deposited by evaporation technique. However direct coating of gold on a glass wafer is not possible, since gold does not adhere to glass surface well. In order to supply enough adhesion to the surface an adhesion layer, which adheres to both glass and gold, is used. In our case this layer is chromium. Therefore, first chromium is coated over the wafer surface, and then gold is coated on the chromium surface.

Patterning of chromium gold (Cr/Au) layer is done by the lift off technique. Patterned Cr/Au layer is desired to be 1 μm. 0.1 μm of this 1 μm is Cr and remaining 0.9 μm is Au. In order to make lift off with such a thick metal, the underlying photoresist thickness is made 4 μm. However while removing the unwanted metal on this photoresist using an ultrasonic cleaner some residues were left on the sides of the lines. Also some of the Cr/Au layer that was supposed to adhere to the surface were peeled off the surface. This leads to two conclusions. First conclusion is that step coverage of the evaporated metal is so good that it cannot be easily broken during lift off. Second conclusion is that adhesion to the surface is not good so metal peels of the surface in some regions. In order to eliminate these problems a short glass etching is made to the wafers before evaporation. This glass etching makes the surface rough and also makes some extra step height and undercut. A rough surface increases adhesion hence solves the second problem. As seen in Figure 4.3 this height difference and undercut helps to weaken the step coverage of the metal hence solves the first problem. Therefore, after glass etching lift off problems are solved, and a successful lift off is made.

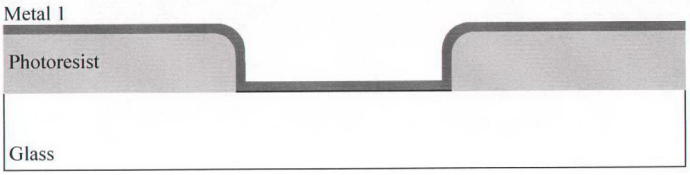

(a)

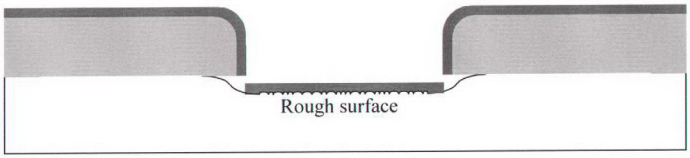

(b)

Figure 4.3: Standard way of lift off is given in (a). In order to have good adhesion and reduced step coverage, a short glass etch is performed before evaporation. Resulting cross section is given in (b). Glass surface at the etched places are rough. Also undercut reduces step coverage. It is drawn as if the step is already broken as an exaggerated case.

After depositing and patterning the first metal layer successfully, next step is to deposit the isolation layer and pattern it. Isolation layer should be a dielectric material with high dielectric constant. Also it should have a high breakdown voltage. In the design stage it is chosen as silicon nitrate (Si_3N_4). Si_3N_4 is chosen since it is a durable material, which can survive the later processing steps. It has a relatively high dielectric constant of approximately 7.

Deposition of Si_3N_4 is performed by Plasma Enhanced Chemical Vapor Deposition (PECVD) technique. Etching technique is used to pattern Si_3N_4. Transene Transetch N Si_3N_4 etchant is used to etch Si_3N_4. Since Si_3N_4 is a transparent material, it is not possible to understand if it is etched or not by observing

a color change. Therefore, precise timing, calculated using the etch rate of the Si_3N_4 etchant, should be made to perform precise etching. Otherwise there would be undercut which is observed by means of a microscope.

After patterning Si_3N_4 deposition of sacrificial layer and second metal layer steps follow. They are explained in the next section. Also the whole process flow including the steps given above is explained in detail in appendix A.

4.3 Sacrificial Layer and Second Metal Layer

Photoresist (S1828) is used as the sacrificial layer in the process. Reasons for using photoresist are ease of patterning and ease of removal at the end of the process. However it also has a drawback. It cannot withstand high temperatures without deformation. Therefore, high temperature steps are not allowed after sacrificial layer deposition. In fact there is only one step remaining after sacrificial layer deposition. It is the deposition of second metal layer.

Second metal layer is deposited by electroplating. In order to perform this, a thin seed layer is deposited using sputtering initially. Thickness of this seed layer should be 0.2-0.3 μm. If it is thinner, it is observed that nonuniform electroplated metal thicknesses are obtained at different places of the wafer due to the high resistance of the thin seed layer. Also deposition temperature of the seed layer is important. If it is high, photoresist is deformed and if it is low adhesion of the seed layer to the surface is reduced. In fact deposition temperature is kept at 120°C which is the maximum temperature that sacrificial photoresist can withstand.

After deposition of seed layer, second metal pattern is transferred on the seed layer. Then electroplating is done. During electroplating, density of the applied current determines the plating rate. It should be fine tuned together with the electroplating time to obtain a desired thickness.

After electroplating, photoresist on the top is removed with acetone. Then seed layer under the photoresist, which remained unplated, is etched. Etchant of the seed layer should be selective to the electroplated metal so that it does not etch the structures.

After the seed layer is etched, remaining sacrificial photoresist is removed with acetone. While removing the sacrificial photoresist one should be careful not to damage the structures since they are very fragile when they are released. Also an important point in sacrificial layer removal is stiction due to surface tension of acetone used in photoresist removal. In order to prevent stiction wafer is immediately dipped into prophanol to dissolve acetone. Then it is dipped into hot methanol to dissolve prophanol and then dried. Since methanol has low surface tension and evaporates easily, stiction problem is reduced. After methanol is dried release process is completed which ends the fabrication process.

4.4 Summary

Fabrication process for RF MEMS switches and phase shifters is composed of three layers. First one is Metal 1, which is first metal layer that defines CPWs. Second one is isolation for DC isolation of electrostatic actuation plates. Third one is Metal 2, which is the second metal layer for producing beams and bridges.

Brief flow of process is given as

1. Pattern transfer of Metal 1 mask.
2. Short glass etching for better adhesion and increased step height.
3. Evaporation and lift off.
4. Si_3N_4 deposition using PECVD and patterning using Transene Transetch N.

5. Sacrificial resist deposition and pattern transfer to define posts.

6. Seed layer deposition with sputtering.

7. Pattern transfer on seed layer to define beams and bridges.

8. Electroplating.

9. Photoresist removal and seed layer etching.

10. Sacrificial layer removal

Detailed flow of the process is given in appendix A. However this process flow is not the final process flow since it can be optimized for better performance. Also it can be altered so that different device structures can be constructed or the process can be merged with MMIC or CMOS processes to fabricate integrated systems.

After devices are fabricated using the fabrication process that is briefly described in this chapter they are tested. Test results and comments on them are given in the following chapter.

CHAPTER 5

FABRICATION AND TEST RESULTS

In this study different RF MEMS switches and phase shifters were designed and implemented. Components are designed according to the information given in chapter 2 and 3, and they are fabricated according to the fabrication procedure given in chapter 4. Section 5.1 gives the fabrication results for the implemented structures. Section 5.2 gives the test results for these structures.

5.1 Fabrication Results of the Implemented Structures

Structures were fabricated using the micromachining facilities at METU. First, masks were generated using the layouts drawn in the computer. Then RF MEMS switches and phase shifters were fabricated on the same wafer, which is corning 7740 glass. Properties of corning 7740 glass is given in Table 5.1 together with the other materials used in implementation of the structures.

Table 5.1: Properties of the materials used in the implementation of the structures.

Material	Place used	Conductivity (Siemens/m)	Relative permittivity	Loss tangent
Corning 7740 Glass	Substrate	NA	5.75	0.005
Gold	First metal	$4.1*10^7$	NA	NA
Silicon Nitrate	Isolation dielectric	NA	7	
Nickel	Structural metal	$1.45*10^7$	NA	NA

Figure 5.1 shows the scanning electron microscope (SEM) photograph of the series capacitive switch. As seen from the figure connection of beam to post is not sharp but has a smooth curvature, which reduces the pull in voltage. Similar curvature is also seen in the SEM photo of the T-wing type switch given in Figure 5.2. Closer view of this curvature is presented in Figure 5.3. This curvature is due to the rounding of sacrificial photoresist during hard bake.

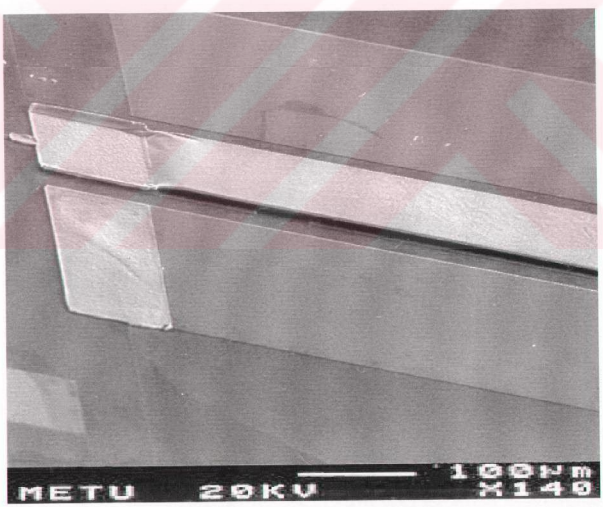

Figure 5.1: SEM photograph of the series capacitive switch.

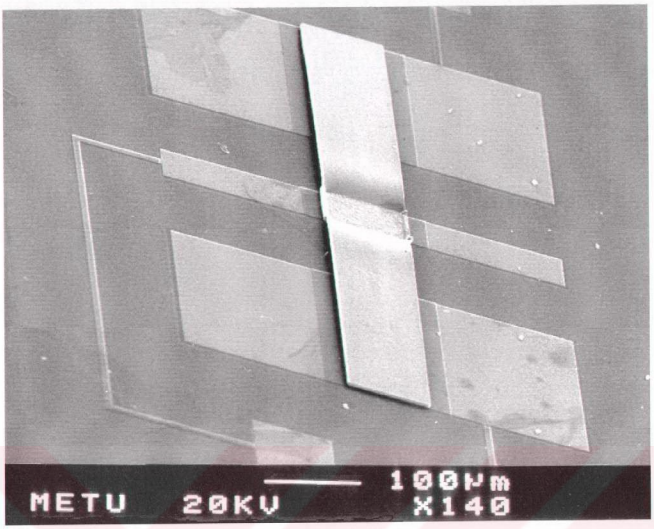

Figure 5.2: SEM photograph of the T-wing type switch.

Figure 5.3: SEM photograph of the anchor point of a T-wing switch.

Figure 5.4 shows a portion of the loaded line phase shifter constructed using T-wing type switches. Switches are periodically placed over the CPW and are 5 μm above.

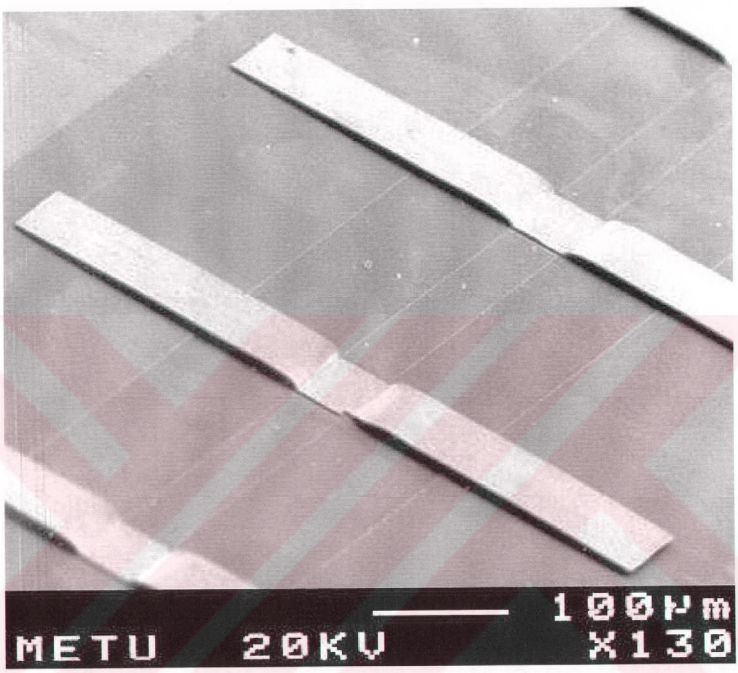

Figure 5.4: SEM photo of the T-wing type loaded line phase shifter.

5.2 Test Results

Devices are tested using the Cascade Microtech probe station and the HP 8720D 0.05-20 GHz vector network analyzer, which is seen in Figure 5.5. Calibration of the system was performed on a calibration substrate supplied by

Cascade Microtech. A full two-port calibration was performed in order to exclude the effects of the probes and additional transmission lines between the network analyzer and the devices.

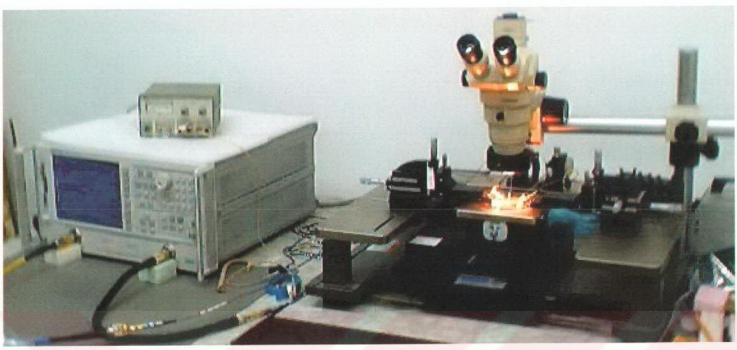

Figure 5.5: Photograph of the test setup. A phase shifter on the wafer is being tested by means of the probestation on the right and the network analyzer on the left. Actuation voltage is applied by the DC supply on the network analyzer.

5.2.1 Test results for Series Capacitive Contact Switch

Figure 5.6 gives the measured isolation for the off state of the series capacitive switch together with the simulation results. Simulation results mostly agree with the test results as seen from the figure. The reason for the small difference can be due to a sacrificial photoresist thickness that is slightly smaller than the desired value, which is 5μm. When sacrificial photoresist thickness is smaller off state capacitance increases leading to a decreased isolation.

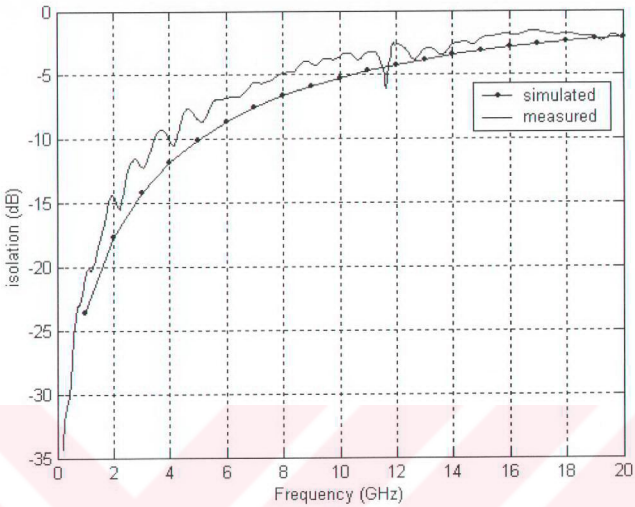

Figure 5.6: Isolation vs. frequency plot for the series capacitive switch.

Figure 5.7 shows the reflection from the series capacitive switch for the on state. As seen in the figure reflection coefficient is significantly lower than the simulated case. There are two reasons for this difference. First reason is the calibration error effect of which can be observed as a glitch in reflection coefficient characteristic around 11 GHz. Second reason is the roughness of the surface, which significantly decreases the on state capacitance. As this capacitance is decreased resonance frequency of the switch is shifted to 15 GHz for the tested case instead of 5 GHz for the simulated case. The roughness of the surface has mainly two parts. First part is the roughness of the deposited metallization and isolation layer. However this part does not have a significant effect on the total surface roughness. Second part, which is more important, is the roughness due to the residues on the surface. These are metals and photoresists, which could not be removed when

etching the seed metal layer and removing the sacrificial photoresist. These residual materials prevent a good contact between the surface of the isolation dielectric and structural metal. The space between these two surfaces due to poor contact reduces the capacitance significantly.

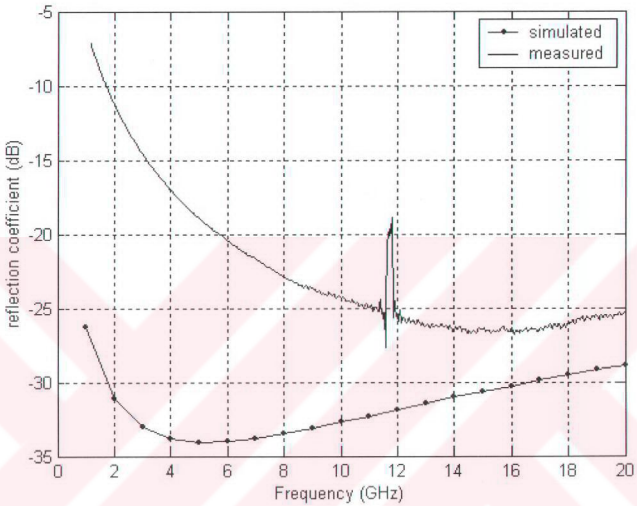

Figure 5.7: Reflection coefficient vs. frequency plot of the series capacitive switch.

This capacitance change more drastically affects insertion loss, which is given in Figure 5.8. As seen from the figure insertion loss is increased approximately five times. Therefore, surface roughness of the fabricated devices is very important in terms of RF performance. Also the effect of calibration error is seen in the figure as a glitch around 11 GHz.

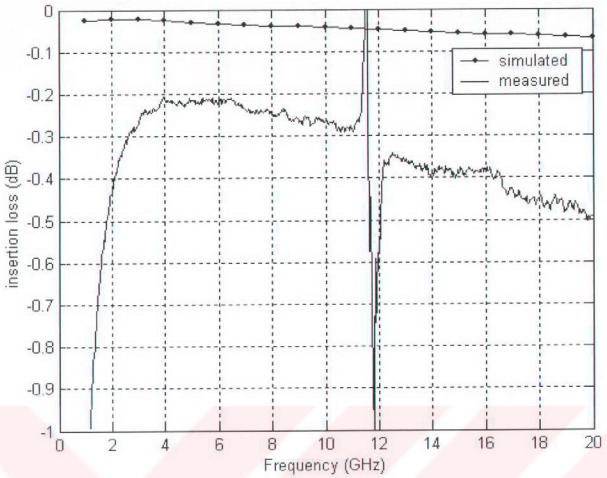

Figure 5.8: Insertion loss vs. frequency plot for series capacitive switch.

Measurement results for the single-pole double-throw switch, bridge type shunt switch, and T-wing type shunt switch could not be obtained, hence cannot be given in this thesis, due to the problems encountered in the fabricated devices.

First problem is that pull down voltage of the switch exceeded the breakdown voltage of the dielectric hence it was not possible to actuate the switch. There are two factors that cause this problem. First one is the quality of the deposited silicon nitride layer. Its breakdown voltage was expected to be 600V/μm but it actually is approximately 200V/μm. Second factor is the properties of the structural metal, which is electroplated nickel. Its stress gradient, which leads to bending of the beams, and Young's modulus, which determines the stiffness hence the pull down voltage of the beams are not optimized enough. If they are optimized it is possible to obtain an unbended beam whose stiffness is also known prior to design.

Second problem is the stiction of the beams to the base. This problem occurs during the removal of the sacrificial photoresist. The surface tension of the liquids used during the release process, pull the beam down and stick it on the base metal. When all of the beam sticks to the base metal elastic deformation occurs around the posts, which leads to a deformed structure even the beam is somehow released after the stiction. Therefore, it is not possible to obtain an undeformed beam to measure the off state performance of the switch.

Due to the problems above measurement results for the single-pole double-throw switch, bridge type shunt switch, and T-wing type shunt switch could not be obtained. In order to obtain successful results for these switches following items should be optimized in the process. High quality silicon nitride deposition. Electroplating without stress gradient. Release of the structures without stiction. These optimization steps are addressed as future work at the end of the thesis since it was not possible to optimize all of them in a limited time.

5.2.2 Test Results for Loaded Line Phase Shifters

Results for two loaded line phase shifters are given in this section. One of the phase shifters is phase shifter 2 in Table 3.1, and the other is phase shifter 3 in Table 3.1. Most important difference between them is the spacing between bridges. Phase shifter 2 has 200 μm spacing and phase shifter 3 has 400 μm spacing between bridges. Results for the T-wing type phase shifters could not be obtained due to the stiction of the beams on the base metal.

Reflection coefficient vs. frequency plot for phase shifter 2 is obtained for 8 different actuation voltage values. As seen in Figure 5.9 reflection coefficient does not change significantly for these actuation states. Similarly insertion loss, which is given in Figure 5.10, does not change much with the actuation voltage. In fact change in insertion loss with actuation voltage, which is given in Figure 5.11, is so small that it can be neglected. Therefore, it is possible to say that this phase shifter can give phase shift without changing the signal amplitude. However both reflection

coefficient and insertion loss are too far away from the desired values, which are given as simulated datas on the plots. There seems to be two reasons for this discrepancy between the simulated and measured results. First reason is the possible error in the calibration of the measurement setup. This calibration error leads to a frequency characteristic different from the simulated results as can be observed from the figures. Second reason is the lower spacing between the bridge and the signal line due to smaller sacrificial layer thickness. This decrease in spacing would reduce the characteristic impedance of the loaded line to a lower value causing impedance mismatch hence reflection.

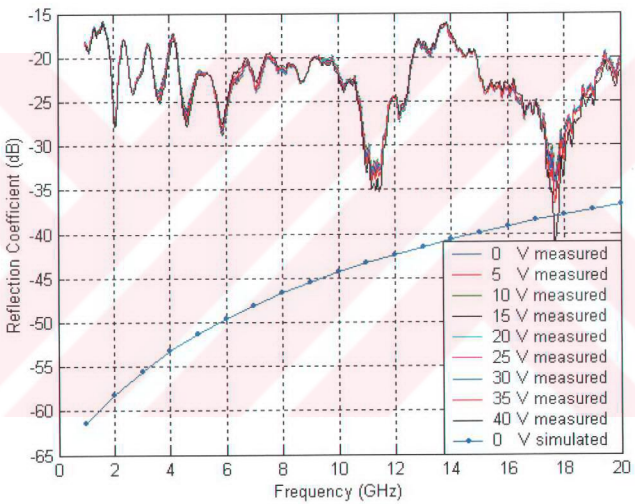

Figure 5.9: Reflection coefficient for different actuation voltages of a loaded line phase shifter

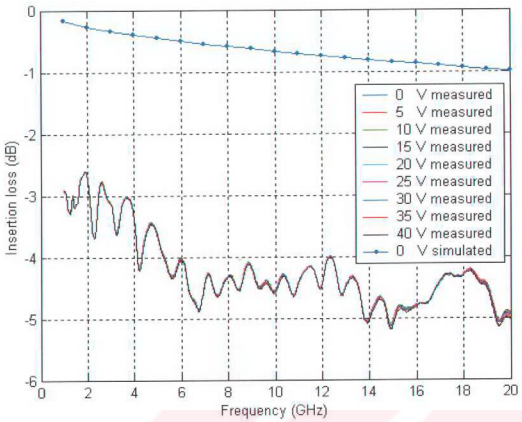

Figure 5.10: Insertion loss vs. frequency plot for different actuation voltages. 0 V is the no actuation case, where bridges have zero displacement.

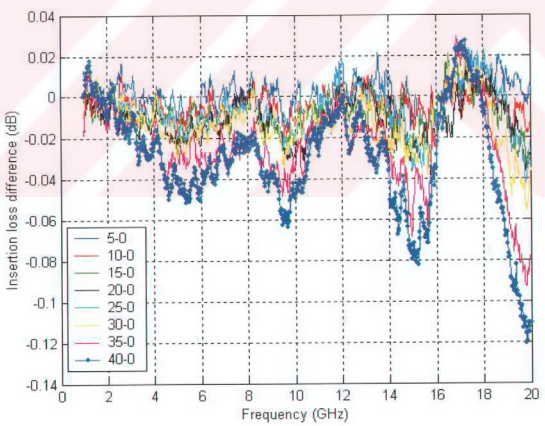

Figure 5.11: Difference between insertion losses of different actuation voltages and the insertion loss of no actuation state.

The different phase shifts obtained for different actuation voltages are given in Figure 5.12. As seen from the figure phase shift is almost linearly increasing with frequency. This means the phase shifter is a nondispersive one. Also one other thing is that the phase shift is nonlinearly increasing with the actuation voltage. This is due to the nonlinear change in the capacitance of the bridge with actuation voltage.

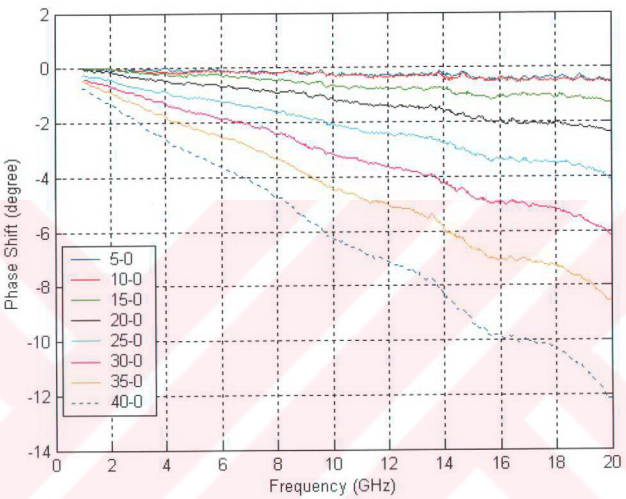

Figure 5.12: Phase shift for different actuation voltages.

Results for phase shifter 3 are similar to that of phase shifter 2. Reflection from the phase shifter 3 for the same actuation voltages is given in Figure 5.13. As seen from the figure it does not change significantly with actuation voltage. Also insertion loss given in Figure 5.14 does not change with actuation voltage. As seen from these figures reflection coefficient and insertion loss are similar in both phase shifters.

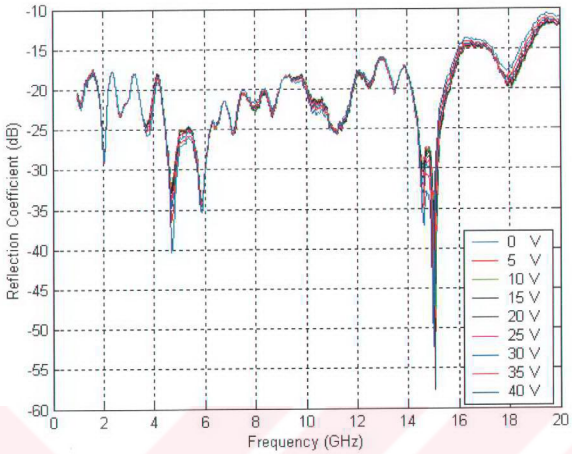

Figure 5.13: Reflection from phase shifter 3 for different actuation voltages.

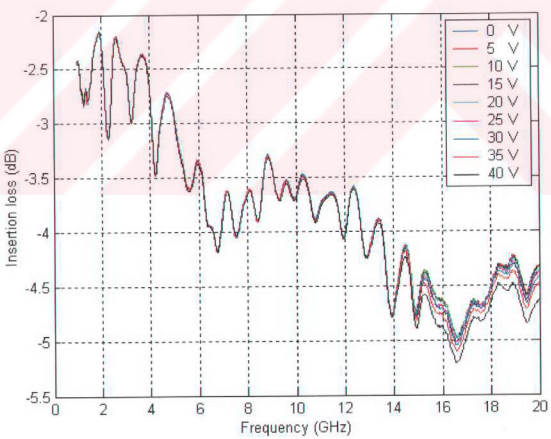

Figure 5.14: Insertion loss of phase shifter 3 for different actuation voltages.

Although insertion loss and reflection coefficient are similar in two phase shifters, phase shift values are different for two phase shifters. Phase shift of phase shifter 3, which is given in Figure 5.15, has similar characteristic with phase shifter 2, which is given in Figure 5.12, but slightly higher values. The reason for higher phase shift is the increased amount of deflection in the bridges of the phase shifter 3 for the same actuation voltage. Since the center line of phase shifter 3 is wider compared to phase shifter 2, it has more actuation capacitance hence more electrostatic force for the same actuation voltage.

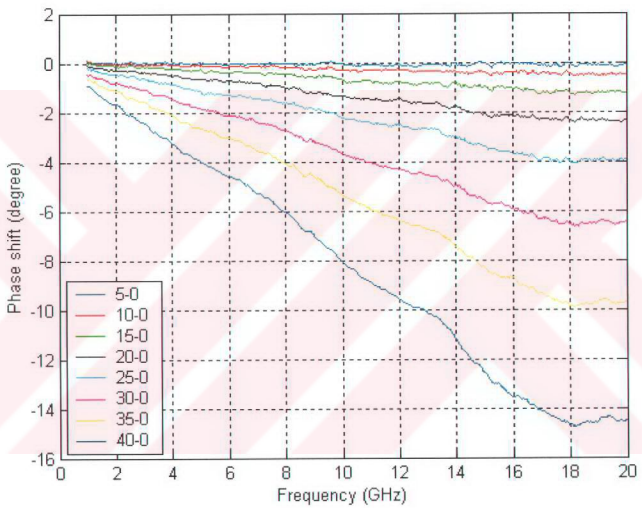

Figure 5.15: Phase shift of phase shifter 3 for different actuation voltages.

When phase shift from phase shifter 3 is compared with the simulated values, which is given in Figure 5.16, it is seen that measured data is almost one third of the simulated data. The reason is that measurements are performed up to 40V instead of

120V, which is the pull in voltage of the bridge. Hence, maximum available deflection is not used for phase shift, but only a small portion of it is used. However when the 40V actuated case is simulated for the bridge, it is observed that phase shift for 40V actuation is far below the measured phase shift. In fact Figure 5.17 shows the simulated and measured phase shift data for the 40V actuation. As seen from the figure when the unactuated bridge height is reduced to 4 μm from 5 μm, phase shift increases, and when it is reduced to 3 μm it becomes approximately equal to the measures case. From this result it is possible to say that actual bridge height is close to 3 μm instead of 5 μm.

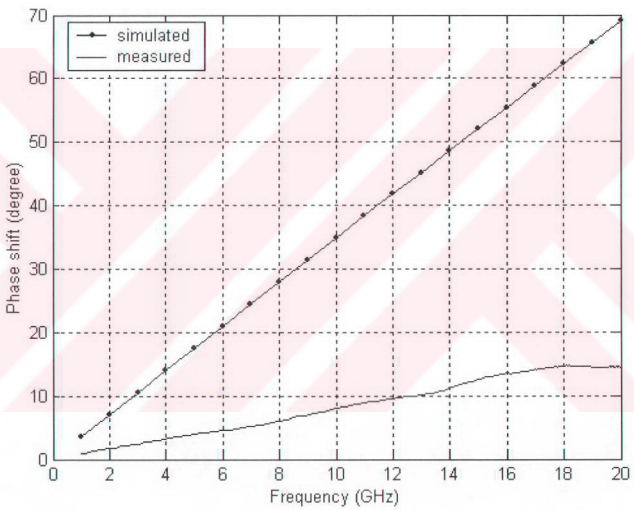

Figure 5.16: Phase shift for simulated and measured cases of phase shifter 3. Simulations are performed for a four bridge portion of the original phase shifter by decreasing the height from 5 μm to 4 μm, and this data is multiplied with ~28 as a scaling factor.

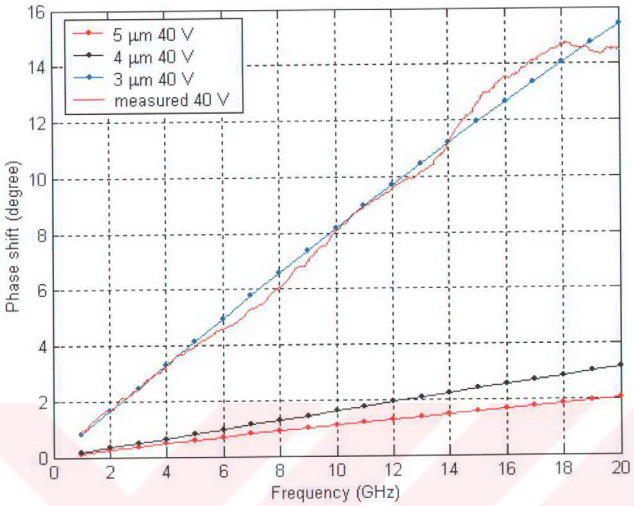

Figure 5.17: Phase shift values for phase shifter 3. Simulations are performed for three different bridge heights. Displacement for these heights for 40V actuation is obtained with Coventorware, and the actuated cases are simulated in HFSS, and phase shift data are obtained.

If we assume a 3 μm of bridge height then the reflection coefficient and insertion loss values become as the ones given in Figure 5.18 and Figure 5.19 respectively. As seen from these figures a bridge height of 3 μm makes the measured and simulated results to approach each other. Then it is possible to say that reflection and insertion loss measurements also lead to an implemented bridge height of 3 μm.

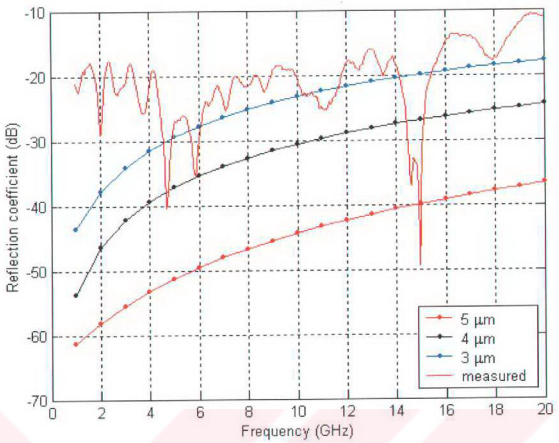

Figure 5.18: Reflection coefficient values for phase shifter 3.

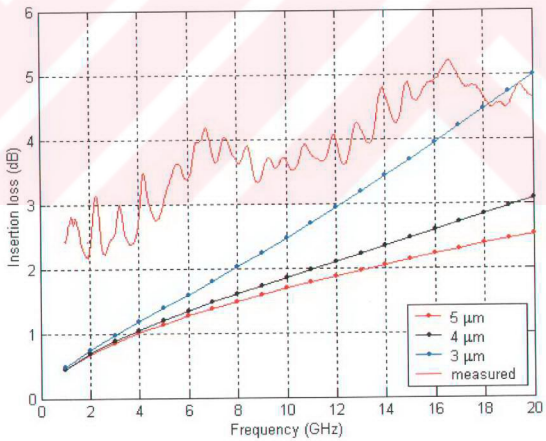

Figure 5.19: Insertion loss graph for phase shifter 3.

According to the measurements, there is a discrepancy between the measured results and the simulated results. This discrepancy has different sources. First one is the error due to calibration of the measurement setup. Second one is the error due to fabrication of the devices. Two of these errors are the difference between the designed and implemented thicknesses of the CPW metals and the spacing between the bridge and the CPW. CPW thickness was designed as 1 μm but it turned out to be ~0.1 μm. Spacing was designed to be 5 μm but it turned out to be 3 μm.

5.3 Summary and Conclusion of Fabrication and Test Results

RF MEMS switches and phase shifters were fabricated using the process given in chapter 4. Components were tested using a probestation and a network analyzer. Test results for the series capacitive switch and two different bridge type loaded line phase shifters were given. Results for the remaining three switch types, T-wing phase shifters, and discrete phase shifters could not be given due to the problems encountered during the fabrication of the devices.

Measurement results for the switch are close to the simulated value especially for the off state. The difference in the on state is mainly due to the extra capacitance introduced by the roughness of the contact surface and residual materials between the beam and the signal line. This roughness can be decreased by improving the process conditions, which is addressed as a part of the future research.

Measured results for the phase shifters are different from the simulated results. Specifically measured reflection coefficient and insertion loss is higher. The difference between the measured and simulated results is due to the calibration error and various fabrication errors.. Although measurement results of the phase shifter are different from the simulation results they indicate that they operate according to the operation principle. In other words their operation characteristic is as expected, which means that they are successful in operation; hence the objective of making a phase shifter is achieved. Further research is concentrated on improving the design.

CHAPTER 6

CONCLUSIONS AND FUTURE WORK

The research presented in this thesis involves the design and implementation of RF MEMS switches and phase shifters. However main objective of this research is to introduce RF MEMS technology to Turkey. In order to achieve this following targets were determined

1. Understanding the RF MEMS technology and devices by making a literature search about research on RF MEMS technology.
2. Fabricating previously implemented devices to understand the micromachining processes involved in the RF MEMS technology.
3. Developing a custom process that can be accomplished using the facilities at METU.
4. Introducing novel designs that are to be implemented using the developed process.

In order to achieve these goals two different switch structures were designed, and these switches were applied to different phase shifter structures. These switches and phase shifters were implemented according to the fabrication process developed in the scope of this thesis, using the microelectronics facilities of METU.

Based on the results obtained during this research, the following conclusions can be drawn.

1. During the design of RF MEMS switches and phase shifters an extensive search on the design of RF MEMS components was made. As a result of this research, valuable knowledge and experience was obtained. This experience and knowledge is recorded in this thesis in order to help the researchers in Turkey, who will do further research on the development of new RF MEMS components.

2. The designed switches and phase shifters were implemented using the microelectronics facilities at METU. A custom process was developed in order to implement these designs. Possible problems in a fabrication process were faced, and effects of the process errors due to these problems are observed. Development of this process introduces an important experience, which is very important in further designs. Basically design rules due to the process difficulties were developed using this experience. These rules are important in terms of designing components that does not have critical dimensions that will create problem during fabrication.

3. Implemented structures were tested by utilizing the facilities at the millimeter wave laboratory in the METU EEE department. The test results give valuable information, which is impossible to obtain through simulations. Effects of process errors were observed through measurements. Determining these effects is important in terms of making a design that can afford the possible process errors and also a design that is more immune to these errors.

4. In general this research constructed a knowledge base for the future research on RF MEMS technology in Turkey. This knowledge base is constructed using the information obtained from the literature search, the experience obtained from the design of the structures, the experience obtained from the development of the fabrication process, and the information obtained from the measurement results of the implemented structures.

Although extensive work has been done in order to design and implement the switches and phase shifters, there are some items that can be improved. Some of these items can be listed as:

1. More accurate models that include the nonideal behavior introduced by the fabrication process can be developed to simulate the performance of a real life design.

2. Improved designs that employ the resonance property of the switches can be made.

3. New structures that can be implemented using RF MEMS switches and phase shifters can be designed and implemented.

4. Fabrication process can be improved to produce better devices. Steps that require special attention are the sacrificial layer deposition and patterning and structural layer formation.

5. New steps can be included in the fabrication process to produce different designs. Also process can be integrated into a CMOS or MMIC process to make more complicated systems.

In conclusion Switches and phase shifters using RF MEMS technology was designed and implemented for the first time in Turkey. Beneficial experience for the future work was gained during the design and implementation phase of this research.

REFERENCES

[1] C. Goldsmith, T. H. Lin, B. Powers, W. R. Wu, B. Norvell, "Micromachined Membrane Switches for Microwave Applications," IEEE Microwave Theory and Techniques Symposium, pp. 91-94, 1995

[2] J. J. Yao, M. F. Chang, "A Surface Micromachined Miniature Switch for Telecommunications With Signal Frequencies From DC to 40 GHz," 8th Int. Conference on Solid-State Sensors and Actuators, pp. 384-387, 1995

[3] C. Goldsmith, J. Randall, S. Eshelman, T. H. Lin, D. Denniston, S. Chen, B. Norvell, " Characteristics of Micromachined Switches at Microwave Frequencies," IEEE Microwave Theory and Techniques Symposium, pp. 1141-1144, 1996

[4] C.L. Goldsmith, Zhimin Yao, Susan Eshelman, David Denniston, "Performance of Low-loss RF MEMS Capacitive Switches," IEEE Microwave and Guided Wave Letters, Vol. 8, Issue 8, August 1998

[5] C. Chang, P. Chang, "Innovative Micromachined Microwave Switch With Very Low Insertion Loss," Sensors and actuators A, Vol. 79, Issue 1, pp 71-75, 2000

[6] J. Rizk, G.-L. Tan, J. B. Muldavin, G. M. Rebeiz, "High-Isolation W-Band MEMS Switches," IEEE Microwave and Wireless Components Letters, Vol. 11, no. 1, pp. 10-12, January 2001

[7] J. B. Muldavin, G. M. Rebeiz, "High-Isolation Inductively Tuned X band MEMS Shunt Switch," IEEE Microwave Theory and Techniques Symposium, Vol. 1, pp. 169-172, 2000

[8] J. B. Muldavin, G. M. Rebeiz, "High-Isolation CPW MEMS Shunt Switches-Part 1: Modeling," IEEE Transactions on Microwave Theory and Techniques, Vol. 48, Issue 6, pp. 1045-1052, June 2000

[9] J. B. Muldavin, G. M. Rebeiz, "High-Isolation CPW MEMS Shunt Switches-Part 2: Design," IEEE Transactions on Microwave Theory and Techniques, Vol. 48, Issue 6, pp. 1053-1056, June 2000

[10] S. P. Pacheco, L. P. B. Katehi, C. T.-C. Nguyen, "Design of Low Actuation Voltage RF MEMS Switch," IEEE Microwave Theory and Techniques Symposium, Vol. 1, 2000, pp. 165-168

[11] D. Hah, E. Yoon, S. Hong, "A Low Voltage Actuated Micromachined Microwave Switch Using Torsion Springs and Leverage," IEEE Microwave Theory and Techniques Symposium, Vol. 1, 2000, pp. 157-160

[12] D. Hyman, A. Schmitz, B. Warneke, T. Y. Hsu, J. Lam, J. Brown, J. Schaffner, A. Waltson, R. Y. Lou, G. L. Tangonan, M. Mehregany, J. Lee, "GaAs Compatible Surface Micromachined RF MEMS Switches," Electronics Letters, Vol. 35, pp. 224-226, February 1995

[13] H.D. Wu, K.F. Harsh, R.S. Irwin, W. Zhang, A.R. Mickelson, Y.C. Lee, "MEMS Designed for Tunable Capacitors," Proceedings of the 1998 IEEE Microwave Theory and Techniques Society, pp 127-129, 1998

[14] J. J. Yao, S. T. Park, R. Anderson, J. DeNatale, "A Low Power Low Voltage Electrostatic Actuator for RF MEMS Applications," Solid-State and Actuator Workshop, Hilton Head Island, South California, pp 246-249, June 2000

[15] C.L. Goldsmith, A. Malczewski, Z.J. Yao, S. Chen, J. Ehmke, D.H. Hinzel, "RF MEMS Variable Capacitors for Tunable Filters," Int. J. RF and microwave computer aided engineering, pp 362-374, 1999

[16] N. S. Barker, G. M. Rebeiz, "Distributed MEMS True Time Delay Phase Shifters and Wide Band Switches," IEEE Transactions on Microwave Theory abd Techniques, Vol. 46, pp. 1881-1890, November 1998

[17] E. G. Berker, A. S. Nagra, Y. Liu, P. Periaswamy, T. R. Taylor, J. Speck, R. A. York, " Monolithic Ka-Band Phase Shifters Using Voltage Tunable $BaSrTiO_3$ Parallel Plate Capacitors," IEEE Microwave and Guided Wave Letters, Vol. 10, pp. 10-12, January 2000

[18] O. L. Tan, R. E. Mihailovich, J. B. Hacker, J. F. DeNatale, G. M. Rebeiz, "A Very Low Loss 2-bit X-Band RF MEMS Phase Shifter," IEEE Microwave Theory and Techniques Symposium, Vol. 1, pp. 333-335, 2002

[19] B. Pillans, S. Eshelman, A. Malczewski, J. Ehmke, C. Goldsmith, "Ka-Band RF MEMS Phase Shifters for Phased Array Applications," Radio Frequency Integrated Circuits Symposium, pp. 195-199, 2000

[20] A. Malczewski, S. Eshelman, B. Pillans, J. Ehmke, C. L. Goldsmith, "X-Band RF MEMS Phase Shifters for Phased Array Applications," IEEE Microwave and Guided Wave Letters, Vol. 9, Issue 12, pp. 517-519, December 1999

[21] T. Campbell, "MEMS Switch Technology Approaches the Ideal Switch," Applied Microwave and Wireless, pp. 100-107, May 2001

[22] G. M. Rebeiz, J. B. Muldavin, "RF MEMS Switches and Switch Circuits," IEEE Microwave Magazine, Vol. 2, Issue 4, pp. 59-71, December 2001

[23] S. Jung, K. Kang, J.-H. Park, K.-W. Chung, Y.-K. Kim, Y. Kwon, "Micromacined Frequency-Variable Impedance Tuners Using Resonant Unit Cells," IEEE Microwave Theory and Techniques Symposium, Vol. 1 , pp. 333-336, 2001

[24] K. L. Lange, J. Papapolymerou, C. L. Goldsmith, A. Malczewski, J. Klebe, "A Reconfigurable Double-Stub Tuner Using MEMS Devices," IEEE Microwave Theory and Techniques Symposium, Vol. 1 , pp. 337-340, 2001

[25] J.-C. Chiao, Y. Fu, I. M. Chio, M. DeLisio, L.-Y. Lin, "MEMS Reconfigurable Vee Antenna," IEEE Microwave Theory and Techniques Symposium, Vol. 4 , pp. 1515-1518, 1999

[26] J. H. Schaffner, R. Y. Loo, D. F. Sievenpiper, F. A. Dolezal, G. L. Tangonan, J. S. Colburn, J. J. Lynch, J. J. Lee, S. W. Livingston, R. J. Broas, M. Wu, "Reconfigurable Aperture Antennas Using RF MEMS Switches for Multi Octave Tunability and Beam Steering," Antennas and Propagation Society International Symposium, Vol. 1, pp. 321-324, 2000

[27] G. M. Rebeiz, G. L. Tan, J. S. Hayden, "RF MEMS Phase Shifters: Design and Applications," IEEE Microwave Magazine, Vol. 3, Issue 2, pp. 72-81, June 2002

[28] R. N. Simons, "Coplanar Waveguide Circuits and Systems," Wiley Series in Microwave and Optical Engineering, Wiley Interscience, 2001

[29] C. Veyres, V. F. Hanna, "Extension of the Application of Conformal Mapping Techniques to Coplanar Lines With Finite Dimensions," Int. J. Electron, Vol. 48, No 1, pp. 47-56, January 1980

[30] S. Gevorgian, L. J. P. Linner, E. L. Kollberg, "CAD Models for Shielded Multilayered CPW," IEEE Transactions on Microwave Theory and Techniques, Vol. 43, No 4, pp. 772-779, April 1995

[31] R. E. Collin, "Foundations for Microwave Engineering," McGraw Hill, 2nd edition, 1992

[32] R. N. Simons, "Suspended Coupled Slotline Using Double Layer Dielectric," IEEE Transactions on Microwave Theory and Techniques, Vol. MTT-29, No 2, pp. 162-165, February 2002

[33] R. N. Simons, R. K. Arora, "Coupled Slot Line Field Components," IEEE Transactions on Microwave Theory and Techniques, Vol. MTT-30, No 7. pp. 1094-1099, July 1982

[34] R. Goyal, "Monolithic Microwave Integrated Circuits: Technology and Design," Artech House, 1989

[35] P. M. Zarvacky, N. E. McGruer, R. H. Morrison, D. Potter, "Microswitches and Microrelays With a View Toward Microwave Applications," International Journal on RF and Microwave Computer Aided Engineering, Vol. 9, pp.338-347, 1999

[36] S. Duffy, C. Bozler, S. Rabe, J. Knecht, L. Travis, P. Wyatt, C. Keast, M. Gouker, "MEMS Microswitches for Reconfigurable Microwave Circuitry," IEEE Microwave and Wireless Components Letters, Vol. 11, Issue 3. pp. 106-108, March 2001

[37] M. Ulm, T. Walter, R. M. Fiedler, K. Voigtlaender, E. Kasper, "K-Band Capacitive MEMS Switches," Topical Meeting on Si Monolithic Integrated Circuits in RF Systems, pp. 119-122, 2000

[38] B. Bahl, "Millimeter wave Engineering and Applications," Wiley Interscience, 1984

[39] J. Tsui, "Microwave Receivers and Related Components," Peninsula Publications, 1986

[40] H. J. De Los Santos, "Introduction to Microelectromechanical (MEM) Microwave Systems," Artech House, 1999

[41] C. Goldsmith, J. Randall, S. Eshelman, T. H. Lin, D. Denniston, S. Chen, B. Norvell, " Characteristics of Micromachined Switches at Microwave Frequencies," IEEE Microwave Theory and Techniques Symposium, pp. 1141-1144, 1996

[42] P. Osterberg, H. Yie, X. Cai, J. White, S. Senturia, Self-Consistent Simulation and Modeling of Electrostatically Deformed Diaphragms," Proceedings of the IEEE Micro Electro Mechanical Systems Conference, pp. 28-32, 1994

[43] E. R. Brown, "RF MEMS Switches for Reconfigurable Integrated Circuits," IEEE Transactions on Microwave Theory and Techniques, Vol. 46, No 11, pp. 1868-1880, 1998

APPENDIX A

FABRICATION PROCESS

Step	Process	Specification	Target	Comments
	GLASS WAFER	Corning 7740 Pyrex		
2	GLASS CLEANING	1.2:1 H_2SO_4:H_2O_2		
		10 min		
		DI rinse 2+3 min		
		Hot methanol rinse 2 min		
				Figure A.1 (a)
3	BACKSIDE	Sputter Ti 200°	0.3μm	
	METALLIZATION	Sputter Cu 200°	1.7μm	
				Figure A.1 (b)
4	MASK #1	Dehydration 130° 30 min		
	METAL1 PATTERN	HMDS		
		PR1828 2000 30 sec	4μm	
		Softbake 115° 60 sec		
		Expose 60 sec		
		Develop MF 319 1 min		
		Hardbake 120° 30 min		
5	GLASS ETCH	BHF 5 min		
		DI rinse 4 min		
				Figure A.1 (c)
6	METALLIZATION	Evaporate Cr	0.1μm	Low temp.
		Evaporate Au	0.9μm	
		Hot acetone		Remove resist
		Ultrasonic cleaning		for lift-off
				Figure A.1 (d)
7	DIELECTRIC	PECVD Si_3N_4	0.1μm	

	DEPOSITION			
8	MASK #2	Dehydration 130° 30 min		
	DIELECTRIC	HMDS		
	PATTERN	PR1813 4000 30 sec		
		Softbake 115° 60 sec		
		Expose 25 sec		
		Develop MF 319 1 min		
		Hardbake 120° 30 min		
9	DIELECTRIC ETCH	Transene Transetch N		
		140° 3 min		
				Figure A.1 (e)
10	STRIP	SVC175 75° 15 min		
	PHOTORESIST	DI rinse 3 min		
11	MASK #3	Dehydration 130° 30 min		
	SACRIFICIAL	HMDS		
	PHOTORESIST	PR1828 1500 30 sec	5μm	
	PATTERN	Softbake 115° 60 sec		
		Remove edge bead 2000		
		Expose 90 sec		
		Develop MF 319 5 min		
		Hardbake 115° 30 min		
				Figure A.1 (f)
12	SEED METAL	Sputter Cu 115°	0.3μm	
13	MASK #4	HMDS		No
	MOLD PATTERN	PR1828 2500 30 sec	3.5μm	dehydration
		Softbake 115° 60 sec		No hardbake
		Expose 190 sec		
		Develop MF 319 5 min		
14	ELECTROPLATING	Electroplate Ni	2μm	
		200 mA 27 min		
15	STRIP	Acetone 2 min		Mold
	PHOTORESIST			photoresist
				Removed
16	Cu etch	Ammonia solution 30 min		
17	STRIP	Acetone 30 min		Sacrificial
	PHOTORESIST	IPA 5 min		photoresist
		Hot methanol 5 min		Removed
				Figure A.1 (g)

(a)

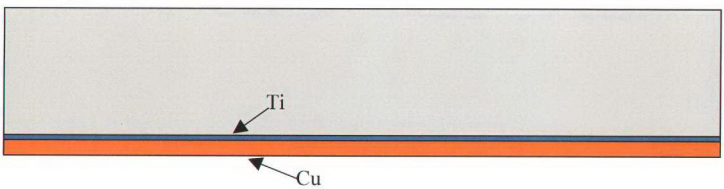

(b)

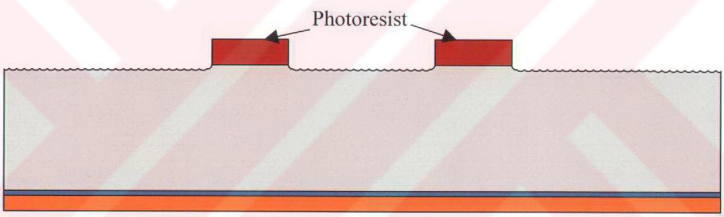

(c)

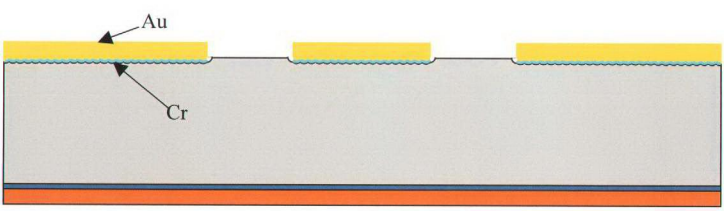

(d)

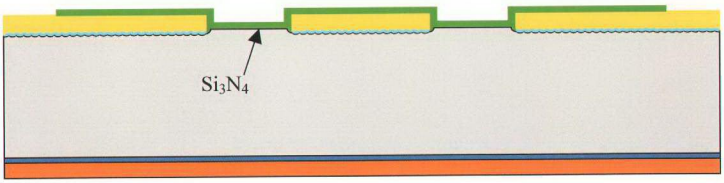

(e)

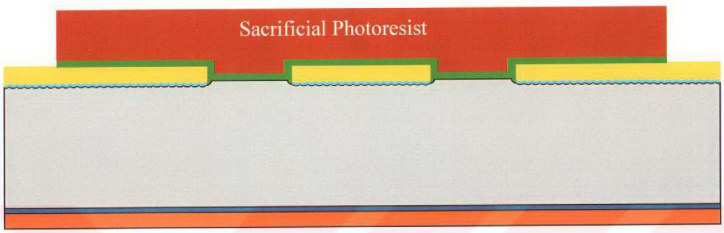

(f)

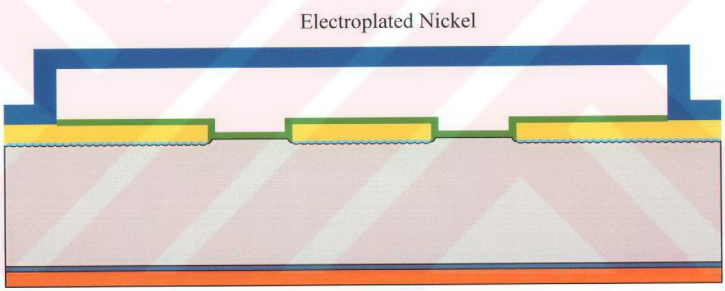

(g)

Figure A.1: Cross section of a standard switch structure throughout the process flow is given. (a) The glass wafer after glass cleaning. (b) Backside of the wafer is coated with Ti/Cu sputtering. (c) Glass is etched after the Metal 1 pattern to make the surface rough and make some undercut to make lift-off easier. (d) Wafer after Cr/Au evaporation and lift-off. (e) Dielectric deposition and patterning. (f) Sacrificial resist coating and patterning. (g) Nickel electroplating and sacrificial resist removal.